2022

ASPECTS ON THE QUANTUM DYNAMICS OF A SYSTEM COUPLED TO A BOSONIC ENVIRONMENT

Qidong Xu
Qidong.Xu.GR@Dartmouth.edu

ASPECTS ON THE QUANTUM DYNAMICS OF A SYSTEM COUPLED TO A BOSONIC ENVIRONMENT

A Thesis

Submitted to the Faculty

in partial fulfillment of the requirements for the

degree of

Doctor of Philosophy

in

Physics and Astronomy

by

Qidong Xu

DARTMOUTH COLLEGE

Hanover, New Hampshire

June 2022

Examining Committee:

Miles Blencowe, Chair

Robert Caldwell

Marcelo Gleiser

Alexander R. H. Smith

F. Jon Kull, Ph.D.
Dean of the Guarini School of Graduate and Advanced Studies

Abstract

In this work we study various aspects of the quantum dynamics for a system coupled to a Bosonic environment, which is described by a collection of quantum harmonic oscillators or a quantum field. We first consider two quantum mechanical oscillator system-bath models obtained by dimensionally truncating linearized gravity coupled to a massive scalar field and scalar QED, and we show that they separately map onto the phase damped oscillator model and the oscillator system subject to two-photon damping. The phase damped oscillator model also corresponds to the optomechanical system with an acoustic field environment, and we study the acoustic environment induced cavity modes dephasing dynamics as well as the possible infrared and ultraviolet divergence dependence on the spatial dimension of the environment with potential experimental realizations. Next, we show that the acoustic phonon field can not only induce the depahsing effects for the system, but also serves as an entanglement channel for two initially separable systems, which bears similarities with the weak, quantum gravitational fields as mediators of quantum entanglement. We then shift our focus to another system-bath model: Unruh-Dewitt (UDW) detectors coupled to a scalar field. We consider two scenarios here; one includes two UWD detectors coupled to a massless scalar field in a gravitational wave spacetime and we show that the entanglement harvested by two detectors depends sensitively on the frequency of the gravitational wave. The resonance effects can be observed when the energy gap of the detectors matches the frequency of the gravitational wave. The

other one consists of a UWD detector initially in the ground state coupled to a non-relativistic particle state of a massive scalar field, and it is found that the transition probability of the detector (which can be interpreted as the probability of detecting the particle at the location of the UWD detector) is qualitatively similar to the non-relativistic probability density of the particle.

Preface

Six years ago, when I embarked on my PhD journey, I didn't come with a traditional academic background. Although I was confident with my physics understanding, most of the learning process was done via a self-taught way in a largely separate environment without contact with physics professors, scholars and students, except for a short and highly valuable research experience with Prof. Zhangqi Yin in Tsinghua University. Looking backwards, I recognize that it would be impossible for me to grow from an eager student to a serious researcher without the help from a number of people that I would like to thank.

First and foremost, I would like to thank my advisor Miles Blencowe for his enormous support over the years. Miles has been a great advisor for both providing important insights and guidance when I got stuck with the research projects and also allowing a great amount of freedom for me to explore physics and come up with my own ideas and projects. Always being patient and caring, Miles is an advisor that I can not be more proud to have worked with.

In addition to Miles, I would like to thank my collaborators Alexander R. H. Smith and Shadi Ali Ahmad for their valuable inputs in our project and enjoyable research and life experience.

I thank every faculty member in the department that I have encountered with, especially Prof. Onofrio and Prof. Viola for the "Nourishing Food Foundation" and many wonderful dinner nights.

I have to thank all my friends who were or still are in the Hanover area; the winter here is too cold to bear without all your supports and laughs. Finally my sincere thanks go to my parents, for their constant support and love.

Citations to Previous Papers

With minor changes, Chapter 2 appear as *Xu, Qidong, and M. P. Blencowe. "Toy models for gravitational and scalar QED decoherence." arXiv:2005.02554 (2020).* Currently under review in New Journal of Physics.

Chapter 3 and Appendix A appear in their entirety as *Xu, Qidong, and M. P. Blencowe. "Cavity mode dephasing via the optomechanical interaction with an acoustic environment." Physical Review A 104.6 (2021): 063509.*

Chapter 4 appears in its entirety as *Xu, Qidong, and M. P. Blencowe. "Entanglement generation by vacuum and thermal phonon fields via the optomechanical interaction." arXiv:2110.13278 (2022).* Currently under review in Physical Review Letters.

Chapter 5 and Appendix B appear in their entirety as *Xu, Qidong, Shadi Ali Ahmad, and Alexander RH Smith. "Gravitational waves affect vacuum entanglement." Physical Review D 102.6 (2020): 065019.*

Chapter 6 and Appendix C appear in their entirety as *Xu, Qidong. "Unruh-DeWitt detector's response to a nonrelativistic particle." Physical Review D 104.8 (2021): 085006.*

Contents

Chapter 1

Introduction

All realistic quantum systems are ultimately open quantum systems, which inevitably interact with external quantum systems that are usually referred as environments. With the advancing quantum technologies, the influence of the environment on the quantum dynamics of the systems can be controlled in a desired way or greatly reduced depending on the properties of the system that the study is interested in. Examples include cavity quantum electrodynamics [1], circuit quantum electrodynamics [2] and cavity optomechanics [3]. Furthermore, one can also view the open quantum system from a different perspective by asking the question: what can we learn about the environment from the system that we have direct access to? In the context of quantum field theories, this question motivated the operational approach to study quantum fields via the coupling of the Unruh-Dewitt (UWD) detectors [4, 5] to the fields, where the UWD detectors are essentially two level quantum systems with some given spacetime worldlines. This thesis shall cover several studies from both perspectives; as these two perspectives are somewhat independent from each other, we will motivate and introduce them separately.

Section 1.1

Cavity mode dephasing and entanglement generation

Despite the increasing control capability towards the environment, there remains one interaction that one can not shield from - gravitational interaction, as indicated by the Einstein equation. It is this unique feature of gravity that motivated a series of the studies in this thesis because gravitational environment might put an upper bound on coherence times of macroscopic superposition states, and therefore results in a macroscopic classical world. A common approach to this problem is to extract the decoherence rate through the off-diagonal matrix elements of the system density

operator. However, when coupled to gravity, the density operator of the system is not a gauge invariant quantity, which is related to the fact that, in general relativity, local diffeomorphisms are gauge symmetries meaning the local correlation functions like $\langle O_1(x_1)...O_n(x_n)\rangle$ do not correspond to physical observables. A remedy to this difficulty might be obtained by noticing that the deffeomorphisms reaching the infinity are true physical symmetries – asymptotic symmetries; one can therefore consider the worldline of an observer starting from infinity and then construct diffeomorphism invariant operators along this worldline [6]. However, the constructed operators are non-local, which are hard to be made use of. Another difficulty arises from the fact that to solve for the time evolution of the system, one usually needs to assume an unnatural initial tensor product state between the system and the gravitational environment, which would result in an upper cutoff dependent decoherence where the upper cutoff depends on the scale of new physics in quantum gravity. Without the UV details of quantum gravity, the scale of new physics can not be known a priori. As an example, string theory gives the scale to be the inverse of the string length: $\frac{1}{l_s}$.

Given the above mentioned issues, a probably more sensible approach is to study the gravitationally induced decoherence through an operational/experimental approach. One example is to consider a massive particle confined in a potential well [7]. Assuming an initial superposition state of two coherent state at different locations, the expectation value of the number density operator exhibits an interference pattern when the two coherent states meet together. The reduction of this interference pattern due to the gravitationally induced decoherence can then be used to quantify the decoherence rate.

In Chapter 2 [based on Xu, Q., & Blencowe, M. P. (2020). arXiv:2005.02554], as a first step, we shall study a quantum mechanical oscillator system-bath model obtained by dimensionally truncating linearized gravity coupled to a massive scalar field as

well as another system-bath model obtained by dimensionally truncating scalar QED. These two models can be regarded as zero dimensional quantum field theory and they are chosen to validate the above mentioned operational approach to the decoherence effects without the need of worrying about the potential gauge problems, and also to validate certain standard approximation methods, thus providing helpful insights and clues to eventually study actual gravitationally induced decoherence. The 0D gravity model allows for an exact time evolution solution for the system density matrix while approximations and numerical methods shall be made to solve for the 0d scalar QED model. The solutions are then used to demonstrate the operational approach to the decoherence effects and we show that these two models effective map onto phase damped oscillator and two-photon damping models.

Chapter 3 [based on Xu, Q., & Blencowe, M. P. (2021). Phys. Rev. A, 104(6), 063509] extends the studies of 0D gravity model in Chapter 2. Despite that the model was proposed with gravitationally induced decoherence considerations, the interaction between the system and the environmental modes is identical to the standard interaction Hamiltonian of an optomechanical system under the conditions of weak couplings, except for that the usual considered optomechanical system only contains a single environment mode while the 0D gravity model comprises *many* bath modes [3]. From this perspective, the model can be interpreted as an optomechanical system comprising a single cavity mode and a dense spectrum of acoustic modes, and we shall find that this model deserves importance in its own rights. In particular, we will show that the possible UV and IR divergences of the system dephasing dynamics are closely related to the spatial dimension and the size of the phonon field environment. Possible experimental realizations for 1D and 2D acoustic environment are also considered with the interaction Hamiltonian derived from the first principle.

In Chapter 4 [based on Xu, Q., & Blencowe, M. P. (2021). arXiv:2110.13278], we

further extend the study in Chapter 3 by shifting our focus from the single cavity dephasing dynamics to two spatially separated, local cavity modes that are coupled optomechanically to a long elastic strip that functions as a quantum thermal acoustic field bath. Utilizing the exact solutions we obtained in the previous Chapter, we study the entanglement dynamics for two cavity modes and we shall find that significant entanglement can be generated periodically regardless of the bath temperature. Thanks to the exact solutions, we can also explicitly demonstrate that the entanglement is only possible when the two cavity modes are causally connected. Our result may then shed light on the nature of weak, quantum gravitational fields as mediators of quantum entanglement.

Section 1.2

Applications of UDW detectors

As we mentioned in the beginning of the Introduction, when we have a system coupled to a bath, the system can be employed to study the properties of the bath. Being simple two-level quantum systems with some given worldlines, UDW detectors are convenient tools engineered for studying the quantum field properties. One of the most famous examples of the UDW detector's application is in the proof of the Unruh effect [4], which states that the definition of vacuum is an observer dependent notion and the Minkowski spacetime vacuum state is actually a thermal state from the perspective of an uniformly accelerated observer. In this thesis, we will cover two studies involving one and two UWD detectors, separately.

In Chapter 5 [based on Xu, Q., Ahmad, S. A., & Smith, A. R. (2020) Phys. Rev. 102(6), 065019], we investigate the entanglement harvesting in a gravitational wave spacetime. Entanglement harvesting refers to the fact that two initially unentangled, spatially separated UDW detectors can become entangled when they are both

locally coupled to a quantum field even if the detectors remain spacelike separated. The entanglement between the detectors is, therefore, 'harvested' from the vacuum, which is already known to be a highly entangled state [8]. By considering a massless scalar quantum field in a gravitational wave spacetime, the entanglement harvested by two detectors shall be shown to be sensitive to the frequency of the gravitational wave, exhibiting resonance effects when the energy gap of the detectors matches the frequency of the gravitational wave. Comparing it to the entanglement harvesting effects in the flat spacetime, this protocol allows a probe to see how the entanglement structure of the field is changed by the spacetime structure.

Besides focusing on the entanglement properties of quantum fields, it is also of interest to study the UDW detectors' response to the field state that represents the matter/particle distribution since the UWD detector is after all an ideal type of particle detectors. In Chapter 6 [based on Xu, Q. (2021). Phys. Rev. D, 104(8), 085006], we study the response of an UDW detector initially in the ground state to a non-relativistic particle state of a massive scalar field. The choice of a non-relativistic particle state allows a convenient comparison between the UWD detector transition probability and the probability density of the corresponding free Gaussian wave packet in the non-relativistic quantum mechanical description. As we will show, the transition probability of the UDW detector splits into the vacuum contribution and the matter contribution, with the latter behaving qualitatively similar to the non-relativistic probability density description.

Chapter 2

Zero-dimensional models for gravitational and scalar QED decoherence

Section 2.1

Introduction

The non-existence of macroscopic mass system quantum superposition states under everyday conditions is commonly understood to be due to interactions with the system environment; air molecules, photons, and internal system defects cause the rapid decoherence of position and energy superposition states into apparent mixtures of either/or alternatives that are indistinguishable from a classical statistical distribution [9, 10, 11]. By placing the system in ultrahigh vacuum, shielding it from external electromagnetic radiation, and cooling the system down to its ground state, quantum mechanics would in principle allow for macroscopic system superposition states to be prepared and measured. However, there is one environment that cannot be screened out–gravity, as expressed dynamically at the classical level through Einstein's field equations [12, 13, 14, 15, 16, 17, 18].

From a fundamental perspective, it is interesting to try to quantify the effect of the gravitational environment on macroscopic mass/energy superposition states; even if the predicted gravitationally induced decoherence times are much longer than for everyday, electromagnetic environments, having a good quantitative understanding of the former would allow us to place in principle, unavoidable bounds on the coherence times of macroscopic superposition states, and furthermore help point the way towards possible future experiments to probe the role of gravity in enforcing macroscopic classicality.

Under terrestrial or space-based laboratory conditions corresponding to weak spacetime curvature [19], it should be sufficient to work with linearized gravity [20], where the matter system-gravitational environment action is quadratic in metric deviations $h_{\mu\nu}$ from Minkowski spacetime $\eta_{\mu\nu}[= \mathrm{diag}(-+++)]$: $g_{\mu\nu} = \eta_{\mu\nu} + \kappa h_{\mu\nu}$, where

$\kappa = \sqrt{32\pi G}$ (with natural units $\hbar = c = 1$). Furthermore, modeling the matter system through quantum excitations of a massive scalar field ϕ, a "first-principles" starting point for investigating gravitational decoherence is the following action:

$$S[\phi, h_{\mu\nu}] = S_M[\phi] + S_E[h_{\mu\nu}] + S_I[\phi, h_{\mu\nu}], \tag{2.1}$$

where the system, environment, and interaction actions are respectively:

$$S_M[\phi] = -\frac{1}{2}\int d^4x \left(\eta^{\mu\nu}\partial_\mu\phi\partial_\nu\phi + m^2\phi^2\right), \tag{2.2}$$

$$S_E[h_{\mu\nu}] = \int d^4x \left(-\frac{1}{2}\partial^\rho h^{\mu\nu}\partial_\rho h_{\mu\nu} + \partial_\nu h^{\mu\nu}\partial^\rho h_{\mu\rho} - \partial_\mu h\partial_\nu h^{\mu\nu} + \frac{1}{2}\partial^\mu h\partial_\mu h\right), \tag{2.3}$$

and

$$S_I = \int d^4x \left(\frac{\kappa}{2}T^{\mu\nu}(\phi)h_{\mu\nu} + \frac{\kappa^2}{4}U^{\mu\nu\rho\sigma}(\phi)h_{\mu\nu}h_{\rho\sigma}\right), \tag{2.4}$$

with $T^{\mu\nu}(\phi)$ the scalar field energy-momentum tensor, $U_{\mu\nu\rho\sigma}(\phi)$ a quadratic in ϕ tensor [21], and $h = h^\mu_\mu$.

Quantization might then proceed through the derivation of a master equation for the density matrix of the scalar matter system, with the (assumed for simplicity) thermal gravitational environmental degrees of freedom traced out [12, 13, 14]. Alternatively, a quantum Langevin equation might be derived for the scalar matter field operator, again with the gravitational environment integrated out. One route to obtaining such effective equations is the closed time path integral approach, which is particularly suited to field systems [22].

However, as a coupled system-environment field theory with a non-quadratic interaction and a gauge symmetry (i.e., general coordinate invariance), the derivation of the quantum gravitational decoherence dynamics presents additional challenges

beyond the usual system-environment models considered in non-relativistic quantum mechanics [23, 24, 25]. One challenge involves the necessity for making various approximations in order to solve for the reduced system dynamics. For example, in the usual open quantum systems analyses, it is assumed that the system+environment is initially in a product state, e.g., the system is in a superposition of two distinct wavepacket or energy states and the environment is in a thermal state. Such a product state can result in an initial "burst" of decoherence that depends on the upper cut-off physics of the environment, which in the case of gravity is unknown. Furthermore, a Born and possibly Markovian approximation is made [23, 24, 25], where the influence of the environment on the system is treated perturbatively to lowest non-trivial order, while the environment is assumed to respond rapidly relative to the system dynamics timescale.

Another challenge concerns requiring gauge invariance of the calculated decoherence rates for them to be meaningful, in particular when assuming a finite temperature environment that comprises gauge degrees of freedom (e.g., photons or gravitons) [24]. A common, direct approach [23, 24, 25] to obtaining decoherence rates for open quantum systems, either with or without gauge degrees of freedom, is to examine the time evolution of the off-diagonal matrix elements of the system density operator in the state basis of interest (e.g., energy eigenstates, position eigenstates etc.). However, the density operator is not a gauge invariant quantity.

A more consistent approach is to extract the decoherence rates through an operational procedure, i.e., involving an in principle measurement that can be ascribed to a particular expectation value of an observable. One such example is the particle detection number density in an atom interference set-up. A minimal way to get scalar matter field quanta initially in superposition states to interfere is by spatially trapping the field quanta in a three-dimensional harmonic confining potential [26];

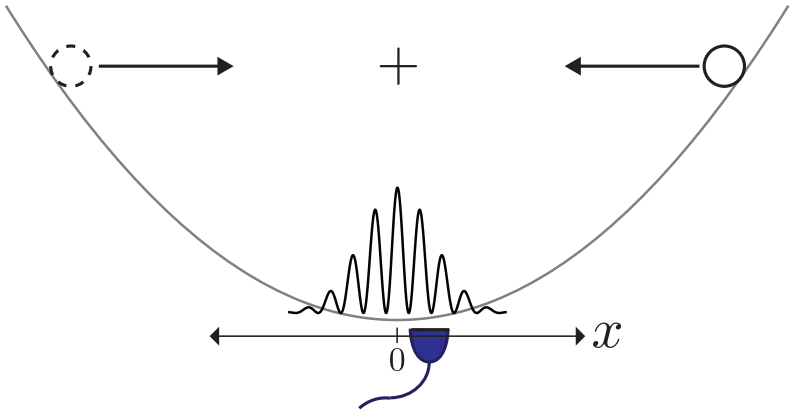

Figure 2.1: Scheme for operationally defining gravitational decoherence. An initial spatial superposition of N nucleon-oscillator coherent states gives rises to a spatial interference pattern in the particle detection probability whenever the particle wavefunctions pass through each other at $x = 0$. The particle detector is indicated centered at some given x-location. A suppression of the x-dependent interference pattern in the particle detection probability is interpreted as gravitational decoherence.

the system action (2.2) is then supplemented by the term

$$-\frac{1}{2}\int d^4x m^2\Omega^2 r^2\phi^2, \tag{2.5}$$

where Ω is the characteristic oscillation frequency and the potential center coincides with the spatial origin $\mathbf{r} = 0$. Referring to Fig. 2.1, we might then consider a thought experiment where an initial ($t = 0$) N-nucleon state corresponding to being in a superposition of two collective coherent states with coordinate parameters $\mathbf{r} = (x, 0, 0)$, $x = x_{01} > 0$, $x_{02} < 0$ (and hence superposition separation $x_{01} - x_{02}$) undergoes gravitational decoherence. Once during every oscillation period, the coherent states in the superposition pass through each other in the region centered at $x = 0$, resulting in an interference pattern for the x-dependence of the local particle detection probability as indicated in the figure. A measure of the degree of coherence is the so-called "inter-

ferometric visibility", defined below in Eq. (2.30); a reduction in visibility over time is interpreted as a signature of gravitationally induced decoherence or dephasing.

In particular, suppose that we have a particle detector with center of mass worldline $(t, \mathbf{r})$ in the vicinity of $\mathbf{r} = 0$ and the particle detection is described by the local field observable $\left(V^{-1}\int_V d\mathbf{r}\phi(\mathbf{r},0)\right)^2$, where $\phi(\mathbf{r},0)$ is the scalar field operator (in the Schrödinger picture), and V is a coordinate averaging volume (assumed very small) that reflects the fact that a real detector is not pointlike, but rather occupies some nonzero volume in space. The visibility can then be obtained in terms of the following expectation value:

$$\mathrm{Tr}\left[\rho(t)\left(V^{-1}\int_V d\mathbf{r}\phi(\mathbf{r},0)\right)^2\right] = V^{-2}\int_V d\mathbf{r}d\mathbf{r}'\mathrm{Tr}\left[\rho(t)\phi(\mathbf{r},0)\phi(\mathbf{r}',0)\right], \quad (2.6)$$

where the density matrix $\rho(t)$ describes the N nucleons initially in a coherent superposition state and interacting with a thermal graviton bath environment. The expectation value (2.6) gives a measure of the spatial particle number density (smeared over the small volume V) and is to be viewed as the field-theoretic counterpart to the configuration space probability density $V^{-1}\int_V d\mathbf{r}\langle\mathbf{r}|\rho_{\mathrm{ho}}(t)|\mathbf{r}\rangle$ for a single, non-relativistic quantum harmonic oscillator described by the evolving density matrix $\rho_{\mathrm{ho}}(t)$.

The just described set-up shares features of atom and molecular wave interferometry experiments [27, 28, 29], but utilizing optical traps [30, 31, 32, 33]. The latter enables the two wavefunction components making up the superposition to interfere multiple times as they oscillate through each other, rather than just once as in most matter wave interferometry set-ups. Furthermore, no complicated boundary conditions or additional coupled degrees of freedom such as spins manipulated by external magnetic fields in a Stern-Gerlach-type apparatus [32] are required in the system-environment action order to implement the interferometer; just a harmonic confining potential is required. We must emphasize however that our set-up should not be

viewed necessarily as a possible way to feasibly measure gravitational decoherence, but rather as an in-principle operational procedure to quantify the decoherence via the above-defined visibility measure.

With the above-describe challenges in mind, in this chapter we shall consider as a first step two toy system-environment models that are in turn closely related through dimensional reduction to the above scalar field-gravity system and to scalar field quantum electrodynamics (QED) [34]. The Lagrangian for scalar QED is

$$L = -(D_\mu\phi)^*(D^\mu\phi) - m^2\left(1+\Omega^2 r^2\right)\phi^*\phi - \frac{1}{4}F_{\mu\nu}F^{\mu\nu}, \tag{2.7}$$

where ϕ is a complex-valued scalar field, $D_\mu = \partial_\mu - ieA_\mu$ is the covariant derivative, and $F_{\mu\nu} = \partial_\mu A_\nu - \partial_\nu A_\mu$ is the electromagnetic field strength tensor. We have also included a three-dimensional harmonic confining potential [c.f. Eq. (2.5)] in order to facilitate operational probes of (de)coherence for initial scalar field spatial quantum superposition states as discussed above.

The models presented in Sec. 2.2 below are "toys" in the sense that there is no spatial coordinate–just a time coordinate–and hence are formally zero-dimensional (0d) field models. Our motivation here is to utilize the toy models in order to validate the above-described operational interferometric approach to decoherence as well as certain standard approximation methods, thus giving confidence in eventually applying a similar approach to quantifying actual gravitationally induced decoherence; the 0d model was in fact utilized in Ref. [12] to lend support for an initial gravitational decoherence derivation.

As zero-dimensional field systems, the toy models lack any gauge symmetry, however. It is for this reason that full scalar field QED is also useful for investigating decoherence and verifying that the considered decoherence measures are gauge invariant. In particular, what constitutes a gauge invariant observable is conceptually

clearer in scalar QED than in gravity and thus the former also serves as a useful pedagogical stepping stone towards addressing gravitational decoherence.

In Sec. 2.2, we introduce the 0d toy model Lagrangians. Section 2.3 analyzes the quantum dynamics of the scalar-weak gravity toy model, by utilizing an exact solution to the full system-environment Schrödinger equation assuming an initial system-environment product state, with the oscillator system state expressed in a number state basis and environment in a thermal state. These solutions are then utilized to determine the decoherence dynamics of initial superpositions of system oscillator coherent states through an operational interference fringe visibility analysis that is the single particle counterpart to that described above. Section 2.4 analyzes both the classical and quantum dynamics of the scalar QED toy model. In particular, both classical and quantum Langevin equations as well as a quantum master equation are derived for the system oscillator interacting with its oscillator bath. By making various approximations, the 0d model is shown to map onto that of a simpler oscillator system with 'two-photon' damping. The master equation is numerically solved to determine the decoherence dynamics of initial superpositions of system oscillator coherent states, again utilizing the operational interference fringe visibility approach. Section 2.5 gives some concluding remarks.

Section 2.2

0d toy models

We consider in turn two distinct oscillator system-environment models described by the following Lagrangians:

$$L_{\text{grav}} = \frac{1}{2}M\dot{x}^2 - \frac{1}{2}M\Omega^2 x^2 + \sum_i \left(\frac{1}{2}m\dot{q}_i^2 - \frac{1}{2}m\omega_i^2 q_i^2\right) - \lambda\left(\frac{1}{2}M\dot{x}^2 + \frac{1}{2}M\Omega^2 x^2\right)\sum_i q_i \quad (2.8)$$

and

$$L_{\text{qed}} = \frac{1}{2}M\left(\frac{d}{dt} + \lambda\sum_i q_i\right)x\left(\frac{d}{dt} + \lambda\sum_i q_i\right)x - \frac{1}{2}M\Omega^2x^2 + \sum_i\left(\frac{1}{2}m\dot{q}_i^2 - \frac{1}{2}m\omega_i^2q_i^2\right). \tag{2.9}$$

Both model Lagrangians describe an oscillator system with mass M and bare frequency Ω that is coupled to a bath of independent oscillators with assumed identical masses m and frequencies ω_i. The two models differ in their system-bath couplings; in particular, the system oscillator couples via its energy to the bath oscillator coordinates in Lagrangian L_{grav}, a 0d analogue of the $T^{\mu\nu}h_{\mu\nu}$ coupling term in Eq. (2.4). On the other hand, the interaction term in Lagrangian L_{qed} is obtained via a 0d analogue of the gauge principle of minimal coupling: $\partial_\mu \to \partial_\mu - ieA_\mu$. Expanding out the kinetic energy part of Lagrangian (2.9) gives both cubic and quartic interaction terms, which are respectively linear and quadratic in the bath coordinates [c.f. Eq. (2.31)]; the full, scalar QED Lagrangian (2.7) possesses analogous nonlinear terms. Note that the coupling strength parameters λ in Eqs. (2.8) and (2.9) have different dimensions.

Lagrangian (2.8) yields the standard Hamiltonian of an optomechanical system under the conditions of weak system-bath coupling, where a single optical mode furnishes the system oscillator degree of freedom, while the bath comprises a very large number of mechanical degrees of freedom. This is in contrast to usually-considered optomechanical systems [35], where only one or a few mechanical degrees of freedom are considered. In the present case, Lagrangian (2.8) might describe the dynamics of a light mode of a cavity embedded within a large elastic crystal, or alternatively a light mode trapped between oppositely facing cavity mirrors and coupled via light pressure to a thin, elastic dielectric membrane with large transverse extent [36, 37]

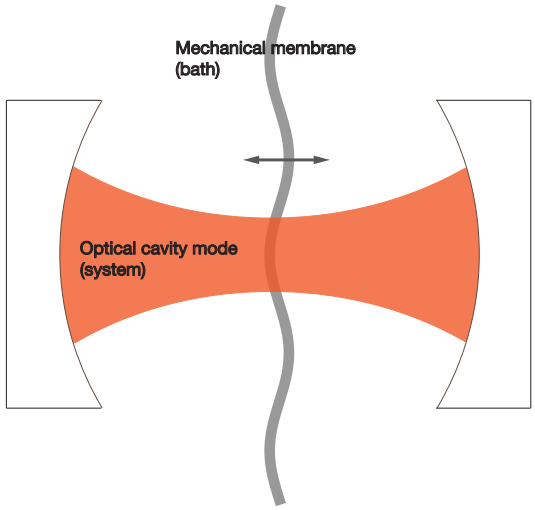

Figure 2.2: Optomechanical scheme where a cavity-trapped light mode (system) between oppositely facing mirrors interacts via light pressure with a thin, transversely vibrating dielectric membrane with large transverse extent (bath). Such a scheme realizes model (2.8) and is explored in more detail in Ref. [37].

(Fig. 2.2). As we shall see later in Sec. 2.3, when placed in an initial superposition of coherent states, such a system mode undergoes dephasing without damping–the latter behavior a consequence of the fact that the interaction Hamiltonian commutes with the system Hamiltonian. The resulting, effective system dynamics coincides with that of the so-called 'phase damped' oscillator [25].

In Sec. 2.4, we show that Lagrangian (2.9) describes approximately an oscillator system subject to two-photon damping [38]. This is in contrast to the usual quantum Brownian oscillator model with single photon damping and results in qualitatively different decoherence dynamics from the latter for initial superpositions of coherent states.

Section 2.3

Scalar gravity model

2.3.1. Solving the model

Starting with the Lagrangian L_{grav} (2.8), the system and bath momentum coordinates are

$$p = \frac{\partial L}{\partial \dot{x}} = M\dot{x}\left(1 - \lambda \sum_i q_i\right), \tag{2.10}$$

$$p_i = \frac{\partial L}{\partial \dot{q}_i} = m\dot{q}_i, \tag{2.11}$$

where we omit the 'grav' subscript from now on. The model Hamiltonian is

$$H = \frac{p^2}{2M}\left(1 - \lambda \sum_i q_i\right)^{-1} + \frac{1}{2}M\Omega^2 x^2\left(1 + \lambda \sum_i q_i\right) + \sum_i \left(\frac{p_i^2}{2m} + \frac{1}{2}m\omega_i^2 q_i^2\right). \tag{2.12}$$

For weak system-environment (bath) coupling, we can Taylor expand the kinetic energy coupled bath term to obtain approximately

$$H = \left(\frac{p^2}{2M} + \frac{1}{2}M\Omega^2 x^2\right)\left(1 + \lambda \sum_i q_i\right) + \sum_i \left(\frac{p_i^2}{2m} + \frac{1}{2}m\omega_i^2 q_i^2\right). \tag{2.13}$$

Quantizing and expressing the Hamiltonian (2.13) in terms of the oscillator system and bath creation and annihilation operators, which are defined through the respective relations $x = \sqrt{\frac{\hbar}{2M\Omega}}(a + a^\dagger)$, $p = i\sqrt{\frac{M\Omega\hbar}{2}}(a^\dagger - a)$, $q_i = \sqrt{\frac{\hbar}{2m\omega_i}}(a_i + a_i^\dagger)$, $p_i = i\sqrt{\frac{m\omega_i\hbar}{2}}(a_i^\dagger - a_i)$, the scalar gravity model Hamiltonian is

$$H = \hbar\Omega\left(a^\dagger a + \frac{1}{2}\right)\left(1 + \sum_i \lambda_i\left(a_i + a_i^\dagger\right)\right) + \sum_i \hbar\omega_i\left(a_i^\dagger a_i + \frac{1}{2}\right), \tag{2.14}$$

where the system-bath coupling is redefined as $\lambda_i = \sqrt{\frac{\hbar}{2m\omega_i}}\lambda$. We recognize in Eq. (2.14) the familiar form of the standard optomechanical Hamiltonian, but with a bath of mechanical oscillator modes (labelled by index i) in contrast to the usually considered situation of just one mechanical mode [35].

Solving for the quantum evolution, we will make the common assumption that the system and bath are in an initial product state $\rho_s \otimes \rho_{\text{bath}}$. While the latter assumption facilitates solving for the quantum dynamics, it is not always justified experimentally, since it necessarily requires that the system quantum state can be sufficiently isolated and prepared quickly enough compared to the interaction time scale with the bath degrees of freedom. While such an approximation may be justified for an electromagnetic environment under certain conditions, a mass-energy system can never be isolated from its gravitational environment. Nevertheless, as we shall see, the ability to solve exactly for the scalar gravity model quantum dynamics will give insights into the consequences of assuming a product state.

It is convenient to work in a basis of system number states and bath coherent states $|n, \{\alpha_i\}\rangle$; the time evolution for such a state can be written as:

$$e^{-\frac{iHt}{\hbar}}|n, \{\alpha_i\}\rangle = \exp\Bigg(-\frac{it}{\hbar}\Big[\hbar\Omega\left(n+\frac{1}{2}\right)\big(1+\sum_i \lambda_i(a_i + a_i^\dagger)\big) + \sum_i \hbar\omega_i\left(a_i^\dagger a_i + \frac{1}{2}\right)\Big]\Bigg)|n, \{\alpha_i\}\rangle\,. \tag{2.15}$$

Following the analysis of Ref. [39], Eq. (2.15) can be evaluated as:

$$\begin{aligned} e^{-\frac{iHt}{\hbar}}|n,\{\alpha_i\}\rangle = \exp\Bigg(& -it\left[\Omega\left(n+\frac{1}{2}\right)+\sum_i\left(\frac{\omega_i}{2}-\frac{\Omega^2\lambda_i^2\left(n+\frac{1}{2}\right)^2}{\omega_i}\right)\right] \\ & -\sum_i\frac{i\left(n+\frac{1}{2}\right)^2\lambda_i^2\Omega^2}{\omega_i^2}\sin\omega_i t+\frac{1}{2}\sum_i\frac{\lambda_i}{\omega_i}\left(n+\frac{1}{2}\right)\Omega \\ & \times\left[\alpha_i^*\left(1-e^{i\omega_i t}\right)-\alpha_i\left(1-e^{-i\omega_i t}\right)\right]\Bigg) \\ & \times\left|n,\left\{\alpha_i e^{-i\omega_i t}-\frac{\Omega\left(n+\frac{1}{2}\right)}{\omega_i}\lambda_i\left(1-e^{-i\omega_i t}\right)\right\}\right\rangle. \end{aligned} \tag{2.16}$$

Supposing the bath to initially be in a thermal state, we can express its initial density matrix in the coherent basis as follows [40]:

$$\rho_{\text{bath}} = \prod_i\frac{1}{\pi\left(e^{\beta\hbar\omega_i}-1\right)}\int d\alpha_i^2\exp\Big(-|\alpha_i|^2\left(e^{\beta\hbar\omega_i}-1\right)\Big)|\alpha_i\rangle\langle\alpha_i|, \tag{2.17}$$

where $\beta^{-1} = k_B T$, with k_B Boltzmann's constant and T the bath temperature. Decomposing the initial system-environment state in the number state basis:

$$\rho_{\text{initial}} = \sum_{n,n'} C_{nn'}|n\rangle\langle n'|\otimes\rho_{\text{bath}}, \tag{2.18}$$

we have for the time evolution of the number state outer products after tracing out the bath degrees of freedom:

$$\begin{aligned} |n(t)\rangle\langle n'(t)| = |n\rangle\langle n'|\exp\Bigg(& -it\Big[\Omega(n-n')+\sum_i\frac{\Omega^2\lambda_i^2}{\omega_i}(n'+n+1)(n'-n)\Big] \\ & +i\sum_i\frac{\lambda_i^2\Omega^2}{\omega_i^2}\sin(\omega_i t)(n'+n+1)(n'-n) \\ & -2\sum_i\left(\frac{\Omega\lambda_i(n-n')}{\omega_i}\right)^2\coth\left(\frac{\beta\hbar\omega_i}{2}\right)\sin^2\left(\frac{\omega_i t}{2}\right)\Bigg). \end{aligned} \tag{2.19}$$

As we shall show later below in Sec. 2.3.2, the time evolution of an arbitrary ini-

tial reduced oscillator system state can be obtained by decomposing in terms of the number state outer product solutions (2.19).

In order to carry out the sum over bath degrees of freedom in Eq. (2.19), we will assume a bath spectral density with exponential cut-off frequency ω_c:

$$\pi \sum_i \lambda_i^2 \delta(\omega - \omega_i) = C\omega e^{-\omega/\omega_c}. \tag{2.20}$$

The linear in ω "Ohmic" dependence well below the cut-off is utilized since a thermal graviton bath is Ohmic [12]; a cut-off is necessary in order to avoid infinities in the intermediate stages of the analysis and the exponential form is primarily motivated by calculational convenience, enabling exact solutions to be obtained for the oscillator system reduced dynamics in the number state basis. While the short distance, cut-off physics is in principle known for a concrete material system realisation such as for the vibrating membrane environment in Fig. 2.2 [37], the corresponding short distance, 'Planckian' physics is by contrast not known for gravity. As we shall see below, the cut-off dependence can be absorbed in part through a frequency and non-linear Kerr-type self-interaction renormalization; the cut-off does however affect the initial decoherence dynamics.

Using Eq. (2.20) to replace the sum in Eq. (2.19) with an integral over the continuous variable ω, we obtain

$$\begin{aligned} |n(t)\rangle\langle n'(t)| = |n\rangle\langle n'| \exp\Bigg(& -i\Omega(n-n')t + i\frac{C\Omega^2}{\pi}(n-n')(n+n'+1)[\omega_c t \\ & - \tan^{-1}(\omega_c t)] - \frac{2C\Omega^2}{\pi}(n-n')^2 \int_0^\infty d\omega\omega \coth\left(\frac{\beta\hbar\omega}{2}\right) \frac{\sin^2(\frac{\omega t}{2})}{\omega^2} e^{-\omega/\omega_c} \Bigg). \end{aligned} \tag{2.21}$$

Note that for a material system realization, the environment would have a finite

extent resulting in a non-zero, lower frequency cut-off ω_1: $0 < \omega_1 \ll \omega_c$ [37]; here we set the lower frequency cut-off $\omega_1 = 0$, reflecting the actual gravitational environment with effectively infinite spatial extent. The integral in the above expression can then be evaluated analytically to give

$$\begin{aligned}&\int_0^\infty d\omega\omega \coth\left(\frac{\beta\hbar\omega}{2}\right)\frac{\sin^2\left(\frac{\omega t}{2}\right)}{\omega^2}e^{-\omega/\omega_c}\\ =&\frac{1}{4}\ln\left(1+t^2\omega_c^2\right)+\frac{1}{2}\ln\left[\frac{\Gamma^2\left(\frac{1}{\beta\hbar\omega_c}+1\right)}{\Gamma\left(\frac{1-it\omega_c}{\beta\hbar\omega_c}+1\right)\Gamma\left(\frac{1+it\omega_c}{\beta\hbar\omega_c}+1\right)}\right].\end{aligned} \tag{2.22}$$

Taking the limit $\beta\hbar\omega_c \to \infty$ (i.e, upper cut-off frequency large compared to the bath temperature), we have

$$\frac{\Gamma^2\left(\frac{1}{\beta\hbar\omega_c}+1\right)}{\Gamma\left(\frac{1-it\omega_c}{\beta\hbar\omega_c}+1\right)\Gamma\left(\frac{1+it\omega_c}{\beta\hbar\omega_c}+1\right)} \to \frac{\beta\hbar}{\pi t}\sinh\left(\frac{\pi t}{\beta\hbar}\right). \tag{2.23}$$

With approximation (2.23), Eq. (2.21) becomes

$$\begin{aligned}|n(t)\rangle\langle n'(t)| = |n\rangle\langle n'|\exp\Bigg[&-i\Omega(n-n')t\\ &+i\frac{C\Omega^2}{\pi}(n-n')(n+n'+1)\left[\omega_c t-\tan^{-1}(\omega_c t)\right]\\ &-\frac{C\Omega^2}{\pi}(n-n')^2\left(\frac{1}{2}\ln\left(1+t^2\omega_c^2\right)+\ln\left[\frac{\beta\hbar}{\pi t}\sinh\left(\frac{\pi t}{\beta\hbar}\right)\right]\right)\Bigg].\end{aligned} \tag{2.24}$$

We now discuss the various terms appearing in Eq. (2.24). First, note that the outer product is time-independent for $n = n'$, a consequence of the fact that the system oscillator Hamiltonian commutes with the system-bath interaction Hamiltonian. The first, pure imaginary term $-i\Omega(n-n')t$ in the argument of the exponential is just the

free oscillator system evolution. The second pure imaginary term

$$i\frac{C\Omega^2}{\pi}(n-n')(n+n'+1)\left[\omega_c t-\tan^{-1}(\omega_c t)\right] \tag{2.25}$$

is upper cut-off dependent and comprises both a linear term in system number, which renormalizes the system oscillator frequency Ω, and a quadratic term in system number that is in fact of the same form as the free evolution of a Kerr nonlinear oscillator expressed in the number state basis:

$$H=\hbar\Omega a^\dagger a+\hbar\Lambda_{\rm kerr}(a^\dagger a)^2. \tag{2.26}$$

Thus, we should properly include a Kerr-type nonlinearity in our starting Hamiltonian (2.14), with the environmentally induced term $i\frac{C\Omega^2}{\pi}(n-n')(n+n')\omega_c t$ renormalizing the nonlinear interaction strength $\Lambda_{\rm kerr}$. The latter term may be thought of as somewhat analogous to the Newtonian gravitational self-interaction arising from the interaction of a matter system with its gravitating environment. Since we are primarily concerned with decoherence in this chapter, we will neglect the quadratic in number term, supposing that it renormalizes an existing Kerr nonlinearity with resulting negligible renormalized coupling strength $\Lambda_{\rm kerr}$. For $t\gg\omega_c^{-1}$, the $\tan^{-1}(\omega_c t)$ term in (2.25) tends to $\pi/2$; this term can be absorbed through a shift in the time coordinate: $t\to\tilde{t}=t-\pi/(2\omega_c)$.

Taking into account the system frequency and Kerr nonlinearity renormalizations as just described, Eq. (2.24) simplifies to

$$\begin{aligned}|n(t)\rangle\langle n'(t)| = |n\rangle\langle n'|\exp\Bigg(&-i\Omega(n-n')t\\&-\frac{C}{\pi}(n-n')^2\left(\frac{1}{2}\ln\left(1+t^2\omega_c^2\right)+\ln\left[\frac{\beta\hbar}{\pi t}\sinh\left(\frac{\pi t}{\beta\hbar}\right)\right]\right)\Bigg),\end{aligned} \tag{2.27}$$

where we have redefined the coupling constant as $C \to \tilde{C} = C\Omega^2$ and dropped the tilde. The real term on the second line of the argument of the exponential results in decoherence, i.e., exponential decay of the outer product for $n \neq n'$. In the high temperature (equivalently long time) limit corresponding to $t \gg \beta\hbar \gg \omega_c^{-1}$, Eq. (2.27) can be approximated asymptotically as

$$|n(t)\rangle\langle n'(t)| = |n\rangle\langle n'| \exp\left(- i\Omega(n-n')t - (n-n')^2 C \left[\frac{1}{\pi} \ln\left(\frac{\beta\hbar\omega_c}{2\pi} \right) + (\beta\hbar)^{-1} t \right] \right). \tag{2.28}$$

From Eq. (2.28), it is clear that the outer product terms for $n \neq n'$ decay exponentially with rate given by $(n-n')^2 C k_B T/\hbar$. Note however, that for early, 'Planckian' (by analogy with gravity) times $t \lesssim \omega_c^{-1}$, the rate of decoherence is governed by the upper cut-off ω_c, resulting in the logarithm term appearing in Eq. (2.28); depending on the magnitude of the ratio $\hbar\omega_c/k_B T \gg 1$, there may already be a significant 'burst' of decoherence during the 'Planckian' regime before the later, high temperature exponential decoherence regime. The fact that the decoherence rate depends on the upper cut-off frequency ω_c is a consequence of assuming an initial system-environment product state [41]. The latter assumption is tantamount to supposing that the system initial state can be prepared on time scales shorter than ω_c^{-1} (or equivalently, the system-environment interaction is switched on over a time scale shorter than ω_c^{-1}). While this may be possible for low energy, solid state system environments (i.e., phonons), for an actual gravitational environment with corresponding characteristic Planck time scale, the system state cannot be similarly isolated from the gravitational environment; an analysis which accounts for the system remaining correlated with the environment while its state is being prepared on timescales that are long compared with ω_c^{-1}, is expected to result in a subsequent decoherence rate that does not depend on the upper cut-off frequency of the environment.

2.3.2. Decoherence

In the following, we will use Eq. (2.27) to determine the decoherence dynamics of the oscillator system for initial coherent state superpositions of the form

$$\rho_{\text{init}} = N\left(|\alpha_1\rangle + |\alpha_2\rangle\right)\left(\langle\alpha_1| + \langle\alpha_2|\right) \otimes \rho_{\text{bath}}, \tag{2.29}$$

where $|\alpha_1\rangle$ and $|\alpha_2\rangle$ denote coherent states and N is the normalization constant. We consider coherent states since they describe most closely a cooled down, macroscopic oscillator center of mass system. We emphasise that we do not rely on any of the approximations that are often invoked in the study of open quantum system dynamics (beyond assuming an initial product state). In particular, the following analysis is valid for both short/long time scales and high/low temperatures.

Note from the form of (the exact) Eq. (2.27), that the system will evolve into a classical mixture of number states with probability coefficients that are identical to the coefficients of the initial system state. In contrast to other types of system-bath interaction where the final steady state of the system is usually temperature dependent, for the present model the temperature only determines how fast the system decoheres–not its long time limit steady state. From Eq. (2.27), we also see that the decoherence rate is proportional to $(n - n')^2$ for a superposition of two number states $|n\rangle$ and $|n'\rangle$. Thus, for a superposition of coherent states, we expect that the larger the average energy difference, the more rapid the decoherence. This trend is apparent in the oscillator system Wigner function [42] snapshots shown in Fig. 2.3. For the initial, example superposition state with $\alpha_1 = 3$, $\alpha_2 = -7$, the negative Wigner function regions disappear in the long time limit (signifying loss of quantum coherence). On the other hand, for the initial example superposition states with nearby coherent state parameter magnitudes: $\alpha_1 = -\alpha_2 = 3$, $\alpha_1 = 3$ and $\alpha_2 = -5$,

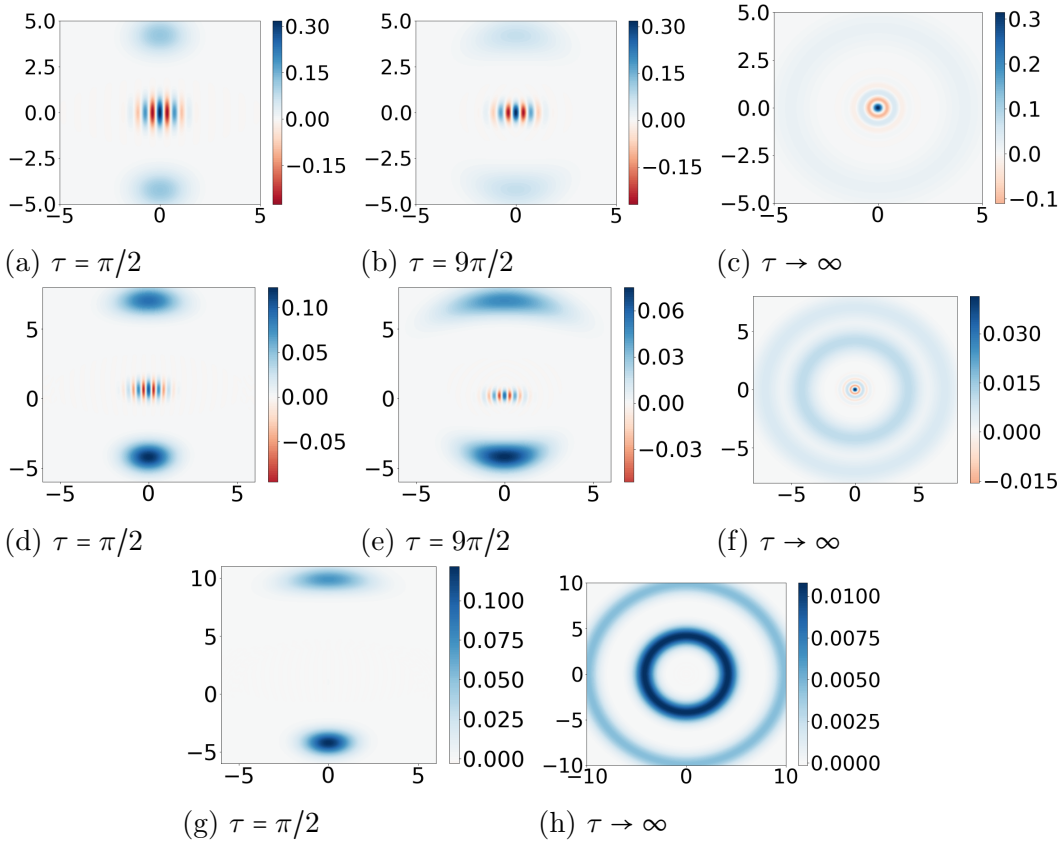

Figure 2.3: Wigner function snapshots at different times $\tau = \Omega t$ for the oscillator system. The horizontal coordinate is the dimensionless position $x\sqrt{M\Omega/\hbar}$ and the vertical coordinate is the dimensionless momentum $p/\sqrt{M\Omega\hbar}$. Example coherent state parameters are (a)-(c) $\alpha_1 = 3$, $\alpha_2 = -3$; (d)-(f) $\alpha_1 = 3$, $\alpha_2 = -5$; (g), (h) $\alpha_1 = 3$, $\alpha_2 = -7$. Other fixed system-bath parameters are: $\beta\hbar\Omega = 1$, $\omega_c/\Omega = 10^3$, $C/\pi = 0.001$.

negative Wigner function regions remain in the long time limit (signifying remaining quantum coherence), as is seen more clearly for the zoomed-in Fig. 2.4. Such trends are consistent with decoherence only resulting for initial spatial superpositions where the states making up the superposition have sufficiently distinct average energies; initial spatial superpositions with the same (or nearby) average energies for the states making up the superposition do not completely decohere. Note also from the Wigner function snapshots in Fig. 2.3 and Fig. 2.4 that the initial coherent superpositions phase-diffuse first into crescent-like regions and then eventually into rings. This is consistent with the fact that, as mentioned above, the final state is always a mixture

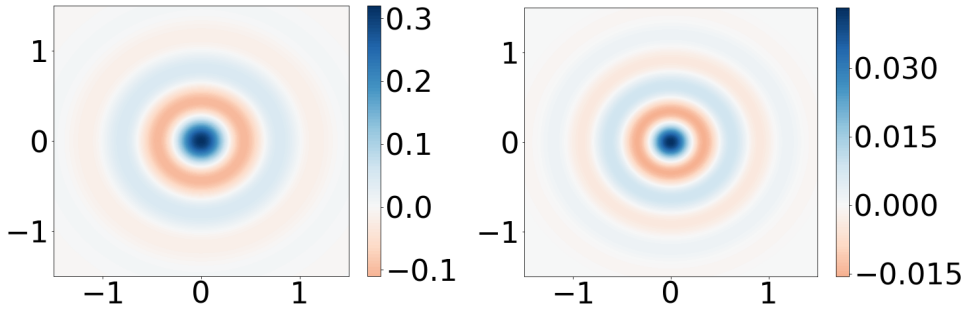

(a) $\tau \to \infty$ (b) $\tau \to \infty$

Figure 2.4: Zoomed-in snapshots of the Wigner function: (a) $\alpha_1 = -\alpha_2 = 3$; (b) $\alpha_1 = 3$, $\alpha_2 = -5$.

of number states.

The above findings are in accord with first investigations on the gravitational decoherence of massive scalar quantum field initial superposition states [12, 13], where it is found that superpositions comprising distinct energy states decohere.

Following from the discussion in Sec. 2.1, an operational way (i.e., in principle measurement procedure) to quantify the coherence is through the system oscillator position detection probability density $P(x,t) = \langle x|\rho(t)|x\rangle$ [c.f. the full field-theoretic counterpart Eq. (2.6)] when the two (initially coherent) wavefunctions making up the superposition pass through each other at $x = 0$; these time instants are $\tau_n = \Omega t_n = \pi(n + 1/2)$, $n = 0, 1, 2, \ldots$ for the initial coherent state superposition examples considered above, as can be seen for the early time snapshots in Fig 2.3. The presence of coherence is manifested in $P(x,t)$ having an oscillatory dependence about $x = 0$. The latter operational approach corresponds to a two-slit inteference measurement, where the harmonic potential plays the role of the slits by (periodically) bringing the wavefunction components in the initial superposition together. Figure 2.5 shows the position probability distribution function in the long time limit, steady state for the various example initial coherent state superpositions; we can see that the probability density indicates interference fringes in the vicinity of $x = 0$ consistent with the

presence of negative-valued Wigner function regions shown in Fig. 2.3; the snapshots can be interpreted as the marginal probability distributions obtained by integrating over the momentum coordinate Wigner function distributions. In particular, the interference remains for $\alpha_1 \simeq -\alpha_2$, where the average energies of each coherent state making up the initial superposition are not too dissimilar. Note that the other, larger scale scale probability variations in Fig. 2.5 are due to the final, steady state being a mixture of different number states, as mentioned earlier above.

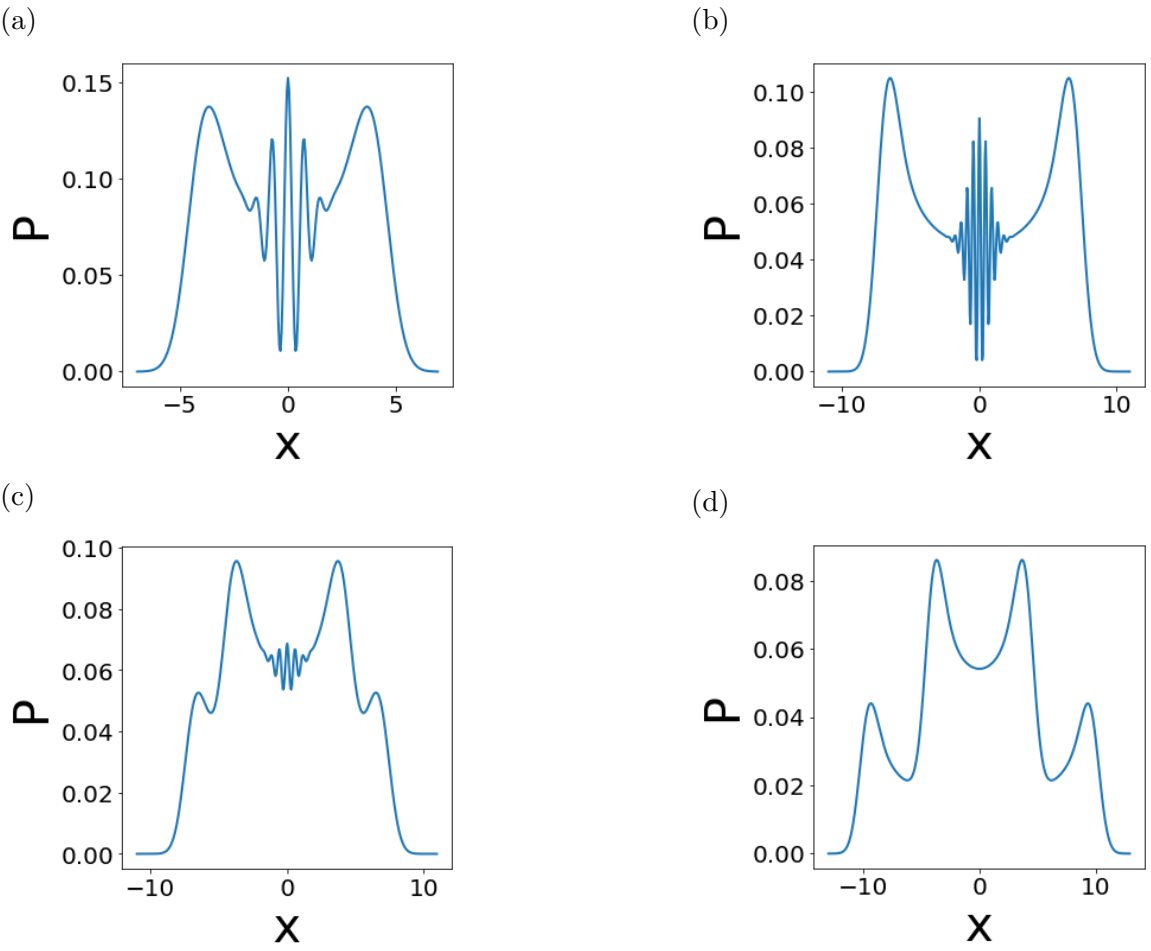

Figure 2.5: Snapshots of the (unnormalized) position probability density P versus the dimensionless position coordinate $x\sqrt{M\Omega/\hbar}$ in the long time limit, steady state; the probability density is specified up to an overall normalization constant. (a) $\alpha_1 = -\alpha_2 = 3$; (b) $\alpha_1 = -\alpha_2 = -5$; (c) $\alpha_1 = 3$ and $\alpha_2 = -5$; (d) $\alpha_1 = 3$ and $\alpha_2 = -7$. The system-bath parameters are: $\beta\hbar\Omega = 1$, $\omega_c/\Omega = 10^3$, $C/\pi = 0.001$.

We adopt the commonly used 'visibility' as a measure of the size of the interference fringes, defined as

$$\nu = \frac{P_{\max} - P_{\min}}{P_{\max} + P_{\min}}, \tag{2.30}$$

where $P_{\max}$ is the central maximum of the probability density $P(x)$ at $x = 0$, and $P_{\min}$ is the first local minimum of the probability to the right (or left) of the central maximum. The decrease in visibility over time starting from the initial superposition state (2.29), provides an operational, quantitative measure of decoherence; Fig. 2.6 gives the visibility as a function of time for various example, initial coherent state, bath temperature, and system-bath coupling parameters. As to be expected, the visibility decreases more rapidly the higher the temperature and the stronger the coupling. Also, the more dissimilar in magnitude $\alpha_2 < 0$ is from $\alpha_1 > 0$ (and hence the larger the average energy difference) in the initial coherent state superposition, the more rapid is the decrease in visibility.

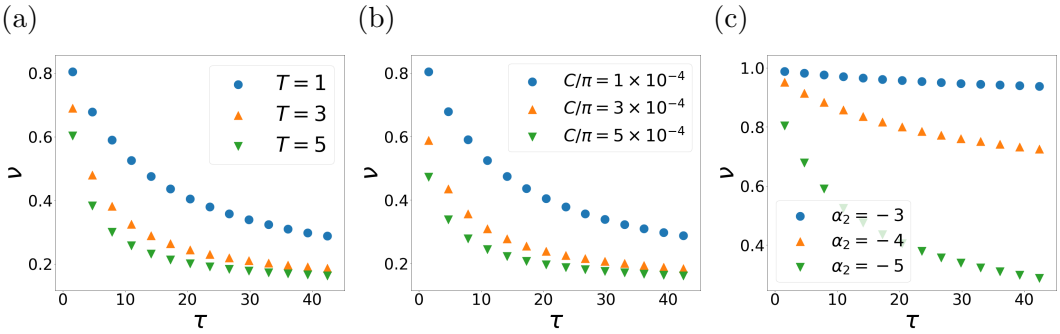

Figure 2.6: Visibility as a function of dimensionless time $\tau = \Omega t$. The example parameters are (a) $\alpha_1 = 3$, $\alpha_2 = -5$, $C/\pi = 0.0001$, with dimensionless temperature $k_B T/(\hbar\Omega)$; (b) $\alpha_1 = 3$, $\alpha_2 = -5$, $k_B T/(\hbar\Omega) = 1$; (c) $\alpha_1 = 3$, $C/\pi = 0.0001$, $k_B T/(\hbar\Omega) = 1$.

Section 2.4

Scalar QED model

In contrast to the scalar-gravity 0d toy model, the scalar QED toy model does not admit an exact, analytical solution for its quantum dynamics. We will therefore utilize various approximation methods towards solving for its quantum dynamics. In particular, we consider both quantum Langevin and master equation approaches, and approximations within these approaches that take advantage of the assumed weak system-bath interaction to show that the model maps onto the oscillator system with two-photon damping.

2.4.1. Classical Langevin equation

We start with the Lagrangian L_{qed} (2.9) and will first derive the Langevin equation that describes the classical oscillator system dynamics interacting with the oscillator bath following the approach of Ref. [43]. Expanding out the kinetic energy term of Eq. (2.9), we have

$$L = \frac{1}{2}M\dot{x}^2 - \frac{1}{2}M\Omega^2 x^2 + \sum_i \left(\frac{1}{2}m\dot{q}_i^2 - \frac{1}{2}m\omega_i^2 q_i^2\right) + M\lambda x\dot{x}\sum_i q_i + \frac{1}{2}M\lambda^2 x^2 \sum_{i,j} q_i q_j, \quad (2.31)$$

where we omit the 'qed' subscript from now on. The system and bath momentum coordinates are

$$p = \frac{\partial L}{\partial \dot{x}} = M\dot{x} + M\lambda x\sum_i q_i, \quad (2.32)$$

$$p_i = \frac{\partial L}{\partial \dot{q}_i} = m\dot{q}_i, \quad (2.33)$$

and the model Hamiltonian is

$$H = \frac{p^2}{2M} + \frac{1}{2}M\Omega^2 x^2 + \sum_i \left(\frac{p_i^2}{2m} + \frac{1}{2}m\omega_i^2 q_i^2 \right) - \lambda x p \sum_i q_i. \tag{2.34}$$

Hamiltonian (2.34) is to be compared with the gravity toy model Hamiltonian (2.13), which differs solely in the form of the system coordinate part of the interaction term; both models have in common a quadratic system coordinate coupling, to be contrasted with the usually studied oscillator system-oscillator bath model with interaction term that is linear in the coupled system and bath coordinates.

Hamilton's equations for the system and bath coordinates are

$$\dot{p}_i = -m\omega_i^2 q_i + \lambda x p, \tag{2.35}$$

$$\dot{q}_i = \frac{p_i}{m}, \tag{2.36}$$

$$\dot{p} = -M\Omega^2 x + \lambda p \sum_i q_i, \tag{2.37}$$

$$\dot{x} = \frac{p}{M} - \lambda x \sum_i q_i. \tag{2.38}$$

Formally integrating the equations of motion (2.35), (2.36) for the bath coordinates and expressing in terms of the system coordinates:

$$\begin{aligned} q_i(t) - \frac{\lambda x(t)p(t)}{m\omega_i^2} = &\left[q_i(0) - \frac{\lambda}{m\omega_i^2} x(0)p(0) \right] \cos\omega_i t + \frac{p_i(0)}{m\omega_i} \sin\omega_i t \\ &- \frac{\lambda}{m\omega_i^2} \int_0^t d\tau \cos\omega_i(t-\tau) \frac{d}{d\tau} \left(x(\tau)p(\tau) \right), \end{aligned} \tag{2.39}$$

where we have performed an integration by parts that allows to identify system renormalization and damping terms as we shall see below. Substituting the solution (2.39) for $q_i(t)$ into the equations of motion (2.37), (2.38) for the system coordinates leads

to the following non-linear Langevin equations:

$$\dot{x} = \frac{\partial H^m}{\partial p} + \lambda^2 x \int_0^\tau d\tau K(t-\tau)\frac{d}{d\tau}\left(x(\tau)p(\tau)\right) - \lambda x F(t), \tag{2.40}$$

$$\dot{p} = -\frac{\partial H^m}{\partial x} - \lambda^2 p \int_0^t d\tau K(t-\tau)\frac{d}{d\tau}\left(x(\tau)p(\tau)\right) + \lambda p F(t), \tag{2.41}$$

where the renormalized system Hamiltonian is

$$H^m = \frac{p^2}{2M} + \frac{1}{2}M\Omega^2 x^2 - \lambda^2 \sum_i \frac{1}{2m\omega_i^2} x^2 p^2, \tag{2.42}$$

the bath memory kernel is

$$K(t-\tau) = \sum_i \frac{1}{m\omega_i^2}\cos\omega_i(t-\tau), \tag{2.43}$$

and the bath random force function is

$$F(t) = \sum_i \left(\left[q_i(0) - \frac{\lambda}{m\omega_i^2} x(0)p(0) \right] \cos\omega_i t + \frac{p_i(0)}{m\omega_i}\sin\omega_i t \right). \tag{2.44}$$

In particular, the first term on the right hand side of the equals sign in the Langevin equations (2.40),(2.41) describes the Hamiltonian evolution, the second term describes nonlinear damping, and the third term the random force. Note that the bath induces a quartic anharmonic potential in the system Hamiltonian (2.42). Such a term is analogous to a Coulomb self-interaction potential in the scalar QED field system. After making the rotating wave approximation (RWA), the interaction term reduces to a Kerr-type nonlinearity [c.f. Eq. (2.26)]. Together with 'two-photon' damping [see Eq. (2.71) below], the resulting open system quantum dynamics can generate quantum states with negative-valued Wigner function regions in the long-time limit, starting from initial Gaussian states [44]. In the following, with decoherence dynamics

our main subject of interest, we will neglect this induced potential energy term, supposing that it renormalizes an existing anharmonic potential with resulting negligible renormalized coupling strength.

Assuming a thermal equilibrium canonical ensemble distribution for the initial bath coordinates $q_i(0), p_i(0)$ in Eq. (2.44), it can be shown that the fluctuation dissipation relation (FDR) between the memory kernel and the random force follows:

$$\langle F(t)F(\tau)\rangle = k_B T K(t-\tau), \tag{2.45}$$

where k_B is Boltzmann's constant and T is the bath temperature. We shall assume that the bath responds rapidly on the time-scale of the system oscillator dynamics, so that memory kernel is approximated as $K(t-\tau) = k_0\delta(t-\tau)$, where k_0 is a constant. The Langevin equations (2.40), (2.41) then become

$$\dot{x} = \frac{p}{M} + \frac{1}{2}\lambda^2 k_0 x \frac{d}{dt}(xp) - \lambda x F, \tag{2.46}$$

$$\dot{p} = -M\Omega^2 x - \frac{1}{2}\lambda^2 k_0 p \frac{d}{dt}(xp) + \lambda p F, \tag{2.47}$$

with the FDR (2.45) taking the form

$$\langle F(t)F(\tau)\rangle = k_B T k_0 \delta(t-\tau). \tag{2.48}$$

The above delta function-approximated memory kernel can be obtained from a bath spectral density $n(\omega)$ with upper cut-off frequency ω_c in the limit $\omega_c \to \infty$. In particular, for a dense bath spectrum, we can approximate the sum over bath degrees of freedom with a bath spectral frequency integral:

$$\sum_i (\cdots) \to \int_0^\infty d\omega n(\omega)\,(\cdots)\,. \tag{2.49}$$

Assuming a Lorentzian spectral density

$$n(\omega) = \frac{mk_0}{\pi}\frac{\omega^2\omega_c^2}{\omega^2+\omega_c^2}, \tag{2.50}$$

the memory kernel (2.43) then becomes

$$K(t-\tau) = \frac{k_0\omega_c}{2}e^{-\omega_c|t-\tau|}. \tag{2.51}$$

Taking the infinite limit $\omega_c \to +\infty$, we obtain the above delta function-approximated memory kernel:

$$\lim_{\omega_c\to+\infty} K(t-\tau) = k_0\delta(t-\tau). \tag{2.52}$$

Note that we could equally well have assumed a spectral density with exponential cut-off function instead, as for the gravity toy model [c.f. Eq. (2.20)]; while the calculations are somewhat more straightforward for the Lorentzian spectral density, we do not expect any qualitative differences in the resulting system quantum dynamics. The motivation to use the Lorentzian spectral density here is purely calculational convenience. The classical, non-linear Langevin equations (2.46), (2.47) can be numerically solved as stochastic differential equations as we show in the following sections when comparing with the corresponding quantum dynamics.

2.4.2. Quantum Langevin equation

The quantum description is obtained through the correspondence principle where x, p and p_i, q_i become operators satisfying the canonical commutation relations:

$$[x,p] = i\hbar,\ [x_i,p_j] = i\hbar\delta_{ij}, \tag{2.53}$$

with all other commutators vanishing. From Eq. (2.34), the quantum Hamiltonian operator is

$$H = \frac{p^2}{2M} + \frac{1}{2}M\Omega^2 x^2 + \sum_i \left(\frac{p_i^2}{2m} + \frac{1}{2}m\omega_i^2 q_i^2 \right) - \frac{\lambda}{2}\sum_i q_i(xp + px), \tag{2.54}$$

where the interaction term on the second line is symmetrized in x and p in order that H is Hermitian. Formally integrating Heisenberg's equations of motion for the bath operators, we obtain the following quantum Langevin equations for the system position and momentum operators:

$$\begin{aligned} \dot{x} = & \frac{p}{M} - \lambda^2 \sum_i \frac{1}{2m\omega_i^2} x\,(xp + px) \\ & + \lambda^2 x \sum_i \int_0^\tau d\tau \frac{\cos\omega_i(t-\tau)}{2m\omega_i^2} \frac{d}{d\tau}\,(xp + px) - \lambda F(t) x, \end{aligned} \tag{2.55}$$

$$\begin{aligned} \dot{p} = & -M\Omega^2 x + \lambda^2 \sum_i \frac{1}{2m\omega_i^2} p\,(xp + px) \\ & - \lambda^2 p \sum_i \int_0^\tau d\tau \frac{\cos\omega_i(t-\tau)}{2m\omega_i^2} \frac{d}{d\tau}\,(xp + px) + \lambda F(t) p, \end{aligned} \tag{2.56}$$

where the force noise operator is given by Eq. (2.44) with the system/bath coordinates and momenta replaced by their corresponding operators. It is convenient to express the quantum Langevin equations in terms of the system creation and annihilation operators which are defined through the usual relations $x = \sqrt{\frac{\hbar}{2M\Omega}}(a + a^\dagger)$, $p = i\sqrt{\frac{M\Omega\hbar}{2}}(a^\dagger - a)$:

$$\begin{aligned} \dot{a} = & -i\Omega a - \frac{i\hbar\lambda^2}{2} \sum_i \frac{1}{m\omega_i^2} a^\dagger \left(a^{\dagger 2} - a^2 \right) - \lambda F(t) a^\dagger \\ & + \frac{i\hbar\lambda^2}{2} a^\dagger \sum_i \int_0^t d\tau \frac{\cos\omega_i(t-\tau)}{m\omega_i^2} \frac{d}{d\tau} \left(a^{\dagger 2} - a^2 \right). \end{aligned} \tag{2.57}$$

Under conditions of weak system-environment coupling, Eq. (2.57) can be simplified by applying the RWA as we now show. Making the substitution $a(t) = A(t)e^{-i\Omega t}$ in Eq. (2.57), we obtain

$$\begin{aligned}\dot{A} = &-\frac{i\hbar\lambda^2}{2}\sum_i \frac{1}{m\omega_i^2}A^\dagger\left(e^{4i\Omega t}A^{\dagger 2} - A^2\right)\\ &+\frac{i\hbar\lambda^2}{2}A^\dagger e^{2i\Omega t}\sum_i\int_0^t d\tau\frac{\cos\omega_i(t-\tau)}{m\omega_i^2}\frac{d}{d\tau}\left(A^{\dagger 2}e^{2i\Omega\tau} - A^2e^{-2i\Omega\tau}\right) - \lambda e^{2i\Omega t}F(t)A^\dagger.\end{aligned} \tag{2.58}$$

Dropping fast rotating terms, neglecting time derivatives of $A(\tau)$ (since A evolves at much slower rates than Ω), and setting $A(\tau) = A(t)$ (Markov approximation), Eq. (2.58) becomes approximately

$$\begin{aligned}\dot{A} = &\frac{i\hbar\lambda^2}{2}\sum_i\frac{1}{m\omega_i^2}A^\dagger A^2 - \lambda e^{2i\Omega t}F(t)A^\dagger\\ &-\hbar\Omega\lambda^2\sum_i\int_0^t d\tau\frac{\cos\omega_i(t-\tau)}{m\omega_i^2}e^{2i\Omega(t-\tau)}A^\dagger(t)A(t)^2.\end{aligned} \tag{2.59}$$

Utilizing the Lorentzian spectral density (2.50), Eq. (2.59) becomes

$$\dot{A} = \frac{i\gamma\omega_c}{2\Omega}A^\dagger A^2 - \frac{\gamma\omega_c}{\omega_c - 2i\Omega}A^\dagger A^2 - \lambda e^{2i\Omega t}F(t)A^\dagger, \tag{2.60}$$

where we have dropped fast oscillating terms and where $\gamma = \hbar\Omega\lambda^2 k_0/2$. For $\omega_c \gg \Omega$ and neglecting the anharmonic interaction term, Eq. (2.60) simplifies to

$$\dot{A} = -\gamma A^\dagger A^2 - \lambda e^{2i\Omega t}F(t)A^\dagger. \tag{2.61}$$

Defining the noise operator as

$$b(t) = \frac{-\lambda e^{2i\Omega t}F(t)}{2\sqrt{\gamma}} \tag{2.62}$$

and utilizing Eqs. (2.44), (2.50) and the RWA, the usual noise operator (anti)commutation rules follow:

$$\begin{aligned}[b(t), b^\dagger(t')] &= \delta(t-t'),\\ \{b(t), b^\dagger(t')\} &= \delta(t-t')\big[2n(2\Omega)+1\big],\end{aligned} \tag{2.63}$$

where the Bose-Einstein thermal average occupation number is evaluated at twice the system oscillator frequency: $n(2\Omega) = \left(e^{2\hbar\Omega/k_BT}-1\right)^{-1}$. Finally, transforming back to the non-rotating frame, $A(t) = a(t)e^{i\Omega t}$, we obtain our desired, RWA quantum Langevin equation:

$$\dot{a} = -i\Omega a - \gamma a^\dagger a^2 + 2\sqrt{\gamma}e^{-2i\Omega t}ba^\dagger. \tag{2.64}$$

From Eq. (2.64), we see that the parameter γ has the dimensions of inverse time and characterizes the strength of a nonlinear damping term, while the third term is the nonlinear force noise operator. Equation (2.64) can be solved numerically as a quantum stochastic differential equation or approximately by first deriving the equations for the various moments in a, b, and their Hermitian conjugates and truncating at some order.

2.4.3. Quantum master equation

An alternative way to express the quantum dynamics is via the quantum master equation, where the time evolution is given by the oscillator system reduced density matrix. To second order in the interaction potential and assuming that the bath responds much more rapidly than the system oscillation timescale (Born-Markov approximation), the master equation for system density matrix ρ in the interaction picture is approximately [23, 24, 25],

$$\frac{d\rho}{dt} = -\frac{1}{\hbar^2}\int_0^t dt' \mathrm{Tr}_B\left[V(t),\left[V(t'),\rho(t)\otimes\rho_B\right]\right], \tag{2.65}$$

where ρ_B is the initial thermal state of the bath, Tr_B denotes the trace over the bath state and $V(t)$ is the system-bath interaction Hamiltonian expressed in the interaction picture:

$$\begin{aligned} V(t) &= \frac{i\hbar\lambda}{2}\sum_i \sqrt{\frac{\hbar}{2m\omega_i}} e^{iH_0 t}\left(b_i^\dagger + b_i\right)\left(a^{\dagger 2} - a^2\right)e^{-iH_0 t} \\ &= \frac{i\hbar\lambda}{2}\sum_i \sqrt{\frac{\hbar}{2m_i\omega_i}}\left(b_i^\dagger e^{i\omega_i t} + b_i e^{-i\omega_i t}\right)\left(a^{\dagger 2}e^{2i\Omega t} - a^2 e^{-2i\Omega t}\right). \end{aligned} \tag{2.66}$$

In order to simplify the next steps, we introduce the following shorthand notation:

$$\mathcal{A}(t) = a^{\dagger 2}e^{2i\Omega t} - a^2 e^{-2i\Omega t} \tag{2.67}$$

$$\mathcal{B}(t) = \sum_i \sqrt{\frac{\hbar}{2m\omega_i}}\left(b_i^\dagger e^{i\omega_i t} + b_i e^{-i\omega_i t}\right). \tag{2.68}$$

Expanding out Eq. (2.65) and substituting in Eqs. (2.67) and (2.68), we obtain:

$$\begin{aligned} \frac{d\rho}{dt} = \frac{\lambda^2}{4}\int_0^t dt' \{&\left[\mathcal{A}(t)\mathcal{A}(t')\rho - \mathcal{A}(t')\rho\mathcal{A}(t)\right]\langle\mathcal{B}(t)\mathcal{B}(t')\rangle \\ &+ \left[\rho\mathcal{A}(t')\mathcal{A}(t) - \mathcal{A}(t)\rho\mathcal{A}(t')\right]\langle\mathcal{B}(t')\mathcal{B}(t)\rangle\}, \end{aligned} \tag{2.69}$$

where

$$\langle\mathcal{B}(t)\mathcal{B}(t')\rangle = \sum_i \frac{\hbar}{2m\omega_i}\left[(n(\omega_i)+1)e^{-\omega_i(t-t')} + n(\omega_i)e^{i\omega_i(t-t')}\right]. \tag{2.70}$$

Using the bath spectral density (2.50) and applying the RWA, we obtain the following quantum master equation:

$$\frac{d\rho}{dt} = i\Omega[\rho, a^\dagger a] + \frac{\gamma}{2}(n+1)\left([a^2\rho, a^{\dagger 2}] + [a^2, \rho a^{\dagger 2}]\right) + \frac{\gamma}{2}n\left([a^{\dagger 2}\rho, a^2] + [a^{\dagger 2}, \rho a^2]\right), \tag{2.71}$$

where $n = n(2\Omega) = \left(e^{2\hbar\Omega/k_BT} - 1\right)^{-1}$. In Eq. (2.71), we recognize an oscillator subject to 'two-photon' damping.

As a consistency check, we can obtain an equation for the expectation value of a starting either from the quantum Langevin equation (2.64) with $\langle a\rangle = \mathrm{Tr}\left(a(t)\rho(0)\right)$ or from the master equation (2.71) with $\langle a\rangle = \mathrm{Tr}\left(a(0)\rho(t)\right)$; both approaches coincide to give

$$\langle \dot{a}\rangle = -i\Omega\langle a\rangle - \gamma\langle a^\dagger a^2\rangle + 2\gamma n(2\Omega)\langle a\rangle. \tag{2.72}$$

2.4.4. Validity of the RWA and quantum vs classical dynamics

Starting with the 0d analogue scalar QED model Lagrangian (2.9), in the previous sections we derived a Markov approximated classical Langevin equation (2.46), (2.47), a Markov-RWA quantum Langevin equation (2.64), and a corresponding Markov-RWA quantum master equation (2.71). In the following, we will test the validity of the RWA at the classical level, as well as compare the classical versus RWA quantum dynamics for the averaged quantities $\langle a\rangle$ and $\langle a^\dagger a\rangle$.

It is convenient to express the classical Langevin equations (2.46), (2.47) in terms of the complex coordinates (a, a^*) corresponding to the quantum annihilation/creation operators:

$$\dot{a} = -i\Omega a + \frac{i\gamma}{2\Omega}\frac{d}{dt}(a^*a^* - aa)a^* - \sqrt{\frac{2\gamma}{\hbar\Omega}}\tilde{F}a^*, \tag{2.73}$$

where $\tilde{F} = F/\sqrt{k_0}$, so that $\langle \tilde{F}(t)\tilde{F}(\tau)\rangle = k_BT\delta(t-\tau)$. The corresponding classical RWA Langevin equation is [c.f. Eq. (2.64)]:

$$\dot{a} = -i\Omega a - \gamma a^2 a^* - \sqrt{\frac{2\gamma}{\hbar\Omega}}\tilde{F}a^*. \tag{2.74}$$

In order to solve the non-RWA (2.73) and RWA (2.74) Langevin equations, we treat

them as classical stochastic differential equations:

$$da = -i\Omega a dt + \frac{i\gamma}{2\Omega}\frac{d}{dt}(a^* a^* - aa)a^* dt - \sqrt{\frac{2\gamma k_B T}{\hbar\Omega}}a^* dW, \tag{2.75}$$

$$da = -i\Omega a dt - \gamma a^2 a^* dt - \sqrt{\frac{2\gamma k_B T}{\hbar\Omega}}a^* dW, \tag{2.76}$$

where W is the standard Wiener process, i.e., a continuous-time random walk [45]. Figures 2.7 and 2.8 give numerical solutions to these classical stochastic equations as well as to the quantum master equation (2.71) (the latter solved using QuTiP [46]) for a range of damping parameters γ and bath temperatures T. These parameters are respectively expressed in terms of the dimensionless $Q = \Omega/\gamma$ factor and thermal average bath occupation number n. The quantum system is initially in a coherent state $|\alpha\rangle$ for which $a|\alpha\rangle = \alpha|\alpha\rangle$, while the corresponding classical system is given an initial amplitude $a(0) = \alpha$, in order to allow a direct comparison between the quantum and classical dynamics. From Fig. 2.7, it can be seen that increasing n and Q^{-1} both lead to faster decay of the amplitude, signalling the non-linear nature of the damping and noise terms in the system Langevin and quantum master equations. It can also be seen that the difference between non-RWA, RWA and classical vs quantum is barely visible with the chosen parameters. However, such differences clearly show up in Fig. 2.8 where we consider the time evolution of the average system number $\langle a^\dagger a\rangle$. In particular, throwing away fast rotating terms due to the RWA results in smoothing of the oscillating behaviour of the non-RWA time evolution of $\langle a^\dagger a\rangle$. Furthermore, the quantum simulation of $\langle a^\dagger a\rangle$ decays faster than the corresponding classical approximation.

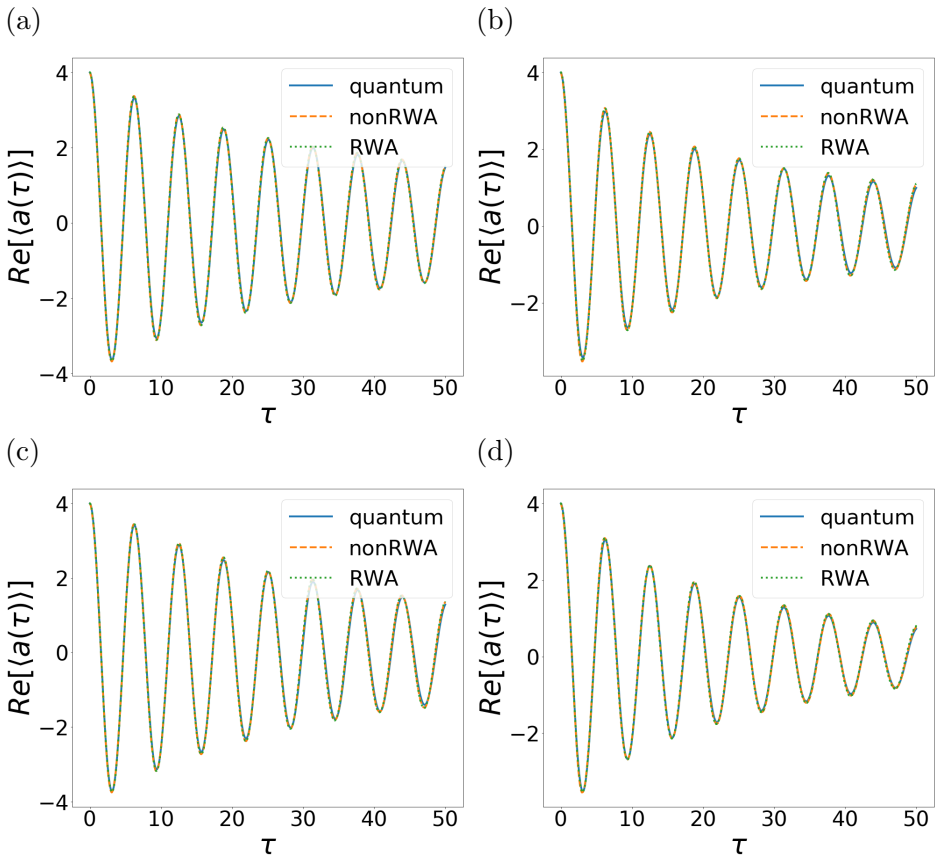

Figure 2.7: Plots of the dimensionless average position $\langle x\rangle\sqrt{M\Omega/(2\hbar)} = \mathrm{Re}\left[\langle a\rangle\right]$ as a function of dimensionless time $\tau = \Omega t$. The initial value $\alpha = a(0) = 4$ in each plot. The time evolution of the classical amplitude $a(t)$ is the result of averaging over 3000 stochastic trajectories. The example parameters are (a) $Q^{-1} = 0.003$, $n = 3$; (b) $Q^{-1} = 0.005$, $n = 3$; (c) $Q^{-1} = 0.003$, $n = 5$; (d) $Q^{-1} = 0.005$, $n = 5$.

2.4.5. Decoherence

In the following, we consider the evolution of system oscillator initial coherent state superpositions of the form

$$|\psi(0)\rangle = N\left(|\alpha\rangle + |-\alpha\rangle\right), \tag{2.77}$$

where N is a normalization constant. Figure 2.9 displays the evolving state through its Wigner function representation [42] for a selection of α, n, and Q parameter values–obtained by numerically solving the master equation (2.71). Quantum co-

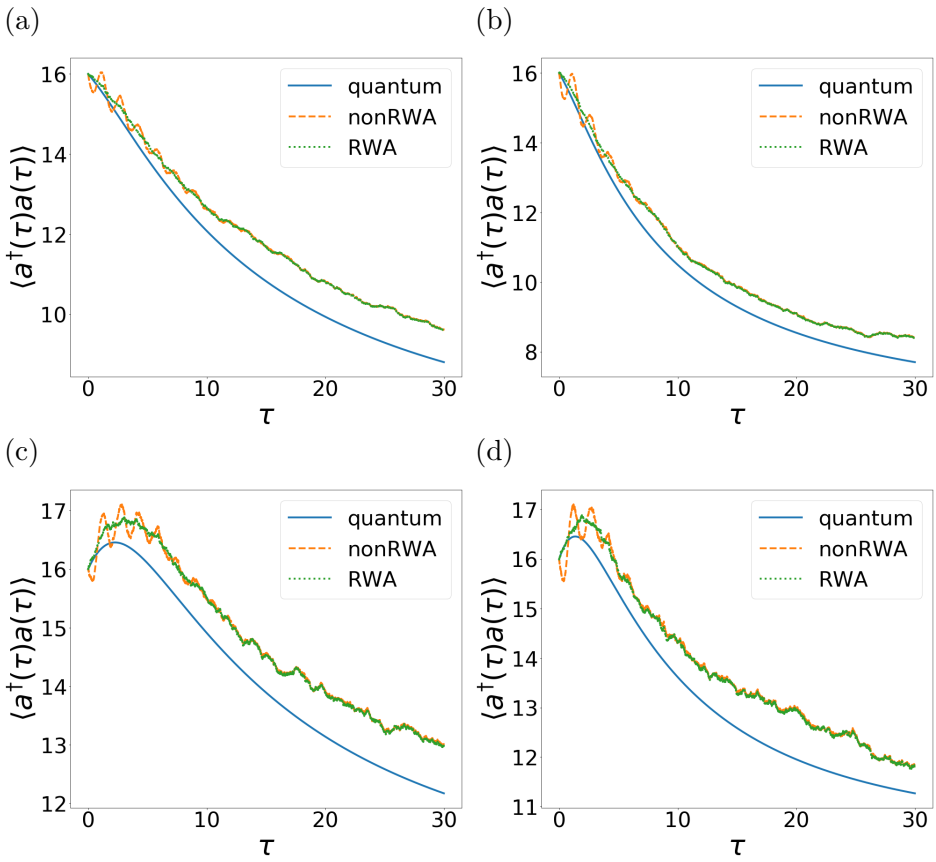

Figure 2.8: Plots of the average system number $\langle a^\dagger a\rangle$ as a function of dimensionless time $\tau = \Omega t$. The initial value $\alpha = a(0) = 4$ in each plot. The time evolution of the classical absolute amplitude squared $a(t)a^*(t)$ is the result of averaging 5000 stochastic trajectories. The example parameters are (a) $Q^{-1} = 0.003$, $n = 3$; (b) $Q^{-1} = 0.005$, $n = 3$; (c) $Q^{-1} = 0.003$, $n = 5$; (d) $Q^{-1} = 0.005$, $n = 5$.

herence manifested in the presence of negative-valued Wigner function regions can survive longer than the amplitude damping time. This is to be contrasted with the commonly-investigated quantum Brownian oscillator model with single photon damping, described by the following master equation:

$$\frac{d\rho}{dt} = i\Omega[\rho, a^\dagger a] + \frac{\gamma}{2}(n+1)\left(2a\rho a^\dagger - a^\dagger a\rho - \rho a^\dagger a\right) + \frac{\gamma}{2}n\left(2a^\dagger \rho a - aa^\dagger\rho - \rho aa^\dagger\right). \tag{2.78}$$

For the latter master equation, decoherence proceeds more rapidly than amplitude damping. Note that the initial, even superposition state (2.77) is an eigenstate of the

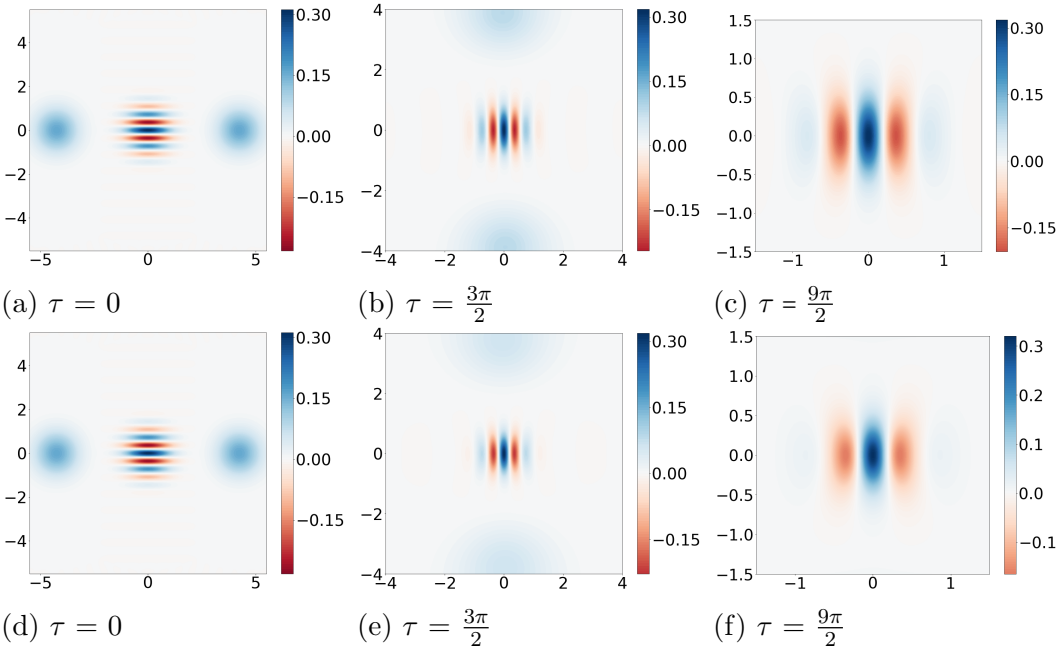

(a) $\tau = 0$ (b) $\tau = \frac{3\pi}{2}$ (c) $\tau = \frac{9\pi}{2}$

(d) $\tau = 0$ (e) $\tau = \frac{3\pi}{2}$ (f) $\tau = \frac{9\pi}{2}$

Figure 2.9: Wigner function snapshots at different times. Horizontal coordinate is for dimensionless position $x\sqrt{M\Omega/\hbar}$ and vertical coordinate is for dimensionless momentum $p/\sqrt{M\Omega\hbar}$. The example parameters are (a), (b) and (c): $\alpha = 3$, $n = 3$ and $Q^{-1} = 0.001$; (d), (e) and (f): $\alpha = 3$, $n = 5$ and $Q^{-1} = 0.001$.

operator a^2 since $a^2|\pm\alpha\rangle = \alpha^2|\pm\alpha\rangle$, so that the two-photon loss term in the master equation (2.71) preserves coherence [38]. In contrast, the even superposition state (2.77) flips to the odd superposition state $N(|\alpha\rangle - |-\alpha\rangle)$ under the action of a single annihilation operator a, hence the single photon loss term in the master equation (2.78) does not preserve coherence.

Figure 2.10 gives snapshots of the system oscillator position probability density $P(x,t) = \langle x|\rho(t)|x\rangle$ when the two initial coherent state wavefunctions making up the superposition pass through each other at $x = 0$ (at time instants $\tau_k = \Omega t_k = \pi(k+1/2)$, $k = 0, 1, 2, \ldots$). These snapshots can be interpreted as the marginal probability distributions obtained by integrating over the momentum coordinate of Wigner function distributions that are similar to those shown in Fig. 2.9 (but for different parameter values). The presence of quantum coherence is manifested in $P(x,t)$ having an oscillatory dependence about $x = 0$. In contrast to the gravity toy model (c.f.,

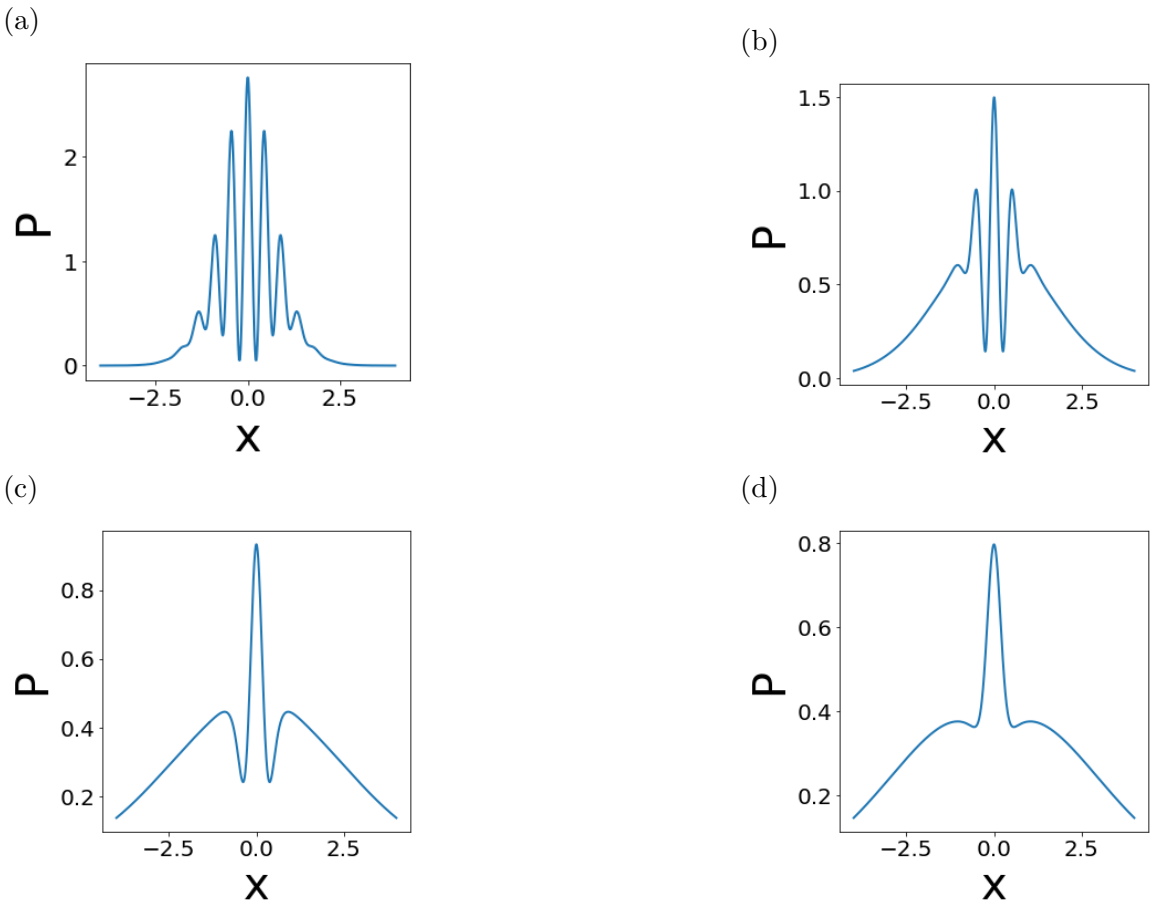

Figure 2.10: Snapshots of the (unnormalized) position probability density P vs dimensionless position coordinate $x\sqrt{M\Omega/\hbar}$ when the two initial coherent states in the superposition pass through each other at $x = 0$ at times (a) $\tau = \pi/2$, (b) $\tau = (6 + 1/2)\pi/2$, (c) $\tau = (42 + 1/2)\pi/2$ and (d) $\tau = (190 + 1/2)\pi/2$. The example parameters are $Q^{-1} = 0.0005$, $\alpha = 5$, and $n = 3$. The probability density should be understood with an overall normalization constant.

Fig. 2.5), the interference fringes survive longer than the initial coherent state peaks; even after 190 cycles a small amount of interference is still present, while the initial coherent states have decayed away.

Proceeding as in Sec. 2.3.2 for the scalar gravity model, We can operationally quantify the decoherence of an initial superposition of coherent states by using the fringe visibility measure ν (2.30) for the position detection probability density. Figure 2.11 shows the time dependence of the visibility ν for a range of parameter choices.

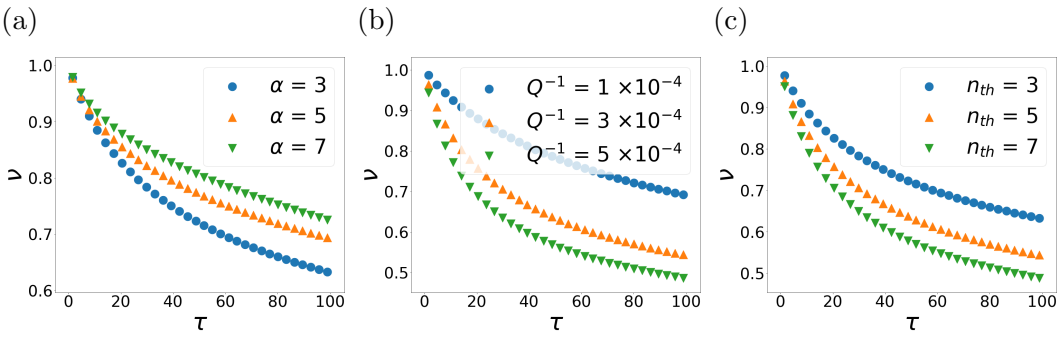

Figure 2.11: Visibility as a function of dimensionless time $\tau = \Omega t$. The example parameters are (a) $Q^{-1} = 0.0003$, $n = 3$; (b) $\alpha = 3$, $n = 5$; (c) $Q^{-1} = 0.0003$, $\alpha = 3$.

The rate at which the visibility is reduced increases with larger damping parameter and bath temperature as for the single photon damping case with master equation (2.78), but contrary to single photon damping the visibility reduction rate decreases with larger initial amplitude.

Section 2.5

Concluding Remarks

In this chapter, we have explored two 0d system-bath models that share common features with a scalar field system weakly coupled to gravity, and also with scalar QED. The considered model systems comprise a single harmonic oscillator, with the gravitational and electromagnetic fields replaced by a bath of harmonic oscillators, in each case coupled to the oscillator system via non-quadratic interaction terms that resemble the respective scalar-weak field gravity and scalar QED interactions. We utilized these models as a test bed for an operational interference fringe visibility measure of decoherence, as well as for various standard open quantum systems approximation methods.

In particular, we have gained several insights working with the two models that may be of use for analyzing gravitational decoherence: (1) A relatively straightfor-

ward, interferometric operational approach for verifying decoherence dynamics can be analyzed that does not involve just extracting the off-diagonal terms of the system reduced density matrix (which is not a gauge invariant quantity in the full theory). (2) While the full scalar matter-gravitational system likely cannot be solved exactly as is the case for the corresponding model system, verified standard open quantum systems approximation methods (e.g., deriving a RWA quantum Langevin equation) may be applicable to the full system; the more involved closed time path integral approaches that are commonly applied to such dynamical quantum field system problems [22] can be guided by the simpler approximation method approaches that are common to non-relativistic open quantum systems analyses. (3) 'Planckian', cut-off dependent terms can affect the initial decoherence dynamics. However, by being careful with the choice of initial system-environment state taking into account finite state preparation times, such cut-off dependence may be avoided.

The logical next step will be to apply the considered approximation methods to the scalar QED system, and verify that the interferometric observable quantities for probing decoherence are gauge invariant and accessible to analysis at low energy (i.e., 'table top' experiment) scales. We can then apply the lessons learned from the 0d models as well as the full scalar QED model to the scalar matter–weak gravity system. While the latter quantum field system is of course more challenging to analyze, the insights gained from this chapter might nevertheless serve as a useful guide in developing an operational understanding of gravitational decoherence, just as the 0d model (2.8) proved valuable for the initial field theoretic investigation in Ref. [12].

Chapter 3

Cavity mode dephasing via the optomechanical interaction with an acoustic environment

Section 3.1

Introduction

Cavity optomechanical systems have received considerable attention over the past decades, with applications ranging from the detection of classical gravity waves in the macroscopic domain to the generation and detection of quantum states of mechanical oscillators in the nano-to-mesoscale regimes [35, 47]. Most investigations deliberately consider one or at most a few cavity modes interacting similarly with one or at most a few mechanical modes, with notable exceptions including optomechanical interactions between multiple driven bosonic modes and multiple mechanical resonators [48], the consideration of interacting optical and acoustic waves coexisting in bulk, crystalline solids [49], and environment-induced, driven cavity photon blockade and Rabi oscillations via the optomechanical interaction [50].

In this chapter, we shall take as our starting point the following Hamiltonian:

$$H = \hbar\Omega\left(a^\dagger a + \frac{1}{2}\right)\left(1 + \sum_i \lambda_i\left(b_i + b_i^\dagger\right)\right) + \sum_{i=1}^{N}\hbar\omega_i\left(b_i^\dagger b_i + \frac{1}{2}\right), \tag{3.1}$$

where here a, $a^\dagger$ are the annihilation/creation operators for a cavity mode with frequency Ω, while the b_i, $b_i^\dagger$ are the annihilation/creation operators for N mechanical modes. The cavity and mechanical modes are coupled via the standard optomechanical interaction with coupling constant parameters $\hbar\Omega\lambda_i$. Our particular focus will be on the effective dynamics of the *single* cavity mode system interacting with *many* (i.e., $N \ggg 1$) mechanical modes, with the latter viewed as an acoustic, environmental bath for the cavity system. In contrast to the usual quantum Brownian motion model, where the system-bath coupling is bilinear in their respective creation/annihilation coordinates, Hamiltonian (3.1) does not result in energy damping of the cavity mode system. This is a consequence of the fact that the system Hamiltonian commutes

with the interaction Hamiltonian term. On the other hand, dephasing does result for initial superpositions of energy eigenstates of the cavity system; for this reason, Ref. [25] terms Eq. (3.1) the "phase damped oscillator", and provides a second order Born-Markov approximated solution to the cavity system reduced density matrix dynamics via a master equation approach.

As we shall show, the effective dynamics for the cavity system reduced density matrix can in fact be solved *exactly* up to a summation over bath modes, while the latter summation can be carried out approximately for certain bath spectral densities; the method of solution is based on that of Refs. [39, 40], which consider a single cavity mode interacting with a single mechanical mode, and which again utilizes the fact that the system and interaction term Hamiltonians commute.

Our interest in the Hamiltonian (3.1) and the resulting dephasing dynamics of the cavity mode system reduced state stems from its analogue connection with gravitationally induced decoherence as we discussed in the previous chapter [12, 51]. In the weak gravitational field regime, the leading order term in the interaction action involving a scalar matter field $\phi(x)$ system and gravitational metric deviation $h_{\mu\nu}$ from Minkowski space environment takes the form

$$S_I = \sqrt{8\pi G} \int d^4x T^{\mu\nu}(\phi) h_{\mu\nu} \tag{3.2}$$

in natural units $\hbar = c = 1$, where $T^{\mu\nu}(\phi)$ is the scalar field energy-momentum tensor. This interaction term can result in the dephasing of scalar field energy superposition states without energy damping [12, 13], just as for the cavity mode quantum dynamics following from Hamiltonian (3.1) [51]. Comparing the optomechanical interaction Hamiltonian in Eq. (3.1) with the matter-weak gravity interaction term action (3.2), the linearly coupled acoustic phonon field plays the role of the weak graviton field, while the quadratically coupled cavity mode plays the role of the scalar matter field.

As discussed in the previous chapter, exploring such optomechanical analogs may shed light on gravitationally induced dephasing dynamics of macroscopic matter field superposition states.

However, the cavity system dynamics following from the Hamiltonian (3.1) interpreted as modeling cavity optomechanical bath systems is of interest in its own right, particularly the consequences of the acoustic environment spatial dimension and size for the cavity mode energy quantum superposition dephasing dynamics. We shall find that for 1D and 2D elastic "string" and "membrane" acoustic environments respectively, the cavity system dephasing dynamics depends on the geometric size of the environment–a consequence of an infrared (IR) divergence in the limit as the environment size tends to infinity. In contrast, for a bulk, elastic 3D acoustic environment (which shares the same Ohmic spectral density as for the gravitational wave environment [12]), the cavity dephasing dynamics depends on the size of the optical cavity system embedded within the 3D elastic medium – a consequence of an ultraviolet (UV) divergence in the limit as the size of the cavity tends to zero, i.e., becomes pointlike.

Infrared divergences arising from long wavelength acoustic flexural modes of membrane like structures in the infinite size limit are also encountered in other contexts, for example the thermal expansion of 2D crystals [52] and atom–membrane surface interactions [53, 54, 55, 56, 57, 58].

In Sec. 3.2, we solve for the cavity system reduced density matrix evolution following from the time dependent Schrödinger equation with Hamiltonian (3.1) in the Fock state (i.e., photon number) basis for both ohmic ($s = 1$) and subohmic ($s = 0, -1$) bath spectral densities [see Eq. (3.6)], and with the oscillator environment in an initial thermal state. This section extends the analysis of the revious chapter, which considers only the Ohmic case and infinite-sized environment. In Sec. 3.3,

we consider a model cavity-acoustic environment optomechanical system realization involving a LC oscillator capacitively coupled to a partially metallized, long elastic strip and show how this system maps onto the subohmic $s = -1$ case; several details of the model strip derivation are given in Appendix A. Section 3.4 considers another model system consisting of an optical cavity interacting via light pressure with a large, square elastic membrane [36], which maps onto the subohmic $s = 0$ case; both Secs 3.3 and 3.4 explore quantitatively by considering example, experimentally feasible device parameter values, the cavity mode quantum dephasing dynamics dependence on the acoustic environment size, i.e., the elastic strip length and side dimension of the square membrane. Sec. 3.5 gives a concluding discussion.

Section 3.2

Cavity Dephasing Dynamics

Our starting point is the standard single cavity mode optomechanical Hamiltonian (3.1), but with a bath of mechanical oscillator modes labelled by the index $i = 0, 1, 2, \ldots, N \ggg 1$, instead of the usually considered single mode case [35]. Hamiltonian (3.1) neglects cavity-mechanical oscillator bath interaction terms of the form $a^2(b_i + b_i^\dagger)$ and $a^{\dagger 2}(b_i + b_i^\dagger)$, which describe for example two photons annihilating and creating a bath phonon ($a^2 b_i^\dagger$), or conversely a bath phonon annihilating and creating two cavity photons ($a^{\dagger 2} b_i$). As we shall see later below in Secs. 3.3 and 3.4, such terms can be neglected since the coupling constant λ_i is suppressed for phonon wavelengths much smaller than the cavity size.

We now briefly review the steps for solving the time-dependent Schrödinger equation with Hamiltonian (3.1) [39, 40, 51] as the detailed derivation is already discussed in the previous chapter. We assume that the cavity mode system can be prepared in an initial product state with the bath, the latter of which is assumed to be in a

thermal state: $\rho_{\text{initial}} = \rho_c \otimes \rho_{\text{bath}}$. The cavity system initial state is decomposed in terms of the Fock (i.e., number) state basis, $\rho_c = \sum_{n,n'} c_{nn'}|n\rangle\langle n'|$, and the thermal bath state expressed in a coherent state basis:

$$\rho_{\text{bath}} = \prod_i \frac{1}{\pi\left(e^{\beta\hbar\omega_i} - 1\right)} \int d\alpha_i^2 \exp\Big(- |\alpha_i|^2 \left(e^{\beta\hbar\omega_i} - 1\right)\Big)|\alpha_i\rangle\langle\alpha_i|, \tag{3.3}$$

where $\beta^{-1} = k_B T$, with k_B Boltzmann's constant and T the bath temperature. Solving first the Schrödinger equation for an initial basis state $|n, \{\alpha_i\}\rangle$ and then tracing out the bath, we obtain for the reduced state of the cavity mode: $\rho_c(t) = \sum_{n,n'} c_{nn'}|n(t)\rangle\langle n'(t)|$, where the time-dependent outer product is [51]

$$\begin{aligned} |n(t)\rangle\langle n'(t)| =& |n\rangle\langle n'| \exp\Bigg(- it\Bigg[\Omega(n-n') - (n+n'+1)(n-n')\sum_i \frac{(\Omega\lambda_i)^2}{\omega_i}\Bigg] \\ & - i(n+n'+1)(n-n')\sum_i \left(\frac{\Omega\lambda_i}{\omega_i}\right)^2 \sin(\omega_i t) \\ & - 2(n-n')^2 \sum_i \left(\frac{\Omega\lambda_i}{\omega_i}\right)^2 \coth\left(\frac{\beta\hbar\omega_i}{2}\right)\sin^2\left(\frac{\omega_i t}{2}\right)\Bigg). \end{aligned} \tag{3.4}$$

Note that this outer product is time-independent for $n = n'$, a consequence of the fact that the system oscillator Hamiltonian commutes with the system-bath interaction Hamiltonian.

We now discuss the various terms appearing in Eq. (3.4). The first imaginary term $-i\Omega(n-n')t$ in the argument of the exponential is just the free cavity oscillator system evolution. The second imaginary term gives rise to a cavity frequency renormalization $\Omega' = \Omega - \sum_i (\Omega\lambda_i)^2/\omega_i$ [from the $(n - n')$ part], as well as an induced Kerr nonlinear self-interaction [from the $(n^2 - n'^2)$ part] in the oscillator Hamiltonian:

$$H = \hbar\Omega a^\dagger a + \hbar\Lambda_{\text{kerr}}(a^\dagger a)^2, \tag{3.5}$$

where $\Lambda_{\text{kerr}} = -\sum_i (\Omega\lambda_i)^2/\omega_i$. The third imaginary term cancels the just-described second imaginary term in the short time limit $t \to 0$, while it decays to zero as t increases due to the oscillating sine term; later below, we give a more quantitative specification of the short and long time regimes. Finally, the fourth, real term in the argument of the exponential in Eq. (3.4) can result in dephasing, causing the off-diagonal terms of the system reduced density operator in the number state basis to decrease with increasing time.

In order to obtain a more quantitative understanding of the time dependent behavior of the various terms appearing in the outer product expression (3.4), we will approximate the discrete sum over the acoustic bath modes with a continuous frequency integral as follows:

$$\pi \sum_i \lambda_i^2 f(\omega_i) \approx C \int_{\omega_1}^{\infty} d\omega \omega^s f(\omega) e^{-\omega/\omega_u}, \tag{3.6}$$

where the function $f(\omega)$ is determined by the ω_i dependence of a given term in the argument of the exponential in Eq. (3.4) and C is a frequency-independent coupling strength constant; approximation (3.6) necessarily requires $N \ggg 1$ for a sufficiently dense bath frequency spectrum. Following common convention [59], we term optomechanical cavity-acoustic bath systems with exponent $s = 1$ "ohmic" and systems with exponent $s < 1$ "subohmic". The value of the exponent s is determined by the combined frequency dependences of the acoustic bath mode spectral density and of the optomechanical coupling λ_i. For the concrete example optomechanical model realizations in Secs. 3.3 and 3.4, we will see that the exponents $s = -1$ and $s = 0$ correspond to 1D and 2D acoustic environments, respectively.

Depending on the value of the exponent s and the form of $f(\omega)$, an upper cut-off function with some characteristic cut-off frequency ω_u may be required in order to regularize a possible UV divergence as $\omega \to \infty$. For the model realizations considered

in the following sections, an upper cut-off arises naturally through a suppression of the optical mode system-acoustic bath coupling when the acoustic phonon wavelength becomes smaller than a characteristic optical cavity system dimension. Note that the functional form of the upper cut-off dependences for these model examples is not in fact of the same exponential cut-off form as assumed in Eq. (3.6). Nevertheless, it is still informative to consider the commonly-used exponential cut-off since it readily allows closed form analytical expressions for the various summation terms appearing in Eq. (3.4) approximated as integrals.

Furthermore, a lower frequency cut-off, which we denote as $\omega_1 (\ll \omega_u)$ in Eq. (3.6), may be required depending on the value of the exponent s and form of the function $f(\omega)$, in order to regularize a possible IR divergence as $\omega \to 0$. For the model realizations considered in the following sections, a lower frequency cut-off arises naturally as the fundamental, lowest frequency mode ω_1 of the acoustic environment medium which has a finite size.

Using the integral approximation Eq. (3.6), the two imaginary, induced phase terms in Eq. (3.4) can be evaluated approximately analytically by expressing them in terms of the incomplete Gamma function $\Gamma(s,z) = \int_z^\infty dx x^{s-1}e^{-x}$:

$$\begin{aligned} & it(n+n'+1)(n-n')\sum_i \frac{\Omega^2\lambda_i^2}{\omega_i} \\ & \approx it(n+n'+1)(n-n')\frac{C\Omega^2}{\pi}\int_{\omega_1}^\infty d\omega\omega^{s-1}e^{-\omega/\omega_u} \\ & = it(n+n'+1)(n-n')\frac{C\Omega^2\omega_u^s}{\pi}\Gamma\left(s,\frac{\omega_1}{\omega_u}\right), \end{aligned} \tag{3.7}$$

and

$$\begin{aligned}
&-i(n+n'+1)(n-n')\sum_i \frac{\Omega^2\lambda_i^2}{\omega_i^2}\sin(\omega_i t)\\
&\approx -i(n+n'+1)(n-n')\frac{C\Omega^2}{\pi}\int_{\omega_1}^{\infty} d\omega\omega^{s-2}\sin(\omega t)e^{-\omega/\omega_u}\\
&=-i(n+n'+1)(n-n')\frac{C\Omega^2\omega_u^{s-1}}{\pi}\mathrm{Im}\left[(1-i\omega_u t)^{1-s}\Gamma\left(s-1,\frac{\omega_1}{\omega_u}(1-i\omega_u t)\right)\right]. \qquad (3.8)
\end{aligned}$$

The real, induced dephasing term in Eq. (3.4), with integral approximation (3.6), can only be expressed analytically in certain time range limits; we will consider the high temperature limit defined as $k_BT \gg \hbar/t$ (equivalently $t \gg \beta\hbar$), for which the coth function can be expanded to leading order. The dephasing term can then similarly be expressed approximately in terms of incomplete Gamma functions:

$$\begin{aligned}
&-2(n-n')^2\sum_i\left(\frac{\Omega\lambda_i}{\omega_i}\right)^2\coth\left(\frac{\beta\hbar\omega_i}{2}\right)\sin\left(\frac{\omega_i t}{2}\right)^2\\
&\approx -\frac{2C\Omega^2}{\pi}(n-n')^2\int_{\omega_1}^{\infty} d\omega\omega^{s-2}\coth\left(\frac{\beta\hbar\omega}{2}\right)\sin\left(\frac{\omega t}{2}\right)^2 e^{-\omega/\omega_u}\\
&\approx -\frac{2C\Omega^2}{\pi}(n-n')^2\int_{\omega_1}^{\infty} d\omega\omega^{s-2}\frac{2}{\beta\hbar\omega}\sin\left(\frac{\omega t}{2}\right)^2 e^{-\omega/\omega_u}\\
&=-\frac{2C\Omega^2}{\pi}(n-n')^2\frac{\omega_u^{s-2}}{\beta\hbar}\left\{\Gamma\left(s-2,\frac{\omega_1}{\omega_u}\right)-\mathrm{Re}\left[(1-i\omega_u t)^{2-s}\Gamma\left(s-2,\frac{\omega_1}{\omega_u}(1-i\omega_u t)\right)\right]\right\}.
\end{aligned} \qquad (3.9)$$

In the following three subsections, we shall explore the time dependences of Eqs. (3.8) and (3.9) for the values $s = 1, 0, -1$, respectively. With the presence of the two frequency scales ω_1 and ω_u ($\ggg \omega_1$), we have three different time range scales: the short time limit range $t \ll \omega_u^{-1}$, intermediate time range $\omega_u^{-1} \ll t \ll \omega_1^{-1}$, and the long time limit range $t \gg \omega_1^{-1}$. Note that the high temperature limit corresponds to requiring $k_BT \gg \hbar\omega_1$ for the intermediate time range. We shall focus below on the intermediate and long time ranges, deriving analytical approximations to the induced

(a)	Net induced phase (intermediate time range)	Net induced phase (long time range)
$s = 1$	$it(n+n'+1)(n-n')\frac{C\Omega^2\omega_u}{\pi}$	$it(n+n'+1)(n-n')\frac{C\Omega^2\omega_u}{\pi}$
$s = 0$	$it(n+n'+1)(n-n')\frac{C\Omega^2}{\pi}\left[\ln(\omega_u t)-1\right]$	$-it(n+n'+1)(n-n')\frac{C\Omega^2}{\pi}\left[\ln(\omega_1/\omega_u)+\gamma\right]$
$s = -1$	$it^2(n+n'+1)(n-n')\frac{C\Omega^2}{4}$	$it(n+n'+1)(n-n')\frac{C\Omega^2}{\pi\omega_1}$

(b)	Dephasing term (intermediate time range)	Dephasing term (long time range)
$s = 1$	$-(n-n')^2 C\Omega^2\left[\frac{1}{\pi}\ln(\beta\hbar\omega_u/2\pi)+(\beta\hbar)^{-1}t\right]$	$-(n-n')^2\frac{2C\Omega^2}{\pi\beta\hbar\omega_1}$
$s = 0$	$-(n-n')^2\frac{C\Omega^2}{\pi\beta\hbar}\left[\frac{3}{2}-\gamma-\ln(\omega_1 t)\right]t^2$	$-(n-n')^2\frac{C\Omega^2}{\pi\beta\hbar\omega_1^2}$
$s = -1$	$-(n-n')^2\frac{C\Omega^2}{\pi\omega_1\beta\hbar}t^2$	$-(n-n')^2\frac{2C\Omega^2}{3\pi\beta\hbar\omega_1^3}$

Table 3.1: Leading order in ω_1/ω_u expansion approximations to the net induced phase terms (a) and dephasing terms (b) in the intermediate time range ($\omega_u^{-1} \ll t \ll \omega_1^{-1}$) and long time range ($t \gg \omega_1^{-1}$) for ohmic ($s = 1$) and subohmic ($s = 0, -1$) bath spectral densities.

phase and dephasing terms by expanding in frequency ratio parameter $\omega_1/\omega_u(\lll 1)$. The numerically evaluated sum of the two induced phase terms (3.7) and (3.8) is plotted versus time in Fig. 3.1, while the numerically evaluated dephasing term integral expression given in the second line of Eq. (3.9) is plotted versus time in Fig. 3.2. Both plots are normalized by their corresponding analytical approximations derived below in the $\omega_1 t \to \infty$ limit, facilitating a check of the analytical approximations in the long time limit. The analytical approximations derived below for the net induced phase and dephasing terms are summarized in Table 3.1.

3.2.1. Ohmic, $s = 1$ environment case

We begin with the ohmic case $s = 1$, which corresponds to a 3D acoustic environment medium. The first induced phase term (3.7) is approximately $it(n+n'+1)(n-n')\frac{C\Omega^2\omega_u}{\pi}$, where we have expanded the incomplete Gamma function to leading order using the fact that $\omega_1/\omega_u \lll 1$. We see that this term diverges linearly with the upper frequency cut-off ω_u.

In the intermediate time range ($\omega_u^{-1} \ll t \ll \omega_1^{-1}$), the second induced phase term (3.8) gives approximately $-i(n+n'+1)(n-n')\frac{C\Omega^2}{2}$, while for the long time limit ($t \gg \omega_1^{-1}$) we obtain approximately $-i(n+n'+1)(n-n')\frac{C\Omega^2}{\pi}\frac{\cos(\omega_1 t)}{\omega_1 t}$; in both ranges,

the second phase term is small compared to the above first phase term, as remarked previously.

The dephasing term (3.9) in the high temperature limit and intermediate time range becomes approximately $-(n-n')^2 C\Omega^2 \left[\frac{1}{\pi}\ln\left(\frac{\beta\hbar\omega_u}{2\pi}\right) + (\beta\hbar)^{-1}t\right]$, with a leading linear dependence on time t. Note that in order to obtain the correct, logarithmically diverging term in ω_u appearing in the latter approximation, we instead used the exact solution to the dephasing term for $\omega_1 = 0$ derived in Ref. [51]. In the long time limit ($t \gg \omega_1^{-1}$), the dephasing term (3.9) becomes approximately $-(n-n')^2 \frac{2C\Omega^2}{\pi\beta\hbar\omega_1}$. Interestingly, this result is finite and independent of time, so that the final, reduced state ρ_c of the cavity system mode will only be partially dephased in the Fock state basis. This is a consequence of the finite-sized volume of the acoustic environment medium, as signified by the non-zero fundamental frequency ω_1 of the medium. We will see in the following that partial dephasing also occurs for the $s = 0$ and $s = -1$ cases, again a consequence of the finite dimensions of the corresponding acoustic environments.

In Fig. 3.2, the approach to the above-described, constant long time limit displays oscillatory behavior. This arises from the sub-leading contribution to the dephasing term, which takes the form $-(n-n')^2 \frac{2C\Omega^2}{\pi\beta\hbar\omega_1} \times \frac{\sin(\omega_1 t)}{\omega_1 t}$. Oscillatory behavior also occurs for the $s = 0$ and $s = -1$ cases as seen in Fig. 3.2, arising from similar sub-leading terms.

3.2.2. Subohmic, $s = 0$ environment case

For the subohmic $s = 0$ case, which corresponds to a 2D acoustic environment medium, the first induced phase term (3.7) is approximately $-it(n+n'+1)(n-n')\frac{C\Omega^2}{\pi}\left[\ln\left(\frac{\omega_1}{\omega_u}\right) + \gamma\right]$, to leading order in an ω_1/ω_u ($\ll 1$) expansion, where $\gamma \approx 0.5772\ldots$ is the Euler-Mascheroni constant. Note that this phase term is both logarithmically UV ($\omega_u \to \infty$) and IR ($\omega_1 \to 0$) divergent.

For the intermediate time range ($\omega_u^{-1} \ll t \ll \omega_1^{-1}$), the second induced phase term (3.8) gives approximately $it(n+n'+1)(n-n')\frac{C\Omega^2}{\pi}\left[\ln(\omega_1 t) - 1 + \gamma\right]$. Combining with the above approximate expression for the first phase term, we obtain $it(n+n'+1)(n-n')\frac{C\Omega^2}{\pi}\left[\ln(\omega_u t) - 1\right]$, so that the net induced phase term is logarithmically divergent in the upper frequency cut-off ω_u for the intermediate time range. In the long time limit ($t \gg \omega_1^{-1}$) the phase term (3.8) approximates to $-i(n+n'+1)(n-n')\frac{C\Omega^2}{\pi}\frac{\cos\omega_1 t}{\omega_1^2 t}$. Again, we note that in the long time limit, this phase term becomes negligible compared with the first induced phase term.

The dephasing term (3.9) in the high temperature limit and intermediate time range becomes approximately $-(n-n')^2\frac{C\Omega^2}{\pi\beta\hbar}\left[\frac{3}{2} - \gamma - \ln(\omega_1 t)\right]t^2$. In contrast to the corresponding $s = 1$ dephasing term given in the previous subsection, the $s = 0$ dephasing term is not UV divergent, but instead is IR divergent in the limit $\omega_1 \to 0$. In the long time limit ($t \gg \omega_1^{-1}$), the dephasing term (3.9) becomes approximately $-(n-n')^2\frac{C\Omega^2}{\pi\beta\hbar\omega_1^2}$.

3.2.3. Subohmic, $s = -1$ environment case

For the subohmic $s = -1$ case, which corresponds to a 1D acoustic environment medium, the first induced phase term (3.7) is approximately $it(n+n'+1)(n-n')\frac{C\Omega^2}{\pi\omega_1}$. In contrast to the corresponding $s = 0$ phase term given in the previous subsection, this $s = -1$ phase term is IR divergent but not UV divergent.

For the intermediate time range ($\omega_u^{-1} \ll t \ll \omega_1^{-1}$), the second induced phase term (3.8) gives approximately $-it(n+n'+1)(n-n')\frac{C\Omega^2}{\pi\omega_1}\left[1 - \frac{\pi}{4}\omega_1 t\right]$. Combining with the above approximate expression for the first phase term, we obtain for the net phase term: $it^2(n+n'+1)(n-n')\frac{C\Omega^2}{4}$, which is neither UV nor IR divergent. In the long time limit ($t \gg \omega_1^{-1}$) the phase term (8) approximates to $-i(n+n'+1)(n-n')\frac{C\Omega^2}{\pi}\frac{\cos\omega_1 t}{\omega_1^3 t}$, which becomes negligible compared with the first induced phase term.

The dephasing term (3.9) in the high temperature limit and intermediate time

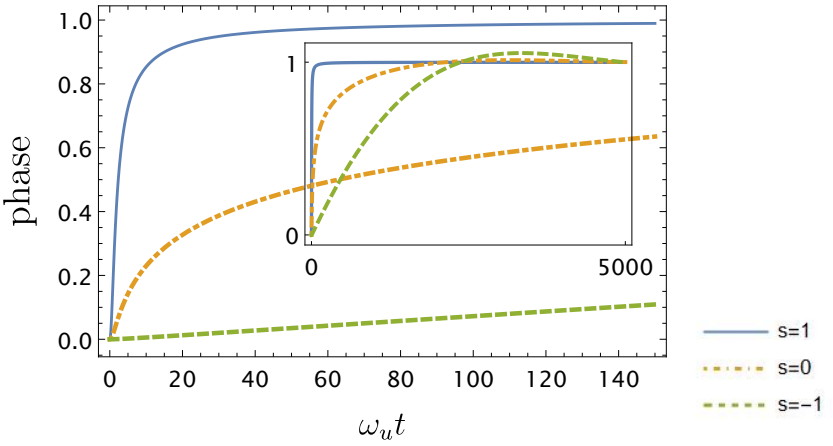

Figure 3.1: Sum of the two induced phase terms Eq. (3.7) and Eq. (3.8) divided by its long time ($t \gg \omega_1^{-1}$) analytical expression as a function of dimensionless time $\omega_u t$, where we set $\omega_1/\omega_u = 0.001$. The inset gives the same normalized phase terms plotted over much longer timescales, indicating the expected approach to 1, hence validating the analytical approximation in the long time limit.

range becomes approximately $-(n-n')^2 \frac{C\Omega^2}{\pi\omega_1\beta\hbar} t^2$. Similarly to the corresponding $s = 0$ dephasing term given in the previous subsection, the $s = -1$ dephasing term is IR divergent. In the long time limit ($t \gg \omega_1^{-1}$), the dephasing term (3.9) becomes approximately $-(n-n')^2 \frac{2C\Omega^2}{3\pi\beta\hbar\omega_1^3}$.

Section 3.3

LC circuit–elastic strip model

In this section we consider a model of a LC circuit capacitively coupled to a long mechanical strip (Fig. 3.3), with several details of the derivation given in the Appendix A. We show that this model system maps onto the subohmic $s = -1$ case considered in Sec. 3.2.3 (although with a different cut-off function and with some modifications to the integral approximation over the bath degrees of freedom). We will only consider dephasing, omitting the induced phase terms, i.e., cavity frequency renormalization

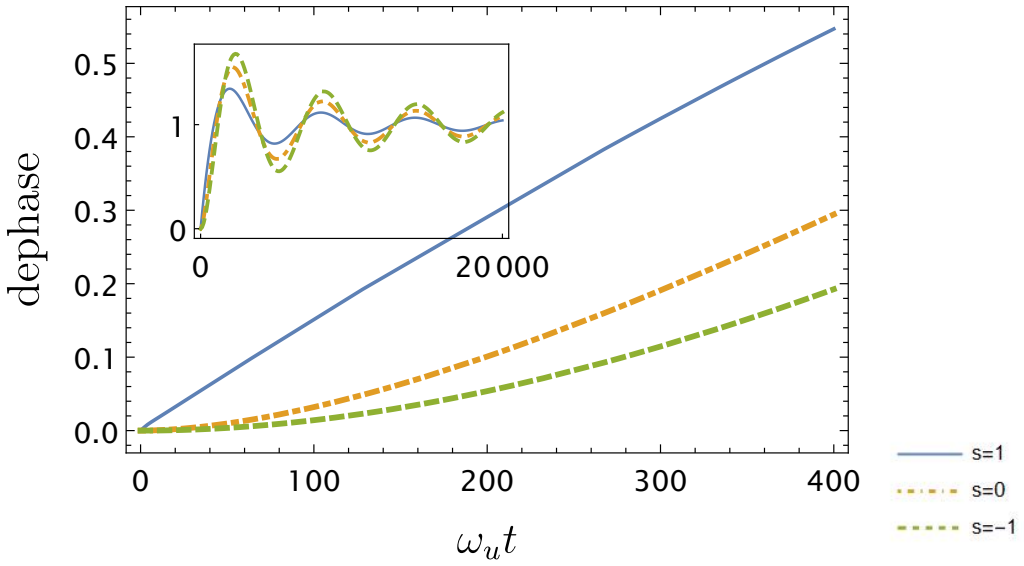

Figure 3.2: The numerically evaluated, exact integral expression for the dephasing term given in Eq. (3.9) divided by its long time ($t \gg \omega_1^{-1}$) analytical expression as a function of the dimensionless time $\omega_u t$, with $\omega_1/\omega_u = 0.001$ and $\beta\hbar\omega_u = 10$. The inset gives the same normalized dephasing terms plotted over much longer timescales, indicating the expected approach to 1, hence validating the analytical approximation in the long time limit.

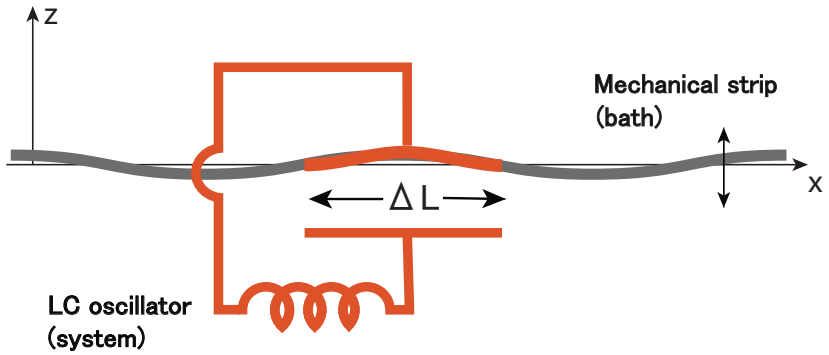

Figure 3.3: Effectively 1D optomechanical scheme comprising a LC circuit oscillator (system) capacitively coupled to a long oscillating strip with (bath) via a metallized length ΔL.

and induced Kerr nonlinearity; the latter phase terms are orders of magnitude smaller than the bare LC circuit frequency phase term for the parameters considered later below in this section. We shall furthermore focus primarily on dephasing during the intermediate time range, where most of the dephasing occurs for the considered parameter values.

Referring to Fig. 3.3, the lower conductor of the capacitor forming the LC circuit is assumed fixed, while the upper conductor is a flexing, metallized segment (length ΔL) of a long elastic mechanical strip (length $L \ggg \Delta L$). The transverse width (W) and thickness (T) dimensions satisfy $T \ll W \lll L$. The lower capacitor plate is assumed also to have length ΔL and the same width W as the strip, with a small equilibrium vacuum gap between upper and lower plates: $d \ll W, \Delta L$. The approximate mutual capacitance between the LC circuit and the undisplaced strip is approximately $\mathsf{C}_0 = \epsilon_0 W \Delta L/d$ and we denote the circuit inductance as L.

Neglecting motion in the transverse y and longitudinal x directions, we denote the flexing mechanical displacement field of the strip in the transverse z direction by $u_z(x,t)$. For sufficiently large tensile forces F applied at the clamped strip ends such that the elastic bending contribution can be neglected, the Lagrangian for the model, LC circuit-mechanical strip system in the resulting string-like limit is as follows:

$$\mathcal{L} = \frac{\rho_m W T}{2}\int_0^L dx \left(\frac{\partial u_z}{\partial t}\right)^2 - \frac{F}{2}\int_0^L dx \left(\frac{\partial u_z}{\partial x}\right)^2 + \frac{1}{2}\mathsf{C}\left[u_z\right]\left(\frac{d\Phi}{dt}\right)^2 - \frac{\Phi^2}{2\mathsf{L}}, \tag{3.10}$$

where $\mathsf{C}\left[u_z\right]$ is the mechanical displacement-dependent capacitance with $\mathsf{C}\left[u_z = 0\right] \equiv \mathsf{C}_0$ the equilibrium capacitance, Φ is the inductor flux coordinate, and ρ_m is the mechanical strip mass density. Note Eq. (3.10) neglects attractive Van der Waals/Casimir forces or the possibility of stray, excess charges on the capacitor plates.

Imposing fixed displacement field boundary conditions at the strip ends, $u_z(0) = u_z(L) = 0$, and solving for the free mechanical normal mode frequencies (see the

Appendix A.1), we have

$$\omega_i = \pi i \sqrt{\frac{F}{2mL}},\ i = 1, 2, \ldots, \tag{3.11}$$

with $m = \rho_m WTL/2$ the effective mass of the mechanical modes. Performing a Legendre transformation to obtain the Hamiltonian from Lagrangian (3.10), introducing the mechanical mode and LC circuit creation/annihilation operators, and expanding the LC circuit frequency $\Omega = 1/\sqrt{\mathsf{LC}}$ and creation/annihilation operators to first order in the displacement field u_z, we obtain the optomechanical Hamiltonian (3.1) after a rotating wave approximation, where the coupling constant λ_i takes the following form (see the Appendix A.2 for derivation details):

$$\lambda_i = -\frac{1}{2d}\left(\frac{\hbar}{2m\omega_i}\right)^{1/2} \sin\left(\frac{\pi i}{2}\right) \operatorname{sinc}\left(\frac{\omega_i}{\omega_u}\right),\ i = 1, 2, \ldots \tag{3.12}$$

Here, $\operatorname{sinc} x \coloneqq \sin x/x$ and the upper cut-off frequency is

$$\omega_u = \frac{2}{\Delta L}\sqrt{\frac{FL}{2m}}. \tag{3.13}$$

Comparing Eq. (3.13) with the mode frequency expression (3.11), we see that the upper cut-off frequency corresponds to the characteristic wavelength $\pi\Delta L$; in the limit where the mechanical mode wavelength becomes much smaller than the capacitor length ΔL, the coupling between the cavity and mechanical strip spatially averages to zero, as expressed by the decaying sinc function appearing in Eq. (3.12).

With equally spaced, harmonic mode frequencies as given by Eq. (3.11), we see from Eq. (3.4) that the dephasing term oscillates, completely vanishing at times

$t = 2\pi n/\omega_1, n = 0, 1, 2, \ldots$, where from Eq. (3.11) the lower cut-off frequency is

$$\omega_1 = \pi\sqrt{\frac{F}{2mL}}. \tag{3.14}$$

We note that such a full rephasing effect is a consequence of having a 1D, harmonic acoustic environment of finite length L with uniformly distributed, discrete modes. This periodic, full rephasing is to be contrasted with the non-zero, long time constant dephasing expressions obtained in Sec. 3.2. The origin for this discrepancy is the breakdown of the integral approximation for the mode sums due to the strongly IR divergent nature of the latter appearing in Eq. (3.4) for the elastic strip model.

An improved integral approximation for the mode sums can be obtained by employing the Euler-Maclaurin series formula to the desired order. In particular, utilizing Eq. (3.12) for λ_i and the Euler-Maclaurin series approximation to first order for example, the integral of the bath spectral density approximation (3.6) in the large strip length L limit is replaced by

$$\pi\sum_i \lambda_i^2 f(\omega_i) \approx C\int_{\omega_1}^{\infty} d\omega\, \omega^{-1} f(\omega)\,\mathrm{sinc}^2\left(\frac{\omega}{\omega_u}\right) + C f(\omega_1), \tag{3.15}$$

where the coupling strength constant is

$$C = \frac{\hbar}{8d^2\sqrt{F\rho_m WT}} \tag{3.16}$$

and we have approximated $\mathrm{sinc}(\omega_1/\omega_u) \approx 1$ since $\omega_1 \ll \omega_u$.

Comparing the integral term in Eq. (3.15) with Eq. (3.6), we see that the LC circuit-elastic strip (string) model corresponds to the $s = -1$ subohmic case, but with upper cut-off of the form $\mathrm{sinc}^2(\omega/\omega_u)$ instead of the previously considered exponential cut-off form $\exp(-\omega/\omega_u)$. Equation (3.15) gives for the dephasing term in the inter-

mediate time range ($\omega_u^{-1} \ll t \ll \omega_1^{-1}$): $-(n-n')^2 \frac{2C\Omega^2}{\pi\omega_1\beta\hbar}t^2$, approximately independent of the form of the upper cut-off. Note that the factor of 2 difference from the corresponding $s = -1$ dephasing expression given in Table 3.1b arises from the additional correction term in Eq. (3.15); including higher order terms in the Euler-Maclaurin series approximation gives a factor closer to 2.5.

From the ω_1^{-1} dependence of the analytical approximation to the $s = -1$ dephasing term (see Table 3.1b), it would seem that the dephasing rate can be made arbitrarily large by progressively increasing the strip length L. However, given that the optomechanical Hamiltonian approximation (3.1) results from expanding the LC circuit frequency to first order in the mechanical displacement field (i.e., weak coupling approximation), we necessarily require that mechanical induced fluctuations in the cavity frequency satisfy $\Delta\Omega \ll \Omega$. From Eqs. (3.1) and (3.12), and assuming a thermal equilibrium state for the mechanical strip modes, the latter requirement gives (see the Appendix A.3 for the derivation details):

$$\sum_{i=1}^{\infty} \frac{\hbar}{8m\omega_i d^2} \sin^2\left(\frac{\pi i}{2}\right) \mathrm{sinc}^2\left(\frac{\omega_i}{\omega_u}\right) \coth\left(\frac{\beta\hbar\omega_i}{2}\right) \ll 1, \tag{3.17}$$

with ω_i and ω_u given by Eqs. (3.11) and (3.13) respectively.

In order to gain a sense of the dephasing rate magnitudes, we assume example parameter values similar to the silicon nitride vibrating string device of Ref. [60] (although allowing for much longer lengths L than the actual 60 μm), and also assume typical superconducting microwave LC circuit parameters. In particular, we adopt the values $\rho_m = 10^3$ kg/m^3, $F = 10^{-5}$ N, $W = 1$ μm, $T = 0.1$ μm, and $L \gtrsim 1$ cm. For the capacitor dimensions, we assume $\Delta L = 10$ μm and $d = 0.1$ μm. The circuit mode frequency is assumed to be $\Omega/(2\pi) = 5$ GHz, and the acoustic bath temperature is taken to be 50 mK. With these assumed values, we have $\omega_i/(2\pi) = 1.6i\frac{10\,\mathrm{cm}}{L}$ kHz and $\omega_u/(2\pi) = 10$ MHz, giving $\omega_1/\omega_u = 2\times10^{-4}\frac{10\,\mathrm{cm}}{L}$. The

dephasing term then becomes approximately $-21(n-n')^2\frac{L}{10\,\mathrm{cm}}\frac{t^2}{\mu s^2}$ in the intermediate time range $0.02\,\mu\mathrm{s} \ll t \ll 100\frac{L}{10\mathrm{cm}}\,\mu\mathrm{s}$. Thus we see that the phase interference between initial energy superposition states of the LC circuit mode is exponentially suppressed on timescales of microseconds for few centimeter long acoustic strip resonators; we note that such dephasing timescales are roughly of the same order as relaxation and decoherence timescales for superconducting circuits reported in recent experiments [61, 62, 63]. Rephasing occurs after a time $\approx 0.6\frac{L}{10\,\mathrm{cm}}$ msec, neglecting other dephasing mechanisms.

Given that the LC circuit mode frequency satisfies $\Omega = 500\,\omega_u$, the cavity-mechanical oscillator bath interaction terms of the form $a^2(b_i+b_i^\dagger)$ and $a^{\dagger 2}(b_i+b_i^\dagger)$ may be neglected as discussed in the beginning of Sec. 3.2 (corresponding to the rotating wave approximation made in the derivation of the Hamiltonian given in Appendix A). Furthermore, condition (3.17) on the strip length can be approximated as $L \ll 16\beta d^2 F \approx 2\times 10^6$ m, which is orders of magnitude longer than in any conceivable circuit optomechanical device operating at cryogenic temperatures, and so the standard optomechanical interaction term in Eq. (3.1) is well-justified. Finally we note that for, e.g., a strip length $L = 10$ cm, the LC induced phase term $\sum_i \Omega^2\lambda_i^2/\omega_i$ is approximately 3×10^3 s^{-1}, which is seven orders of magnitude smaller than the bare LC frequency $\Omega = 2\pi\times 5\times 10^9$ s^{-1}; the LC frequency renormalization and induced Kerr nonlinearity are therefore negligible.

Section 3.4

Optical cavity–elastic membrane model

In this section we consider a model of a 3D optical cavity coupled to a large, square mechanical membrane (Fig. 3.4) [36]. We show that this model system maps onto the subohmic $s = 0$ case considered in Sec. 3.2.3. As in the previous section, we will only consider in detail the dephasing term in the intermediate time range, omitting

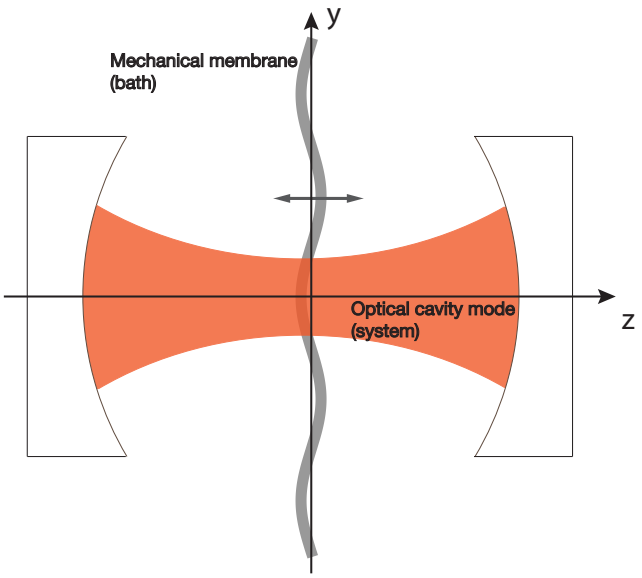

Figure 3.4: Optomechanical scheme comprising a cavity light mode (system) trapped between oppositely facing mirrors interacting via light pressure with a thin dielectric membrane of large transverse extent and undergoing transverse flexural oscillations (bath).

the induced phase term (i.e., cavity frequency renormalization and induced Kerr nonlinearity).

The cavity-membrane model system can be approximately described by the optomechanical Hamiltonian (3.1) (see, e.g., Ref. [64]), with the mechanical normal mode frequencies of the vibrating membrane given by

$$\omega_{i_x i_y} = \pi\sqrt{\frac{\mathcal{F}}{4m}(i_x^2 + i_y^2)},\ i_x, i_y = 1, 2, \ldots, \tag{3.18}$$

where i_x, i_y are the mode labels marking the spatial dependencies of the modes in the transverse x and y coordinate dimensions of the membrane surface, $\mathcal{F}$ is the tensile force per unit length applied at the clamped membrane edges and m is the effective

mass of the mechanical modes:

$$m = \rho_m L^2 T/4, \tag{3.19}$$

with the membrane having side dimension L and thickness T; the tensile force is here assumed to be sufficiently large that the stretching potential energy dominates over the bending potential energy of the mechanical structure, hence defining the so-called membrane limit.

Restricting to cavity Gaussian beam modes, the cavity normal mode frequencies are approximately given by the following expression [65]:

$$\Omega_\sigma = \frac{\sigma\pi c}{l} + \frac{2c}{l}\tan^{-1}\left(\frac{l}{2f}\right),\ \sigma = 1, 2, \ldots, \tag{3.20}$$

where l is the cavity length, f is a length parameter termed the "Rayleigh range" that characterizes the mode beam profile, and c is the speed of light in vacuum.

The optomechanical coupling between the Gaussian beam cavity modes (labeled by σ) and mechanical membrane modes (labeled by i_x, i_y) can be approximated as follows [64]:

$$\lambda_{\sigma,i_x i_y} = (-1)^\sigma \sqrt{\frac{\hbar}{2m\omega_{i_x i_y}}} \frac{(n^2-1)T\Omega_\sigma}{lc} \sin\left(\frac{2\Omega_\sigma z_0}{c}\right) \exp\left(-\frac{\omega_{i_x i_y}^2}{\omega_u^2}\right) \sin\left(\frac{i_x\pi}{2}\right) \sin\left(\frac{i_y\pi}{2}\right), \tag{3.21}$$

where z_0 is the location of the membrane on the cavity's longitudinal axis, with the membrane positioned such that its center coincides with the center of the cavity mode beam 'waist' (i.e., the cavity midpoint with narrowest optical beam width defined as $w_\sigma = \sqrt{2fc/\Omega_\sigma}$), n here denotes the membrane material optical index of refraction,

and

$$\omega_u = \sqrt{\frac{8\mathcal{F}}{\rho_m T w_\sigma^2}} \tag{3.22}$$

is the upper frequency cut-off. Expression (3.21) assumes that the beam waist w_σ is much smaller than the membrane side dimension L.

Comparing Eq. (3.22) with the mechanical mode frequency expression (3.18), we see that the upper cut-off frequency corresponds to a mechanical mode wavelength comparable to the optical beam waist w_σ; in the limit where the mechanical mode wavelength becomes much smaller than the beam waist, the coupling between the cavity and mechanical membrane is exponentially suppressed as the square of the mode frequency.

The integral approximation (3.6) gives

$$\pi \sum_{i_x,i_y} \lambda^2_{\sigma,i_x i_y} f(\omega_{i_x i_y}) \approx C \int_{\omega_1}^{\infty} d\omega f(\omega) \exp\left(-\frac{2\omega^2}{\omega_u^2}\right), \tag{3.23}$$

where from Eq. (3.18) the lower cut-off frequency is

$$\omega_1 = \pi\sqrt{\frac{\mathcal{F}}{2m}}, \tag{3.24}$$

and the coupling strength constant is

$$C = \frac{\hbar}{\mathcal{F}}\left[\frac{(n^2-1)\Omega_\sigma T \sin\left(\frac{2\Omega_\sigma z_0}{c}\right)}{2lc}\right]^2. \tag{3.25}$$

Comparing the right hand sides of Eqs. (3.23) and (3.6), we see that the optical cavity-elastic membrane model corresponds to the $s = 0$ subohmic case, but with upper cut-off of the form $\exp(-2\omega^2/\omega_u^2)$ instead of the previously considered exponential cut-off

form $\exp(-\omega/\omega_u)$.

Equation (3.23) gives for the dephasing term in the intermediate time range ($\omega_u^{-1} \ll t \ll \omega_1^{-1}$): $-(n-n')^2 \frac{1.3C\Omega_\sigma^2}{\pi\beta\hbar}\left[\frac{3}{2} - \gamma - \ln(\omega_1 t)\right]t^2$, approximately independent of the form of the upper cut-off. The factor 1.3 difference with the corresponding $s = 0$ dephasing expression given in Table 3.1b accounts for the error in the continuous frequency integral approximation to the discrete sum over membrane modes given by Eq. (3.23). This factor 1.3 correction was simply determined by trial numerical fitting of the integral approximation over the intermediate time range, since there is no straightforward counterpart to the Euler-Maclaurin formula that gives the correction to the integral approximation of a double sum [66].

In order to gain a sense of the dephasing rate magnitudes, we assume example parameter values similar to the silicon nitride vibrating membrane device of Ref. [67] (although allowing for much longer membrane side dimensions L than the actual 1 mm). In particular, we adopt the values $n = 2$, $\rho_m = 3.4 \times 10^3$ kg/m^3, $\mathcal{F} = 43$ N/m, $T = 50$ nm, and $L \gtrsim 1$ cm. For the optical mode, we assume a cavity length $l = 3.7$ cm and infrared wavelength $\lambda_\sigma = 1064$ nm, corresponding to frequency $\Omega_\sigma/(2\pi) = 2.8 \times 10^{14}$ Hz and beam waist $w_\sigma = 90$ μm, and suppose that the z_0 location of the membrane in the cavity is chosen such that the factor $|\sin(2\Omega_\sigma z_0/c)| = 1$ in the coupling strength constant expression (3.25). With these assumed values, we have $\omega_{i_x i_y}/(2\pi) = 2.5\sqrt{i_x^2 + i_y^2}\frac{10\,\mathrm{cm}}{L}$ kHz and $\omega_u/(2\pi) = 2.5$ MHz, giving $\omega_1/\omega_u = 1.4 \times 10^{-3}\frac{10\,\mathrm{cm}}{L}$. The dephasing term then becomes approximately $-6\times10^{-6}(n-n')^2\left[0.9 - \ln\left(0.02\frac{10\,\mathrm{cm}}{L}\frac{t}{\mu\mathrm{s}}\right)\right]\frac{T}{\mathrm{K}}\frac{t^2}{\mu\mathrm{s}^2}$ in the intermediate time range $0.06\,\mu\mathrm{s} \ll t \ll 45\frac{L}{10\mathrm{cm}}\,\mu\mathrm{s}$, where $\frac{T}{\mathrm{K}}$ refers to the membrane temperature expressed in Kelvin units. In the long time range $\omega_1^{-1} \ll t$, the dephasing term oscillates strongly but does not completely vanish, in contrast to the strip case considered in Sec. 3.3; due to the non-uniform distribution of the membrane vibrational modes, complete rephasing

does not occur.

From the just-derived expression for the dephasing term, we see that it scales approximately quadratically with the membrane edge length L close to the upper limit ω_1^{-1} of the intermediate time range. The resulting estimated dephasing term magnitudes for few centimeter scale-sized membranes are such that the contribution to dephasing of optical mode initial Fock state superposition states due to the membrane environment is expected to be negligible compared to that of other sources, such as photon loss from the cavity.

From the form of the coupling strength constant (3.25), dephasing due to the membrane can also be increased somewhat by reducing the tensile force per unit length $\mathcal{F}$ applied to the membrane edges. However, the membrane approximation assumed in the present investigation eventually breaks down as $\mathcal{F}$ is reduced; the bending potential energy contribution to the mechanical structure would need to be taken into account, with the structure behaving instead as a so-called plate having a qualitatively different flexural vibration mode spectrum.

Given that the cavity mode frequency satisfies $\Omega_\sigma = 10^8\,\omega_u$, the cavity-mechanical oscillator bath interaction terms of the form $a^2(b_i + b_i^\dagger)$ and $a^{\dagger 2}(b_i + b_i^\dagger)$ may be neglected, as discussed in the beginning of Sec. 3.2. In contrast to the cavity-strip system considered in Sec. 3.3, the membrane induced fluctuations in the cavity mode frequency remain constant with increasing membrane edge length L (with the tensile force per unit length $\mathcal{F}$ kept fixed) and are negligible compared to the cavity mode frequency, so that there is no upper limit on the membrane edge length for the validity of the standard optomechanical interaction term in Eq. (3.1). For, e.g., a membrane edge length $L = 10$ cm, the induced phase term $\sum_{i_x,i_y} \Omega_\sigma^2 \lambda_{\sigma,i_x i_y}^2/\omega_{i_x i_y}$ is approximately 2×10^{-3} s^{-1}, which is eighteen orders of magnitude smaller than the bare LC frequency $\Omega_\sigma = 2\pi \times 2.8 \times 10^{14}$ s^{-1}; the cavity frequency renormalization and

induced Kerr nonlinearity are therefore negligible.

Section 3.5

Conclusion

In this chapter, we have investigated the quantum dynamics of optomechanical systems in the unusual situation where the mechanical subsystem comprises a dense spectrum of acoustic modes, functioning effectively as an environment for a single optical mode; in particular, the standard optomechanical interaction results in dephasing without dissipation of initial photon number superposition states of the optical mode.

We found that the optical mode effective dynamics is qualitatively affected by the spatial dimension of the mechanical subsystem, with the dynamics for one dimensional mechanical environments (which can be realized for example as long elastic strings) exhibiting strong power law infrared divergences, two dimensional mechanical environments (such as large area elastic membranes) exhibiting weakly logarithmic infrared and ultraviolet divergences, and three dimensional mechanical environments (such as large volume elastic solids) exhibiting strong power law ultraviolet divergences. The infrared divergences are regularized by accounting for the actual, finite size of the mechanical structures, characterized by the lowest mechanical mode frequency ω_1. On the other hand, the ultraviolet divergences are regularized by the suppression of the optomechanical interaction on length scales smaller than the dimensions of the optomechanical interaction region, characterized by a given upper cut-off frequency $\omega_u (\gg \omega_1)$.

We furthermore found that the cavity mode effective dynamics depends qualitatively on the time scales considered, with three different ranges delineated by the inverse frequencies ω_1^{-1} and ω_u^{-1}. Dephasing predominantly occurs during the so-called 'intermediate' range $\omega_u^{-1} \ll t \ll \omega_1^{-1}$, with a certain degree of rephasing occurring dur-

ing the so-called long time range $\omega_1^{-1} \ll t$.

Two possible realizations were considered in some detail, the first being a long elastic strip capacitively coupled to a LC circuit over a short segment of the strip, and an optical cavity mode coupled via light pressure to a large area elastic membrane. While the estimated dephasing rates resulting from these realizations are relatively small compared with photon loss rates from the cavities, they nevertheless afford useful model systems for clarifying our understanding of system-environment quantum dynamics for the unusual optomechanical type of interaction, where dephasing occurs without dissipation.

The optomechanical models considered in this chapter may be interpreted as analogs for investigating various relativistic quantum information processes, including gravitationally induced dephasing (as briefly discussed in the present work) [12, 13, 51] and gravitationally induced entanglement generation [32]. By being able to carry out exact analytical calculations in the case of the optomechanical coupling, useful insights may be gained concerning the combined dephasing and entanglement dynamics of gravitationally coupled quantum matter systems.

Chapter 4

Optomechanical quantum entanglement mediated by acoustic fields

Section 4.1

Introduction

Thermal environments have often been invoked to explain the decoherence of a quantum system, thus resulting in the observed classical, macroscopic world [68, 69, 70]. However, it is also quite well known that thermal environments can generate quantum entanglement when coupled to otherwise independent quantum subsystems under suitable conditions [71, 72, 73, 74, 75, 76, 77, 78, 79, 80, 81]; several experimental realizations have been proposed [71, 82, 83, 84, 85], with further examples considered in the Ref. [86] review (and references therein).

In this Chapter, we investigate the entanglement dynamics of an experimentally feasible model comprising two spatially separated inductor-capacitor (LC) oscillators that are coupled to a long, partially metallized elastic strip via the optomechanical interaction; here, the elastic strip functions as a thermal phonon environment. A field theoretic description of the environment naturally leads to local, *spatially-dependent* couplings between the oscillators and the field modes. This then allows for an explicit analysis of the causal nature of the entanglement dynamics between the two oscillators arising from the finite elastic wave propagation speed in the elastic strip, analogous to the speed of light in vacuum. Tracing out the elastic strip (phonon) degrees of freedom, we solve *exactly* for the quantum time evolution of the LC oscillators, with particular attention paid to the competing entanglement and dephasing/rephasing dynamics of the LC oscillators.

With the capacitor sizes much smaller than the elastic strip length, the two LC oscillators can also be thought of as variants of the so-called Unruh-DeWitt (UDW) detector [4, 87], with the bare two-level UDW detector replaced by a quantum harmonic oscillator [88] and the usual bilinear coupling between the detector and field

replaced by the quadratic-linear optomechanical-type interaction [3]. A consequence of the optomechanical interaction is that the photon number in each LC oscillator is conserved, so that the oscillators do not undergo transitions between their energy levels, and yet we shall see that entanglement can still develop between the detectors due to their interaction with the common environment. However, we find that the entanglement can only form when the two LC oscillators are 'timelike' separated (i.e., causally connected) as opposed to 'spacelike' separated with respect to the elastic wave propagation (i.e., phonon) speed. This is to be contrasted with the usually considered bilinear, two-level UDW detector-field interaction case where perturbative leading order calculations show that entanglement can be 'harvested' from the quantum field vacuum even for spacelike separated inertial detectors, with the latter undergoing transitions between their ground and excited levels [89, 90, 91, 92]. Furthermore, exact calculations for accelerating oscillator detectors also with bilinear detector-field interactions show spacelike entanglement generation [93]. Such a difference lies in the fact that, with the optomechanical interaction, the oscillator system couples to the environment via its number operator which is time independent in the interaction picture, and therefore obeys the general no-go theorem of Ref. [94] for entanglement generation when the two detectors are 'spacelike' separated.

The optomechanical interaction bears some similarities with the weak field, scalar matter-graviton interaction action [95, 96] given by $S_I = \sqrt{8\pi G}\int d^4x T^{\mu\nu}(\phi)h_{\mu\nu}$, with $T^{\mu\nu}(\phi)$ the scalar field energy-momentum tensor and $h_{\mu\nu}$ the gravitational metric perturbation from flat spacetime; for the LC oscillator-elastic strip model, the LC oscillator is analogous to the scalar matter field while the acoustic phonon excitations of the elastic strip are analogous to graviton excitations of spacetime [97]. Our model can therefore serve as a gravitational entanglement generation analog for informing about recent proposals to observe quantum gravity effects at low energies [98, 99]. In

these proposals, only the effective Newtonian gravitational interaction potential was considered for inducing entanglement between an initial product of matter superposition states, serving as an indirect witness for the existence of the quantum graviton [100]. If gravity is indeed a quantum field entity, then the Newtonian potential corresponds to the nonrelativistic, action at a distance limit of the effective field theory description of the graviton. In this regard, our model analog demonstrates explicitly how the quantum phonon field is responsible for the entanglement generation in the system, with retardation effects exactly taken into account.

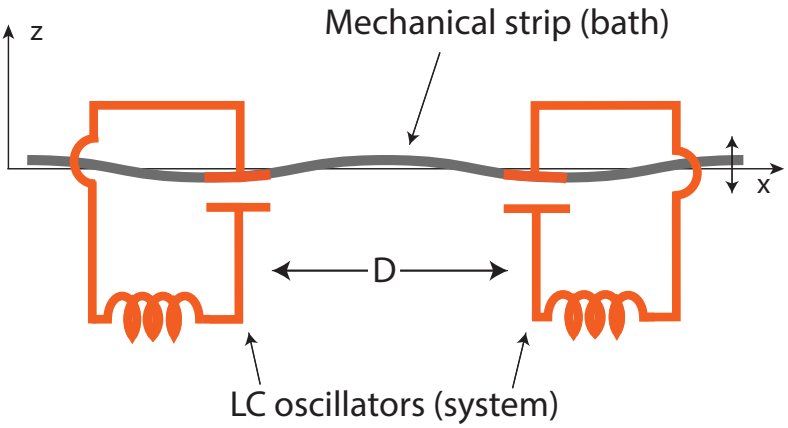

Figure 4.1: Scheme of the model system. Two spatially separated LC circuit oscillators (system) are capacitively coupled to a long oscillating, elastic strip (bath) via two metallized segments.

Section 4.2

The model

Our model scheme (Fig. 4.1) builds on the one considered in Ref. [97], which investigated dephasing only of a single LC oscillator coupled capacitively to a long elastic strip. In particular, we consider two identical LC circuits separated by a distance D, each coupled capacitively via metallized segments (with lengths ΔL) of a long,

elastic mechanical strip with overall length $L > D \gg \Delta L$ that is clamped at both ends. The LC circuits are sited such that the center point between the two capacitors coincides with the strip center. The transverse width (W) and thickness (T) of the strip satisfy $T \ll W \lll L$. The indicated lower capacitor plates are assumed fixed, also with length ΔL, the same width W as the strip, and separated from the upper flexing, metallized ΔL strip segments of the strip by a small equilibrium vacuum gap $d \ll W$. The bare, zero flexing capacitance of each LC circuit is then given by the standard parallel plate expression $\mathsf{C}_b = \epsilon_0 W \Delta L/d$ with ϵ_0 the vacuum permittivity. In the following we shall denote the left circuit capacitance by C_l and right circuit capacitance by C_r, and we denote both circuit inductances by L.

Neglecting displacements in the transverse y and longitudinal x directions, the flexing mechanical displacement of the strip along the transverse z direction can be described by the Hamiltonian

$$\mathcal{H}_{\text{bath}} = \frac{\rho_m WT}{2} \int_0^L dx \left(\frac{\partial u_z}{\partial t}\right)^2 + \frac{F}{2} \int_0^L dx \left(\frac{\partial u_z}{\partial x}\right)^2, \tag{4.1}$$

where $u_z(t,x)$ is the displacement field, ρ_m is the mass density of the strip, and we assume a sufficiently large tensile force F is applied at both ends of the strip so that it behaves effectively as a string with end boundary conditions $u_z(x=0) = u_z(x=L) = 0$.

The Hamiltonian for the two LC circuit system is

$$\mathcal{H}_{\text{sys}} = \frac{Q_l^2}{2\mathsf{C}_l} + \frac{\Phi_l^2}{2\mathsf{L}} + \frac{Q_r^2}{2\mathsf{C}_r} + \frac{\Phi_r^2}{2\mathsf{L}}, \tag{4.2}$$

where Q_l (Q_r) is the left (right) capacitor charge coordinate and Φ_l (Φ_r) is the left (right) inductor flux coordinate. We note that C_l and C_r are implicit functions of the displacement field $u_z(t,x)$, with $\mathsf{C}_l(u_z=0) = \mathsf{C}_r(u_z=0) \equiv C_b$.

Introducing creation/annihilation operators for both the LC circuits and the

elastic strip modes, and expanding the LC circuit resonant frequencies and creation/annihilation operators to first order in the strip transverse displacement field, the total Hamiltonian of the LC system and acoustic phonon bath approximately reduces to the standard optomechanical Hamiltonian

$$\mathcal{H} = \sum_{k=1}^{2}\left[\hbar\Omega_b\left(a_k^\dagger a_k + \frac{1}{2}\right) + \sum_{j=1}^{\infty}\hbar g_{k,j}\left(a_k^\dagger a_k + \frac{1}{2}\right)\left(b_j + b_j^\dagger\right)\right] + \sum_{j=1}^{\infty}\hbar\omega_j\left(b_j^\dagger b_j + \frac{1}{2}\right), \quad (4.3)$$

where a_k ($a_k^\dagger$) are the annihilation (creation) operators for the LC oscillators with bare frequency $\Omega_b = 1/\sqrt{\mathsf{C}_b\mathsf{L}}$, with the subscript $k = 1, 2$ denoting the left, right LC oscillator, and b_j ($b_j^\dagger$) are the annihilation (creation) operators for the elastic strip modes of frequency $\omega_j = \pi j\sqrt{\frac{F}{2mL}}$ with $m = \rho_m WTL/2$ the effective mass of the modes. We note that the usual rotating wave approximation (RWA) is made in order to obtain the standard optomechanical Hamiltonian (4.3), where interaction terms of the form $a_k^2\left(b_j + b_j^\dagger\right)$ and $a_k^{\dagger 2}\left(b_j + b_j^\dagger\right)$ are neglected. The coupling strength between each LC oscillator and the elastic strip modes is given approximately by [97]

$$g_{1(2),j} = -\frac{\Omega_b}{2d}\left(\frac{\hbar}{2m\omega_j}\right)^{1/2}\operatorname{sinc}\left(\frac{\omega_j}{\omega_u}\right)\sin\left(\frac{\pi j}{L}\times\frac{L \mp D \mp \Delta L}{2}\right), \quad (4.4)$$

where $\operatorname{sinc} x := \sin(x)/x$ and the cut-off frequency is $\omega_u = \frac{2}{\Delta L}\sqrt{\frac{FL}{2m}}$, corresponding to the characteristic wavelength $\pi\Delta L$, which is of the same order as the capacitor size; the decaying sinc function results in the coupling to higher frequency modes approaching zero asymptotically for $\omega_j \gg \omega_c$. The term $\frac{L\mp D\mp\Delta L}{2}$ inside the sine function denotes the x coordinate for the center of the left ($-$) and right ($+$) capacitors, respectively.

For the mode frequency ω_j dependence of the above given coupling strength $g_{j,k}$, there is in fact no ultraviolet (UV) divergence when taking the limit $\omega_u \to +\infty$ in the determination of the quantum dynamics of the LC oscillator systems given below; this

is a consequence of the effective one dimensional nature of the elastic strip [97]. Since the capacitor length ΔL is assumed to be much smaller than the length L of the strip, we shall therefore take the 'point-like' UV limit for the capacitors by dropping the upper cut-off regulating sinc function and setting $\Delta L = 0$ for the coupling strength in the following. This then allows closed form analytical solutions for the quantum dynamics.

Supposing that the LC oscillators and the elastic strip state are prepared initially at $t = 0$ in a product state with the latter in a thermal state, the time evolution of the reduced oscillator system density matrix expanded in the Fock state basis can be expressed as follows [97]:

$$\begin{aligned}\rho_{n_1 n_2, n_1' n_2'}(t) = \exp\Big(& -it\Omega_b(n_1 + n_2 - n_1' - n_2') \\ & + ip_1(t)\big[(n_1 + n_1' + 1)(n_1 - n_1') + (n_2 + n_2' + 1)(n_2 - n_2')\big] \\ & + ip_2(t)\big[(n_1 + n_1' + 1)(n_2 - n_2') + (n_2 + n_2' + 1)(n_1 - n_1')\big] \\ & - d_1(t)\big[(n_1 - n_1')^2 + (n_2 - n_2')^2\big] - d_2(t)(n_1 - n_1')(n_2 - n_2')\Big)\rho_{n_1 n_2, n_1' n_2'}(0),\end{aligned} \tag{4.5}$$

where the respective time-dependent terms are given by

$$p_1(t) = \lambda\left(\frac{\pi^2\tau}{6} - \tau\mathrm{Re}[\mathrm{Li}_2(-e^{i\sigma})] + \mathrm{Im}\Big[\frac{1}{2}\mathrm{Li}_3\left(-e^{i(\tau+\sigma)}\right) + \frac{1}{2}\mathrm{Li}_3\left(-e^{i(\tau-\sigma)}\right) - \mathrm{Li}_3(e^{i\tau})\Big]\right), \tag{4.6a}$$

$$p_2(t) = \lambda\left(\frac{\pi^2\tau}{12} + \tau\mathrm{Re}[\mathrm{Li}_2(e^{i\sigma})] - \mathrm{Im}\Big[\mathrm{Li}_3(-e^{-i\tau}) + \frac{1}{2}\mathrm{Li}_3\left(e^{i(\tau-\sigma)}\right) + \frac{1}{2}\mathrm{Li}_3\left(e^{i(\tau+\sigma)}\right)\Big]\right), \tag{4.6b}$$

$$d_1(t) = \sum_{j=1}^{\infty} \frac{1 - \cos(\omega_j t)}{\omega_j^2} g_{1,j}^2 \coth\left(\frac{\beta\hbar}{2}\omega_j\right), \tag{4.6c}$$

$$d_2(t) = 2\sum_{j=1}^{\infty} \frac{1 - \cos(\omega_j t)}{\omega_j^2} g_{1,j} g_{2,j} \coth\left(\frac{\beta\hbar}{2}\omega_j\right), \tag{4.6d}$$

with $\beta^{-1} = k_B T$, where k_B is Boltzmann's constant and T is the bath temperature. The dimensionless numerical constant $\lambda = \frac{\Omega_b^2 \hbar}{16 d^2 m \omega_1^3}$, and $\mathrm{Li}_s(\cdot)$ is the polylogarithm function of order s. Note that we have also introduced the notations for the dimensionless time: $\tau = \omega_1 t$, and the scaled distance ratio: $\sigma = \pi D/L$ in the above expressions. Equation (4.5) neglects any influence due to environments that couple directly to the LC oscillators and the elastic strip systems, since we seek here to understand purely the effects of the optomechanically coupled, long stripline alone on the LC oscillators' reduced quantum dynamics.

We now make several observations based on the form of Eq. (4.5) about the LC oscillators' reduced system dynamics. The first term in the argument of the exponential in Eq. (4.5) is just the free evolution of the system. The $p_1(t)$ and $d_1(t)$ terms correspond to environment induced renormalization and dephasing respectively of the individual LC oscillators, while the $p_2(t)$ and $d_2(t)$ terms encode the effective environment induced mutual dynamics between the two LC oscillators. In particular, we have competing processes here where a non-zero mutual phase term $p_2(t)$ can render the LC oscillators' reduced density matrix non-separable, i.e., we have entanglement generation between the two LC oscillator subsystems; on the other hand, the real dephasing terms $d_1(t)$ and $d_2(t)$ serve to counteract the entanglement generation. However, since both the $d_1(t)$ and $d_2(t)$ terms contain the oscillating factor $1 - \cos(\omega_j)t$, in which the harmonic mechanical mode frequencies are equally-spaced, these two terms completely vanish at times $t = 2\pi j/\omega_1, j = 0, 1, 2, \ldots$. This periodic, full rephasing phenomenon is crucial for the formation of entanglement as we will see below; in particular, it allows for periodic time windows in which to probe the generated entanglement, of course neglecting decoherence effects due to intrinsic environments of the LC oscillators and elastic strip. We note that this full rephasing phenomenon is a consequence of the one dimensional nature of the long elastic strip

with uniformly spaced vibrational modes; only partial rephasing will occur for two dimensional, elastic membranes that have non-uniformly spaced vibrational modes [97].

Section 4.3

Causality

Before we discuss our main results on the entanglement generation dynamics, it is of interest to first analyze the causal aspects of the model dynamics. Although the action following from Hamiltonian (4.1) is not invariant under Lorentz transformations, the Hamiltonian can be expressed in the same form as that for a relativistic massless quantum field in the lab frame, with the speed of light replaced by the acoustic sound (phonon) speed $v_{\rm ph} = \sqrt{\frac{FL}{2m}}$. While the photon number of each LC oscillator is conserved as indicated by Eq. (4.5), the oscillators nevertheless source a local disturbance at $t = 0$ in the phonon field, which propagates along the strip in both directions at the acoustic sound speed. Causality then requires that the physical state of one LC circuit will not be changed by the presence of the other within the time that it takes for phonons to travel the separation distance between the two capacitors: $\Delta t = \frac{D}{v_{\rm ph}} = \sqrt{\frac{2m}{FL}} D$. Performing a partial trace over one of the LC oscillator subsystem's density matrix, one can easily see from Eq. (4.5) that the influence of one LC oscillator on the other is only through the $p_2(t)$ term. Considering the following inequalities for τ and σ: $\tau < \sigma$ (corresponding to $t < \Delta t$) and $\sigma < \pi$ (corresponding to $D < L$), $p_2(t)$ in Eq. (4.6b) can be rewritten as a combination of Bernoulli polynomials that are verified to vanish exactly, thus fulfilling the causality requirement. We stress that such a causally consistent result can only be obtained by an exact, field theoretic treatment of the environment [101, 102] (i.e., taking account of the position-dependent coupling between system and bath and summing over all environmental bath degrees

of freedom); if one approximately truncates to a finite number of field modes in the sum, causality is violated. For example, as we show in Fig. 4.2, a strongly acausal result is obtained with only the contribution from the lowest, fundamental frequency mode of the elastic strip taken into account. By including more modes in the sum, the induced phase term $p_2(t)$ approaches its exact analytical expression, but nevertheless remains acausal.

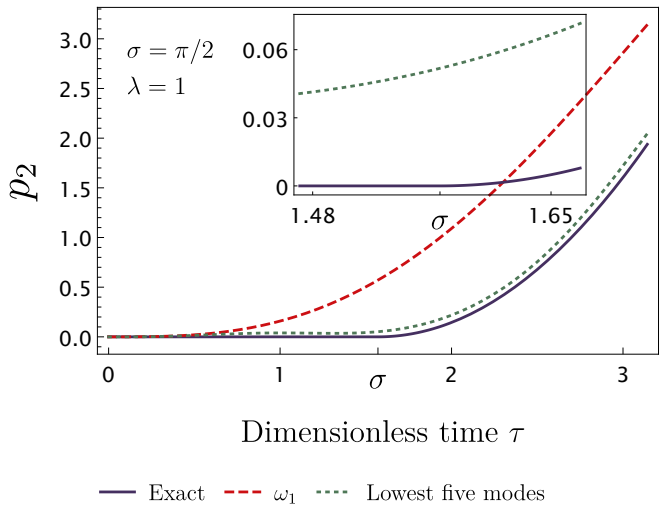

Figure 4.2: The environment induced mutual phase term $p_2(t)$ plotted as a function of dimensionless time $\tau = \omega_1 t$. The constant $\lambda = 1$ and $\sigma = \pi/2$ (corresponding to the LC circuits' separation $D = L/2$). Both the exact analytical expression (4.6b) (solid line) and finite mode sum approximations are shown for comparison: the contribution from the lowest, fundamental mode ω_1 only (dashed line) and the contribution obtained by summing over the lowest five elastic frequency modes only (dotted line). The inset gives the zoomed in plot for p_2 close to $t = \sigma$.

Section 4.4

Zero temperature entanglement

We now discuss the entanglement dynamics in the model. For simplicity, we shall consider an initial ($t = 0$) superposition of zero and single photon states for each

LC circuit: $|\psi(0)\rangle = \frac{1}{2}(|0\rangle_l + |1\rangle_l) \otimes (|0\rangle_r + |1\rangle_r)$, with the labels l (r) denoting the left (right) LC circuit; since the photon number cannot change, each LC circuit then functions effectively as a two-level system where only the relative phases of the various photon number state products can change with time–not the amplitudes. We furthermore assume as before for calculational convenience that the LC oscillators and strip are initially in a product state. The latter is equivalent to suddenly switching on the optomechanical interaction at $t = 0$. While unphysical (the capacitive couplings are always 'on'), such an assumption may be justified by supposing that the LC oscillator superposition states are prepared on a timescale that is much shorter than the phonon travel time between the two oscillators.

We shall first focus on the zero temperature limit of the phonon field (corresponding to the vacuum field state of the strip). Despite the zero temperature limit being a challenge to realize given the presence of low frequency modes of the long elastic strip, the limit allows analytical expressions for the dephasing terms and yields important information about the competition between dephasing and entanglement generation. Taking the limit $\beta \to +\infty$ in Eqs. (4.6c) and (4.6d), we have

$$d_1(t) = \lambda\left(\mathrm{Re}\left[\frac{1}{2}\mathrm{Li}_3\left(-e^{-i(\tau-\sigma)}\right) + \frac{1}{2}\mathrm{Li}_3\left(-e^{i(\tau+\sigma)}\right) - \mathrm{Li}_3\left(e^{i\tau}\right) - \mathrm{Li}_3\left(-e^{i\sigma}\right) + \zeta(3)\right]\right), \tag{4.7a}$$

$$d_2(t) = 2\lambda\left(\mathrm{Re}\left[\mathrm{Li}_3\left(-e^{-i\tau}\right) + \mathrm{Li}_3\left(e^{i\sigma}\right) - \frac{1}{2}\mathrm{Li}_3\left(e^{i(\tau-\sigma)}\right) - \frac{1}{2}\mathrm{Li}_3\left(e^{i(\tau+\sigma)}\right) + \frac{3}{4}\zeta(3)\right]\right), \tag{4.7b}$$

where ζ is the Euler–Riemann zeta function. To determine whether the system is entangled, we utilize the logarithmic negativity [103]: $E_N(\rho) \equiv \log_2(\|\rho^{\Gamma_l}\|)$ as our entanglement measure, where ρ^{Γ_l} is the partial transpose of ρ with respect to the left subsystem and $\|\cdot\|$ denotes the trace norm. A positive value of E_N implies the

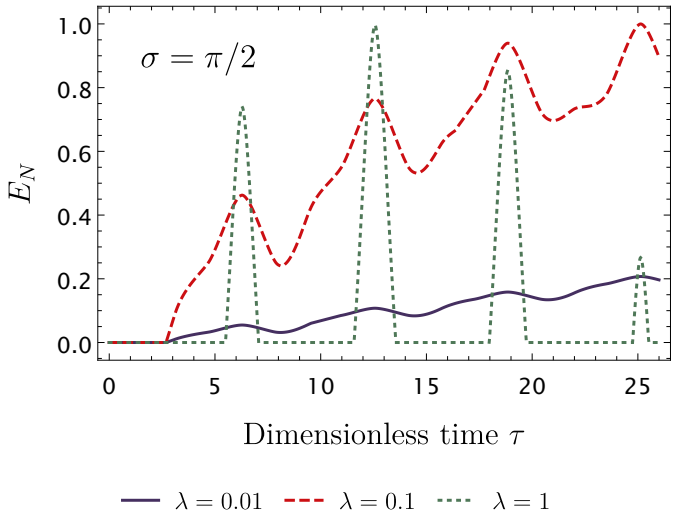

Figure 4.3: Logarithmic negativity plotted as a function of dimensionless time $\tau = \omega_1 t$ with different values of the numerical constant λ. The parameter $\sigma = \pi/2$ (corresponding to the LC circuits' separation $D = L/2$)

presence of entanglement in our (two-level) bipartite system.

With the full time evolution of the system density matrix given by Eq. (4.5) and the calculated time dependent terms $p_1(t)$, $p_2(t)$, $d_1(t)$, and $d_2(t)$, we obtain the logarithmic negativity E_N as a function of the dimensionless time $\tau = \omega_1 t$ shown in Fig. 4.3. It can be seen from Fig. 4.3 that the entanglement dynamics is sensitive to the value of the numerical constant λ, with several features in the time dependence noted as follows: (1) For the parameters considered here, the entanglement can only build up some time later than $t = \Delta t$ (corresponding to $\tau = \sigma$), the time required for phonons to travel the separation distance D between the subsystems. Such a result means that entangled states can only be generated when the two subsystems are 'timelike' with respect to the phonon speed v_{ph}, which is the combined consequence of causality and the effect of zero temperature dephasing; although the environment induced phase term $p_2(t)$ starts to build up immediately after $t = \Delta t$ (Fig. 4.2), some additional time may be required in order to overcome the dephasing in order for

entanglement to develop between the two subsystems. In particular, entanglement would otherwise immediately build up after $t = \Delta t$ in the artificial situation where the dephasing is suppressed [i.e., $d_1(t) = d_2(t) = 0$]. (2) E_N is a local maximum at $\tau = 2j\pi,\ j = 1, 2, 3, \ldots$, corresponding to when both $d_1(t)$ and $d_2(t)$ vanish exactly, as noted previously. Furthermore, depending on the value of the numerical constant λ, E_N can reach its upper bound value 1 for the two-level bipartite system, signaling a maximally entangled system state. (3) With the periodic vanishing of the dephasing terms, the maximally entangled state can always be generated regardless of the separation distance between the LC circuits; a larger separation distance only results in a longer time for the entanglement to build up.

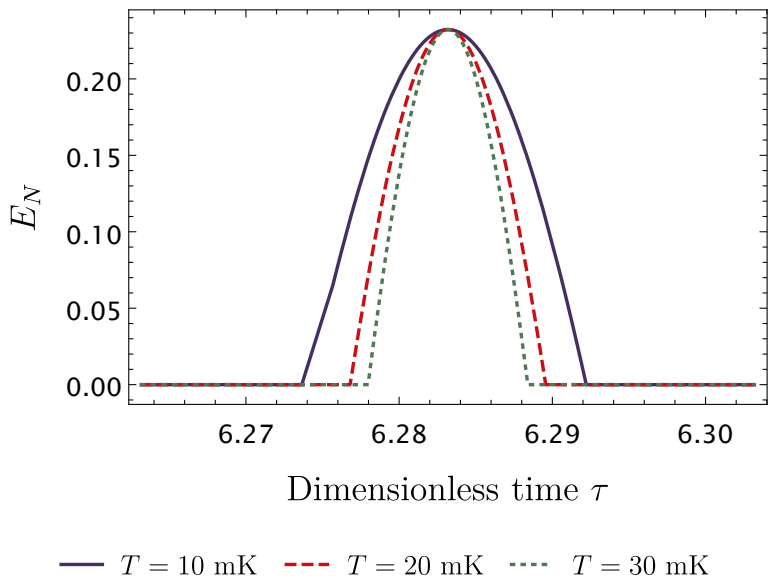

Figure 4.4: Logarithmic negativity plotted as a function of dimensionless time $\tau = \omega_1 t$ for different phonon field temperatures; the utilized parameters of the model are discussed in the text, and correspond to the numerical constant $\lambda \approx 0.045$.

Section 4.5

Finite temperature entanglement and experimental considerations

We now shift our focus to more realistic, finite temperature scenarios, where the entanglement generation can be strongly suppressed due to the much more rapid thermal dephasing as compared with the zero temperature limit. However, as we have seen previously, the entanglement can nonetheless be present in the system around the times $\tau = 2j\pi, j = 1, 2, 3....$ when there is full rephasing (neglecting the other circuit and elastic strip decohering environments). In order to quantitatively investigate the entanglement dynamics, we assume some example parameters for the model that are related to actual experimental devices. In particular, for the elastic strip we adopt the silicon nitride vibrating string parameters from Ref. [104]: $\rho_m = 10^3$ kg/m^3, $F = 10^{-5}$ N, $W = 1$ μm, $T = 0.1$ μm; however, we assume a much longer length $L = 2$ cm than that considered in Ref. [104] (≈ 60 μm). For the LC oscillators, we adopt typical superconducting microwave LC circuit parameters with $\Delta L = 1$ μm, $d = 0.1$ μm, and the circuit mode frequency of $\Omega/(2\pi) = 15$ GHz. The separation distance between the capacitors is taken to be $D = 1$ cm.

Using the above given parameters, we obtain the numerical results shown in Fig. 4.4 for the logarithmic negativity plotted around $\tau = 2\pi$, with different example temperatures achievable in a dilution refrigerator. Note that the amount of entanglement at $\tau = 2\pi$ when there is full rephasing (corresponding to $t \sim 126$ μs) is not changed by the environment temperature. Instead, increasing the temperature narrows the time window (corresponding to a width around 150 ns for $t = 30$ mK in Fig. 4.4) during which the LC circuits system is entangled.

In order to experimentally probe the entanglement within the system, the initial

and final LC systems' state may for example be prepared and measured by coupling the LC circuits to driven nonlinear Josephson phase qubits [105]. With respect to the unavoidable LC circuit environments, we note that relaxation and dephasing times from around a hundred to a few hundred microseconds have been reported for superconducting circuits [61, 106, 62, 63], thus allowing for the possibility to measure the first entanglement generation peak captured by the logarithmic negativity using available circuit QED experimental methods [2].

Section 4.6

Conclusion

We have investigated the entanglement dynamics for two LC oscillators coupled to a long elastic strip–a model system realization for two separated, localized UDW detectors interacting with a $1+1$ dimensional, massless scalar field. Exact solutions for the quantum time evolution of the oscillators were obtained, and the causality of the quantum dynamics analysed.

In contrast to other findings of entanglement generation for spacelike separated, inertial detectors [89, 90, 91], entanglement only arises in our model for timelike separated detectors, a consequence of the optomechanical interaction where the system number operator is time-independent in the interaction picture [94]. Including the RWA-neglected terms in the interaction may result in small amounts of entanglement generation when the detectors are spacelike separated (since the no-go theorem of Ref. [94] no longer holds with such non-RWA interaction terms present), although a similar exact analysis of the entanglement dynamics is not possible in this case.

Given the analog connection between the standard optomechanical interaction and the localized matter system-weak gravitational field interaction, it would be interesting to go beyond recent non-relativistic, action at a distance analyses [98, 99]

and utilize a quantum field theoretic approach [107, 108, 100] to explore gravitationally generated entanglement between inertial detectors that are initially spacelike separated [109, 110, 111].

Finally, with potential applications to quantum information processing in mind, it would also be interesting to extend our model to multiple LC circuits and investigate possible multipartite entanglement generation via the optomechanical interaction [112] with a common, thermal acoustic environment, such as a long elastic strip or large surface area elastic membrane [97].

Chapter 5

Gravitational waves affect vacuum entanglement

Section 5.1

Introduction

It has long been realized that the vacuum state of a quantum field theory in Minkowski space is highly entangled across spacelike regions; for example see Ref. [8] and references therein. Using algebraic methods, Summers and Werner demonstrated that correlations between field observables across spacelike regions are strong enough to violate a Bell inequality [113, 114, 115]. It was later realized that this vacuum entanglement could be 'harvested' by atoms / detectors that couple locally to the field [116, 117, 118]. This result is surprising, suggesting that the vacuum is a resource for quantum correlations and has since been examined in a wide range of scenarios [119, 120, 121, 122, 123, 124, 125, 126, 127, 128, 129, 130, 131, 132, 133].

This phenomenon can be used to construct an operational measure of vacuum entanglement. Specifically, supposing that two detectors remain spacelike separated for the duration of their interaction with the field, then any entanglement that results between them must be attributed to entanglement 'harvested' from the vacuum that existed prior to the detectors' interaction. Thus, quantifying how entangled two detectors become serves as a proxy for how entangled the vacuum is across the regions in which the detectors have interacted. Such a quantification of vacuum entanglement is similar to the distillable entanglement defined as the number of maximally entangled states that can be 'distilled' from a number of copies of a given quantum state via local operations and classical communication [134].

Entanglement harvesting has been used to probe the effects of nontrivial spacetime structure on vacuum entanglement, such as cosmological effects [135, 136, 119, 137, 138], nontrivial spacetime topology [139, 140, 141], spacetime curvature [142, 143, 144, 145], and black hole horizons [146, 147]. It is the purpose of this chapter

to extend this analysis to examine how a gravitational wave affects the entanglement structure of the vacuum. To do so, we derive the gravitational wave modification to the Minkowski space Wightman function and evaluate the final state of two detectors that are initially unentangled. The final state of the detectors is entangled, and the amount of entanglement depends sensitively on the frequency of the gravitational wave and detectors' energy gap. In particular, we demonstrate that a resonance effect occurs when the detectors' energy gap is tuned to the frequency of the gravitational wave. If the detectors' interaction is centered around the gravitational wave's peak displacement, then the gravitational wave is shown to degrade the harvested entanglement relative to detectors in Minkowski space. However, when the detectors' interaction is not centered at this point in the gravitational wave's cycle, then the harvested entanglement can be either amplified or degraded and oscillates as a function of gravitational wave frequency. Away from this resonance condition, the effect of a gravitational wave on the harvested entanglement is exponentially suppressed.

Moreover, we demonstrate that the transition probability of an inertial detector is unaffected by the presence of a gravitational wave, and thus does not register a different particle content than if it were in Minkowski space. This is consistent with Gibbons' conclusion that gravitational waves do not produce particles [148]. In contrast, we emphasize that the entanglement between two detectors is sensitive to the presence of a gravitational wave. This result is analogous to the observation made by ver Steeg and Menicucci [135] that a single detector is unable to distinguish the field being in a thermal state in Minkowski space or the vacuum in a de Sitter spacetime, whereas the correlations between two detectors can distinguish between these situations. Furthermore, this result agrees with the intuition from the classical theory of gravitational waves which asserts that a gravitational wave cannot be detected by a local detector moving along a geodesic.

Section 5.2

Scalar field theory in a gravitational wave background

A gravitational wave propagating along the z-direction is described by the line element

$$\begin{aligned} ds^2 &= -dt^2 + dz^2 + (1 + A\cos[\omega(t-z)])dx^2 + (1 - A\cos[\omega(t-z)])dy^2 \\ &= -dudv + (1 + A\cos\omega u)dx^2 + (1 - A\cos\omega u)dy^2, \end{aligned} \tag{5.1}$$

where in the last equality we have introduced light cone coordinates $u \coloneqq t - z$ and $v \coloneqq t + z$ defined in terms of Minkowski coordinates (t, x, y, z). Such a spacetime is a solution to the linearized field equation, valid to leading order in $A \ll 1$. On this spacetime, consider a massless scalar field $\phi(\mathsf{x})$ satisfying the Klein-Gordon equation at a spacetime point x,

$$\Box\phi(\mathsf{x}) = 0, \tag{5.2}$$

where $\Box$ is the d'Alembertian operator associated with Eq. (5.1).[1] Solving this equation in light-cone coordinates $\mathsf{x} = (u, v, x, y)$ yields a complete set of solutions [149]

$$u_{\vec{k}}(\mathsf{x}) = \frac{\gamma^{-1}(u)}{\sqrt{2k_-}(2\pi)^{\frac{3}{2}}} e^{ik_a x^a - ik_- v - \frac{i}{4k_-}\int_0^u du\,(g^{ab}k_a k_b)}, \tag{5.3}$$

where $\gamma^{-1}(u) \coloneqq [\det g_{ab}(u)]^{\frac{1}{4}}$, the indices a and b run over $\{x, y\}$, and $\vec{k} \coloneqq (k_-, k_a)$ are separability constants arising from solving Eq. (5.2) in light-cone coordinates. This set of solutions is orthonormal with respect to the usual Klein-Gordon inner product

[1] We could have considered a nonminimal coupling of the field to the Ricci scalar by including a term ξR in the equation above. However, for a gravitational wave spacetime like the one described in Eq. (5.1) R vanishes.

[149, 150].

Quantization proceeds by promoting the field to an operator and imposing the canonical commutation relations [150, 151]. As the solutions to Eq. (5.2) are most easily constructed in light cone coordinates, we quantize the field in this coordinate system. For a free field theory, light cone quantization has been shown to be equivalent to the more familiar equal time quantization procedure [152]. Thus, we can interpret the mode functions in Eq. (5.3) as describing the perturbation to the Minkowski vacuum induced by a gravitational wave. As we shall see, using light cone quantization yields the same detector behaviour in the Minkiwoski space limit ($A \to 0$) as equal-time quantization.

As derived in Appendix B.1, the vacuum Wightman function is

$$\begin{aligned} W(\mathsf{x},\mathsf{x}') &:= \langle 0|\phi(\mathsf{x})\phi(\mathsf{x}')|0\rangle = \int d\mathsf{k}\, u_{\mathsf{k}}(\mathsf{x})u^*_{\mathsf{k}}(\mathsf{x}') \\ &= W_{\mathcal{M}}(\mathsf{x},\mathsf{x}') + W_{\mathrm{GW}}(\mathsf{x},\mathsf{x}'), \end{aligned} \tag{5.4}$$

where $W_{\mathcal{M}}(\mathsf{x},\mathsf{x}')$ is the Minkowski space Wightman function which is independent of the gravitational wave in light-cone coordinates,

$$W_{\mathcal{M}}(\mathsf{x},\mathsf{x}') = \frac{1}{4\pi i\Delta u}\delta\left(\frac{\sigma_{\mathcal{M}}(\mathsf{x},\mathsf{x}')}{\Delta u}\right) + \frac{1}{4\pi^2\sigma_{\mathcal{M}}(\mathsf{x},\mathsf{x}')}, \tag{5.5}$$

where $\Delta\mathsf{x}^\mu := \mathsf{x}^\mu - \mathsf{x}'^\mu$, and

$$\sigma_{\mathcal{M}}(\mathsf{x},\mathsf{x}') := -\Delta u\Delta v + \Delta x^2 + \Delta y^2, \tag{5.6}$$

is the geodesic distance between x and x' in Minkowski space, and the modification of

the Minkowski Wightman function to first order in the gravitational wave amplitude

$$W_{\rm GW}(\mathsf{x},\mathsf{x}') = -\tfrac{A}{4\pi^2}\,\mathrm{sinc}\left(\tfrac{\omega}{2}\Delta u\right)\cos\left(\tfrac{\omega}{2}[u+u']\right)\times\tfrac{\Delta x^2-\Delta y^2}{\Delta u^2}\left[i\pi\delta'\left(\tfrac{\sigma_{\mathcal{M}}(\mathsf{x},\mathsf{x}')}{\Delta u}\right)+\tfrac{\Delta u^2}{\sigma^2_{\mathcal{M}}(\mathsf{x},\mathsf{x}')}\right], \tag{5.7}$$

where $\mathrm{sinc}\,x := \frac{\sin x}{x}$.

Section 5.3

Detectors in the presence of gravitational waves

To operationally probe the effects a gravitational wave has on the vacuum state of a scalar field theory, we employ so-called Unruh-DeWitt detectors. Such detectors are a model of a two-level atom locally coupled to a quantum field. We use these detectors to probe interesting field observables in a gravitational wave background, and to track their deviation from the equivalent observables in Minkowski space. After describing these detectors in detail, we demonstrate that the transition probability of an inertial detector is unaffected by the presence of a gravitational wave.

Then, two initially uncorrelated detectors will be used to examine the effect a gravitational wave has on vacuum entanglement by quantifying how entangled they become as a result of their interaction; this protocol will be referred to as *entanglement harvesting*. We demonstrate that the entanglement harvested by the detectors depends sensitively on the gravitational wave frequency ω and exhibits resonance effects.

5.3.1. The Unruh-DeWitt detectors and the light-matter interaction

The Unruh-DeWitt detector [153, 87] is a simplified model of a two-level atom, with a ground state $|0_D\rangle$ and excited state $|1_D\rangle$, separated by an energy gap 2Ω. The center of mass of the detector is taken to move along the classical spacetime trajectory $\mathsf{x}_D(t)$

parametrized by the detector's proper time t. As an approximation to the light-matter interaction, the detector couples locally with the scalar field $\phi(\mathsf{x})$ along its trajectory. In the interaction picture, the Hamiltonian describing this interaction is

$$H_D(t) = \lambda\chi(t)\left(e^{i\Omega t}\sigma^+ + e^{-i\Omega t}\sigma^-\right)\otimes\phi\left[\mathsf{x}_D(t)\right], \tag{5.8}$$

where λ is the strength of the interaction, $\chi(t) \coloneqq e^{-\frac{(t-t_0)^2}{2\sigma^2}}$ is a switching function with the interpretation that t_0 and σ correspond to when the interaction takes place and its duration, respectively, and $\sigma^+ \coloneqq |1_D\rangle\langle 0_D|$ and $\sigma^- \coloneqq |0_D\rangle\langle 1_D|$ are ladder operators acting on the detector Hilbert space. Although simple, this model captures the relevant features of the light-matter interaction when no angular momentum exchange is involved [154, 155, 123, 128].

5.3.2. Single detector excitation as a proxy for vacuum fluctuations

If an Unruh-DeWitt detector begins ($t \to -\infty$) in its ground state $|0_D\rangle$, due to fluctuations of the vacuum and a finite interaction time, there is a finite probability P that in the far future ($t \to \infty$) it will transition to its excited state $|1_D\rangle$. The probability of such a transition is given to leading order in the interaction strength by [156, 157]

$$P = \lambda^2 \int_{-\infty}^{\infty} dtdt'\,\chi(t)\chi(t')e^{-i\Omega(t-t')}W\left(\mathsf{x}_D(t),\mathsf{x}_D(t')\right). \tag{5.9}$$

This probability may be interpreted as quantifying the ability of a detector (or atom) to be spontaneously excited by vacuum fluctuations. Suppose that the detector is at rest with respect to the Minkowski coordinates introduced in Eq. (5.1), so that its trajectory is the geodesic

$$\mathsf{x}_D(t) = (t,0,0,0). \tag{5.10}$$

Note that for this detector trajectory, the gravitational wave contribution to the Wightman function in Eq. (5.7) vanishes because $\Delta x^2 = \Delta y^2 = 0$. It follows that the transition probability in Eq. (5.9) is not affected by the gravitational wave background. We thus conclude that a single detector cannot detect the presence of a gravitational wave.

The transition probability can be calculated for the trajectory in Eq. (5.10), and coincides with the transition probability for a detector in Minkowski space using an equal-time quantization scheme

$$P = \frac{\lambda^2}{4\pi}\left[e^{-\sigma^2\Omega^2} - \sqrt{\pi}\sigma\Omega\left(1 - \mathrm{erf}[\sigma\Omega]\right)\right], \tag{5.11}$$

see Appendix B.2 for details. The fact that a detector clicks with the same probability as in the Minkowski vacuum is consistent with Gibbons' observation that a gravitational wave will not create particles from the vacuum during its propagation [148].[2]

5.3.3. Detector entanglement as a proxy for vacuum entanglement

To operationally probe vacuum entanglement across spacetime regions, consider two detectors, A and B, each interacting locally with the field ϕ for a finite amount of time, after which the detectors become correlated [116, 118, 117]. If these detectors remain spacelike separated for the duration of their interaction with the field, then any correlations that arise between them must have been harvested from the vacuum state of the field. Thus, their behaviour serves as an operational proxy of vacuum correlations. If it is not the case that the detectors remain spacelike separated, then again correlations may be transferred from the vacuum state of the field to the detec-

[2]This conclusion was arrived at by evaluating the Bogolyubov coefficients between the in and out Minkowski-like regions that sandwich a gravitational wave spacetime and demonstrating the absence of particle creation. This setup models a gravitational wave traveling in Minkowski space. In backgrounds other than Minkowski, gravitational wave perturbations may cause particle production [158].

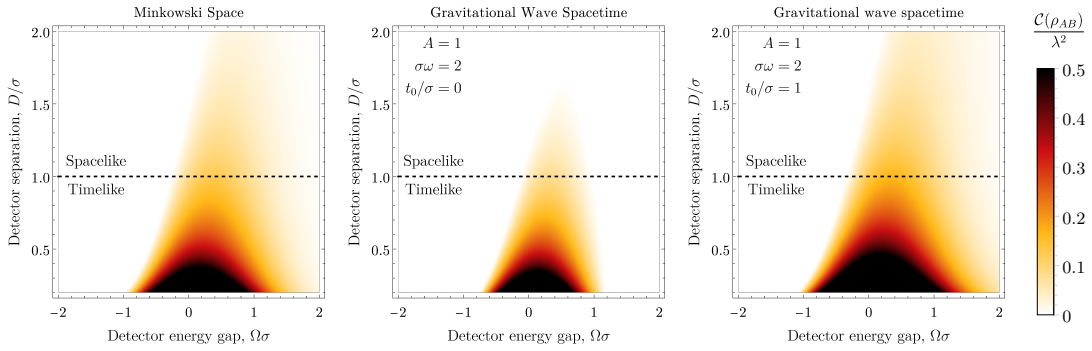

(a) (b) (c)

Figure 5.1: The concurrence $\mathcal{C}(\rho_{AB})/\lambda^2$ is plotted as a measure of entanglement between the two detectors as a function of their energy $\Omega\sigma$ and average proper separation D/σ for detectors situated in (a) Minkowski space and a gravitational wave spacetime with (b) $t_0 = 0$ and (c) with $t_0 = 1$. The gravitational wave contribution degrades the concurrence relative to detectors in Minkowski space for $t_0 = 0$, as can be seen by comparing (a) and (b); however, for $t \neq 0$, as shown in (c), the concurrence can either be amplified or degraded due to the presence of a gravitational wave.

tors. However, in this case even though the detectors do not interact directly, they can still be coupled by a field-mediated interaction, that may now have the time to propagate between the detectors leading to detector correlations.

Consider the following trajectories of detectors A and B specified in Minkowski coordinates

$$\mathsf{x}_A(t) = (t, 0, 0, 0), \tag{5.12}$$

$$\mathsf{x}_B(t) = (t, D, 0, 0). \tag{5.13}$$

Note that since the detectors interact with the field for an approximate amount of proper time σ, detectors moving along these trajectories can be considered approximately spacelike separated throughout the interaction when $D > \sigma$ and timelike when $D < \sigma$; D corresponds to the average proper distance between the detectors.[3] Further-

[3]Technically, because we employ Gaussian switching functions, the tails of which never vanish exactly, the distinction between spacelike and timelike is not exact.

more, suppose these detectors are initially ($t \to -\infty$) prepared in their ground state, and the state of the field is in an appropriately defined vacuum state $|0\rangle$, so that the joint state of the detectors and field together is $|\Psi_i\rangle = |0\rangle_A |0\rangle_B |0\rangle$. Given that the interaction between each detector and the field is described by the Hamiltonian in Eq. (5.8), the final ($t \to \infty$) state of the detectors and field is

$$|\Psi_f\rangle = \mathcal{T} e^{-i \int_{\mathbb{R}} dt \, [H_A(t) + H_B(t)]} |\Psi_i\rangle \,, \tag{5.14}$$

where H_A and H_B are given in Eq. (5.8) and $\mathcal{T}$ denotes the time ordering operator. The reduced state of the detectors is obtained by tracing over the field

$$\begin{aligned} \rho_{AB} &\coloneqq \mathrm{tr}_\phi \left(|\Psi_f\rangle\langle\Psi_f| \right) \\ &= \begin{pmatrix} 1-2P & 0 & 0 & X \\ 0 & P & C & 0 \\ 0 & C^* & P & 0 \\ X^* & 0 & 0 & 0 \end{pmatrix} + \mathcal{O}\big(\lambda^4\big) \,, \end{aligned} \tag{5.15}$$

expressed in the basis $\{|0_A 0_B\rangle, |0_A 1_B\rangle, |1_A 0_B\rangle, |1_A 1_B\rangle\}$, and the matrix elements X and C are given by integrals over the Wightman function evaluated along the detectors' trajectories and are computed analytically in Appendix B.2. These matrix elements are the sum of two terms, $X = X_{\mathcal{M}} + X_{\mathrm{GW}}$ and $C = C_{\mathcal{M}} + C_{\mathrm{GW}}$. The first terms, $X_{\mathcal{M}}$ and $C_{\mathcal{M}}$, correspond to the value X and C would take if the detectors were situated in Minkowski space and coincides with the result obtained using equal-time quantization [139, 141],

$$X_{\mathcal{M}} \coloneqq i \frac{\sigma\lambda^2}{4D\sqrt{\pi}} e^{-\sigma^2\Omega^2 - 2i\Omega t_0 - \frac{D^2}{4\sigma^2}} \left[\mathrm{erf}\left(\frac{iD}{2\sigma} \right) - 1 \right], \tag{5.16}$$

$$C_{\mathcal{M}} \coloneqq \frac{\sigma\lambda^2}{4D\sqrt{\pi}} e^{-\frac{D^2}{4\sigma^2}} \times \left(\mathrm{Im}\left[e^{iD\Omega} \, \mathrm{erf}\left(i\frac{D}{2\sigma} + \sigma\Omega \right) \right] - \sin\Omega D \right). \tag{5.17}$$

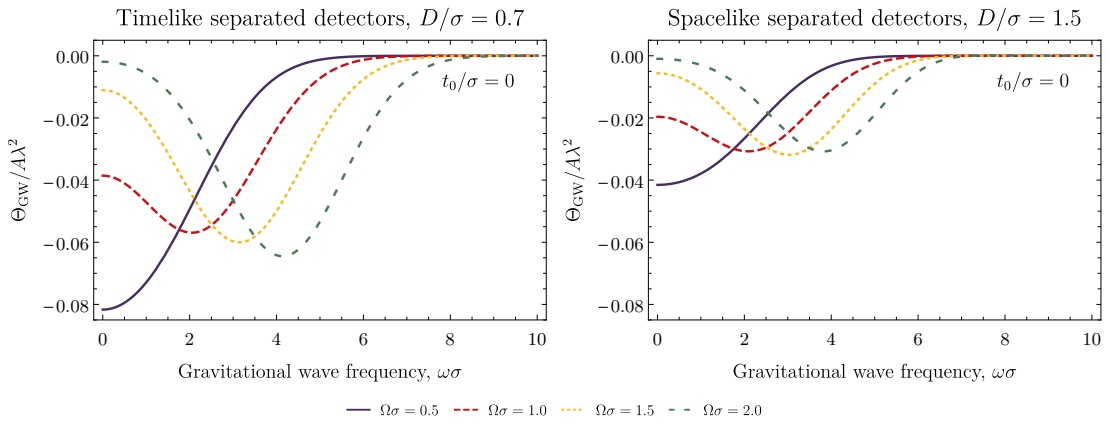

Figure 5.2: The gravitational wave contribution $\Theta_{GW}/A\lambda^2$ to the concurrence is plotted as a function of the gravitational wave frequency $\omega\sigma$ for both timelike (*left*) and spacelike (*right*) seperated detectors for $t_0 = 0$. We see that around the resonance condition $\omega \approx 2\Omega$ the gravitational contribution is negative, which implies a degradation of harvested entanglement relative to detectors in Minkowski space.

The second terms, X_{GW} and C_{GW}, correspond to the modification to the matrix elements X and C stemming from the gravitational wave

$$X_{GW} := \frac{A\sigma\lambda^2}{4D^2\pi^{3/2}} f(\omega, \Omega, \sigma, t_0)\,(I_1 + I_2)\,, \tag{5.18a}$$

$$C_{GW} := -\frac{A\sigma\lambda^2}{4D^2\pi^{3/2}} e^{-\frac{\sigma^2\omega^2}{4}} \cos(\omega t_0)\,(I_3 + I_4)\,, \tag{5.18b}$$

where the terms I_1 and I_2 are complicated functions of ω, D, and σ and the terms I_3 and I_4 are complicated functions of ω, D, σ, and Ω, which have been defined in Appendix B.2, and

$$f(\omega, \Omega, \sigma, t_0) := e^{-\frac{\sigma^2}{4}(\omega-2\Omega)^2 - it_0(\omega+2\Omega)} + e^{-\frac{\sigma^2}{4}(\omega+2\Omega)^2 + it_0(\omega-2\Omega)}. \tag{5.19}$$

To quantify the entanglement harvested by the detectors, which will serve as a proxy measure for vacuum entanglement, we use the concurrence as an entanglement

measure [159]. For the two detector state in Eq. (5.15) the concurrence is [139, 141]

$$\mathcal{C}(\rho_{AB}) = 2\max[\,0,\ |X| - P\,] + \mathcal{O}\big(\lambda^4\big)\,. \tag{5.20}$$

Being a simple difference of a local term P and non-local term $|X|$, the concurrence $\mathcal{C}(\rho_{AB})$ is convenient in interpreting the results to follow. The concurrence can be expressed as sum of the Minkowski space contribution $\Theta_{\mathcal{M}}$ and the modification due to the gravitational wave $\Theta_{\rm GW}$

$$\mathcal{C}(\rho_{AB}) = 2\max[\,0, \Theta_{\mathcal{M}} + \Theta_{\rm GW}] + \mathcal{O}\big(\lambda^4\big)\,, \tag{5.21}$$

where

$$\Theta_{\mathcal{M}} \coloneqq |X_{\mathcal{M}}| - P, \tag{5.22}$$

$$\Theta_{\rm GW} \coloneqq \frac{\mathrm{Re}\,[X_{\rm GW} X^*_{\mathcal{M}}]}{|X_{\mathcal{M}}|}. \tag{5.23}$$

Note that $\Theta_{\rm GW}$ has been expanded to first order in the gravitational wave amplitude A, since this analysis is within the linearized gravity regime.

Figure 5.1 compares the behaviour of the concurrence of the final state of two detectors in Minkowski space with an equivalent pair of detectors in the presence of a gravitational wave as a function of the detectors' energy $\Omega\sigma$ and their separation D/σ; both $t_0 = 0$ and $t_0 \neq 0$ are depicted. Since $X_{\mathcal{M}}$ only depends on t_0 through an overall phase in Eq. (5.16) and $\Theta_{\mathcal{M}}$ depends on $|X_{\mathcal{M}}|$, the Minkowski contribution to the harvested entanglement is unaffected by t_0. From Fig. 5.1, it is seen that in all instances the concurrence (and thus vacuum entanglement) falls off as the distance D/σ between the detectors grows; this could have been anticipated by noting that both $X_{\mathcal{M}}$ and $X_{\rm GW}$ are proportional to $e^{-D^2/4\sigma^2}$. More interestingly, Fig. 5.1b illus-

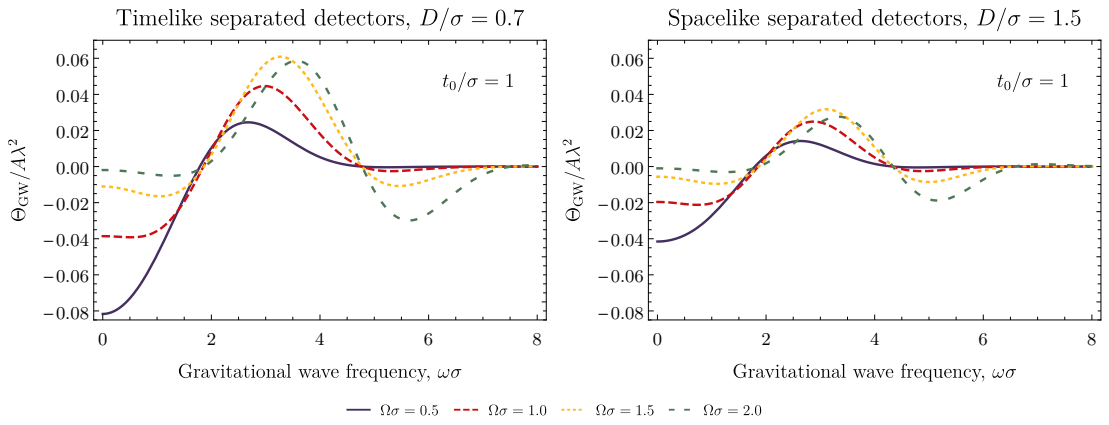

Figure 5.3: The gravitational wave contribution $\Theta_{GW}/A\lambda^2$ to the concurrence is plotted as a function of the gravitational wave frequency $\omega\sigma$ for both timelike (*left*) and spacelike (*right*) separated detectors for $t_0/\sigma = 1$. We see that around the resonance condition $\omega \approx 2\Omega$ the gravitational contribution oscillates around zero, which implies that the gravitational wave can either amplify or degrade the harvested entanglement relative to detectors in Minkowski space.

trates that for $t_0 = 0$ a gravitational wave degrades the concurrence when compared to an equivalent pair of detectors in Minkowski space (Fig. 5.1a). However, when $t_0 \neq 0$, a gravitational wave can both amplify or degrade the concurrence depending on the detector separation and gravitational wave frequency, as can be seen in Fig. 5.1c.

A more detailed study of the gravitational wave contribution to the concurrence is shown in Figs. 5.2 and 5.3 in which $\Theta_{GW}/A\lambda^2$ is plotted as a function of the gravitational wave frequency $\omega\sigma$ for different detector energies $\Omega\sigma$ for both spacelike and timelike separated detectors. From Fig. 5.2, we see that for both spacelike and timelike separated detectors Θ_{GW} is a negative quantity, supporting the conclusion that gravitational waves degrade field entanglement for $t_0 = 0$, as described in the previous paragraph. Moreover, Fig. 5.2 reveals a strong resonance effect when the frequency of the gravitational wave is approximately equal to the energy gap of the detector, $\omega \approx 2\Omega$, around which the harvested entanglement is maximally degraded. This resonance is due to the dependence of Θ_{GW} on the Gaussian profile centered

at $\omega = 2\Omega$ that appears in Eq. (5.19). Away from this resonance, $\Theta_{\rm GW}$ approaches zero asymptotically, which implies that the gravitational wave does not influence the harvested entanglement significantly when $|\omega - \Omega| \gg 1/\sigma$. Note that if the atom had begun in its excited state, $\Omega \to -\Omega$, then $\Theta_{\rm GW}$ would be identical, which implies that for $t_0 = 0$ the harvested entanglement would be degraded by the same amount.

In contrast, Fig. 5.3 depicts $\Theta_{\rm GW}$ when $t_0 \neq 0$, revealing oscillatory behaviour of the concurrence as a function of ω around the resonance condition $\omega \approx 2\Omega$. The frequency of these oscillations is t_0, which can be seen by expanding the numerator in Eq. (5.23) and noting that it is a sum of terms that oscillate with this frequency. It is thus seen that $\Theta_{\rm GW}$ can be positive or negative, indicating that a gravitational wave can either amplify or degrade the harvested entanglement depending on $\omega\sigma$ and t_0/σ. Again, when ω moves away from $\omega \approx 2\Omega$, $\Theta_{\rm GW}$ approaches zero asymptotically.

We end this section with some remarks on our parameter choices. Notice that we choose to survey detector energies $\Omega\sigma \in (-2, 2)$. This upper bound is to ensure the validity of the Taylor expansion A to first-order in Eq. (5.21). To be more precise, in the numerator of Eq. (5.23), $X_{\mathcal{M}}$ approaches zero as $\Omega\sigma$ gets larger, which causes the second order contribution in A (which would only depend on $X_{\rm GW}$) to dominate $\Theta_{\rm GW}$. Such restriction also bounds the value of $\omega\sigma$ due to the resonance effect. Since the period of the gravitational wave as seen by the detectors is $\frac{2\pi}{\omega}$, we find that within the parameter space surveyed, the detectors will not see multiple cycles of gravitational wave throughout the interaction time σ. This fact then makes the value of t_0 more physically relevant since it determines the time at which the interaction with the field is centered.

The effect a gravitational wave has on the total correlations harvested by a pair of detectors is discussed in Appendix B.3, revealing that harvested correlations are affected in a similar fashion as harvested entanglement.

Section 5.4

Conclusion and outlook

We examined the effect that a gravitational wave has on Unruh-DeWitt detectors. To do so, the Wightman function for a massless scalar field living in a gravitational wave background was derived and used to compute the final states of one and two detectors locally coupled to the field for a finite period of time.

It was shown that the transition probability of an inertial detector is unaffected by a gravitational wave, in agreement with Gibbon's observation that a gravitational wave does not excite particles from the vacuum [148]. In contrast, the entanglement structure of the vacuum was shown to be modified by the presence of a gravitational wave as witnessed by the entanglement harvesting protocol. When the detectors are tuned to the frequency of the gravitational wave, it was shown that depending on when the detectors interact with the field relative to where the gravitational wave is in its cycle, the harvested entanglement can be either amplified or degraded relative to an equivalent pair of detectors in Minkowski space.

The relative size of the gravitational wave contribution to the entanglement harvested, $|\Theta_{\mathrm{GW}}/\Theta_{\mathcal{M}}|$, is proportional to the amplitude of the gravitational wave. In general, the amplitudes of gravitational waves detected on Earth tend to be very small, with some whose strain is on the order of 10^{-21} as reported by LIGO [160]. Thus, we think that it would be very difficult to detect the effects of gravitational waves through the entanglement harvesting protocol given our current technological limitations. Since our analysis was carried out in the linearized gravity regime, it would be interesting to extend the analysis to the strong gravity regime where similar resonance effects would presumably exist, which may generate a more easily detectable gravitational wave signal. Moreover, different detector configurations could potentially yield

further amplification of harvested entanglement. Furthermore, in the strong gravity regime it would be interesting to examine the consequences of gravitational-wave memory effect [161, 162] on vacuum entanglement, revealing potential differences in the way in which classical and quantum systems are affected. One might also imagine extending this analysis to investigate gravitational-wave induced decoherence; since one cannot shield from gravity, such a decoherence mechanism might be expected to affect all systems.

Chapter 6

Unruh-DeWitt detector's response to a non-relativistic particle

Section 6.1

Introduction

A conceptual idealized particle detector model in the context of quantum field theory was initially proposed by Unruh [4] to resolve the ambiguity of defining a physical particle state in a general spacetime background. Later, DeWitt simplified this model by introducing a local two-level system moving along a classical trajectory to replace the field description of the detector [5], which is now known as Unruh-DeWitt (UDW) detector. The UDW detector has a simple interpretation of particles; the transition from the ground state to the excited state of the two-level system is regarded as an absorption of the field quanta, and therefore the detection of a particle of the field.

One of the most well-known example of the UDW detector's application is the proof of the Unruh effect [4], which states that from the perspective of an uniformly accelerated observer, the Minkowski spacetime vacuum state is a thermal state. As a simple and useful tool, the UDW detector has also received considerable attention

in many other areas, including the study of black hole thermodynamics [163, 164], Lorentz-violating dispersion relations [165, 166, 167], finite spacial extensions of the detector and the corresponding regularization schemes [168, 169, 170, 171, 172], and the coupling to a fermionic field [173, 174, 175, 176] (for more examples, see recent reviews [177, 178, 179] and references therein). More recently, UDW detectors have been used extensively in the so-called entanglement harvesting protocol [92], where a pair of UDW detectors coupled to a quantum field can be used to extract the vacuum entanglement of the field, and therefore to probe the nontrivial field properties in a wide range of scenarios [89, 91, 122, 180, 181, 182, 183, 184, 185, 186, 187, 141, 188, 189].

However, despite many successful applications of the UDW detectors, most works primarily focus on the vacuum state of a massless quantum field, with a few exceptions for the massive field and single excitation state [190, 191]. As a type of particle detector, it is of natural interest to ask how does the UDW detector respond to the field state that represents the matter/particle distribution, and what are the properties of such field state that can be operationally accessed by coupling the field to the UWD detector. Despite the fact that excitation state exhibits quite different theoretical properties including the entanglement entropy [192] and phase transition [193], these questions are also directly related to the problem of measuring the quantum field as it is known that the projective measurement does not directly generalize to the framework of quantum field theory [194, 195, 196, 197], while the particle detector based model can be promising to formulate the measurement process [198] . It is the purpose of this chapter to investigate the transition probability of the UDW detector in the presence of a non-relativistic particle as a starting point of such attempt, where the transition probability can be interpreted as the probability of finding the particle at the position of the detector.

Working with a non-relativistic particle state allows us to compare the transition probability of the UDW detector with the well-understood probability density of the corresponding free Gaussian wave packet in the non-relativistic quantum mechanical description, which is proportional to the energy density of the field in the non-relativistic limit as we show in Sec. 6.2. To keep the model simple with a focus on particle properties, we consider a massive scalar field living in the two-dimensional Minkowski spacetime, where we can consider the interaction to have a sharp switch-on and switch-off instead of introducing technical details of smearing the detector over time. We find that the total transition probability of the detector splits into the vacuum contribution and the matter contribution, and we show that the matter contribution gives a qualitatively similar description to the probability density of the particle. Such result indicates that our detector model can serve as a faithful field theoretic measurement model for the single particle detection. Unique features inherent to the detector model are found as the matter part contribution oscillates with the interaction time whose period is determined by the difference between the energy gap of the detector and the mass of the particle. Moreover, we observe that there is a strong resonance pattern for the transition probability when the energy gap of the detector is tuned to the mass of the particle.

The chapter is organized as follows. In Sec. 6.2 we give a quick review of the field description for a non-relativistic particle and calculate its energy density. In Sec. 6.3, after introducing the UDW model and a quick review of the transition probability for the detector in the vacuum, we present our main results on the matter part contribution to the transition probability. Both analytical results for the detector coinciding with the particle and numerical results for more general scenarios are discussed. A comparison between the vacuum contribution and the matter part contribution has also been explored with different parameter choices. Sec. 6.4 gives concluding remarks

of the chapter. Throughout this chapter, we use natural units $\hbar = c = 1$ and the metric of the two-dimensional Minkowski spacetime has signature $(-,+)$.

Section 6.2

Single particle description in the two-dimensional Minkowski spacetime

In this section, we briefly review the quantum field description of a non-relativistic particle. Consider a free real scalar field $\phi(t,x)$ of mass m in two-dimensional Minkowski spacetime, which satisfies the Klein-Gordan equation:

$$(-\Box + m^2)\phi(t,x) = 0, \tag{6.1}$$

where $\Box := \partial_\nu \partial^\nu$ is the d'Alembertian operator. Solving this field equation and imposing the canonical quantization for the field, the expression of the field operator can be obtained as

$$\phi(t,x) = \int \frac{dk}{\sqrt{(2\pi)^2 2\omega_k}} \left(a(k) e^{ik_\mu x^\mu} + a^\dagger(k) e^{-ik_\mu x^\mu} \right), \tag{6.2}$$

where $\omega_k = \sqrt{k^2 + m^2}$ is the energy of a single mode and the creation and annihilation operators satisfy the usual commutation rule:

$$[a(k), a^\dagger(k')] = \delta(k - k'). \tag{6.3}$$

A non-relativistic particle localized at x_0 and with momentum k_0 can be described by the initial field state [199]:

$$|\psi(0)\rangle = N \int \frac{dk}{\sqrt{(2\pi)^2 2\omega_k}} e^{-\frac{1}{2\sigma^2}(k-k_0)^2 - ikx_0} a^\dagger(k)|0\rangle, \tag{6.4}$$

where N is the normalization constant. The field state description of the particle is non-relativistic to a good approximation provided the characteristic radius satisfies $\sigma^{-1} \gg m^{-1}$ and the momentum k_0 satisfies $|k_0| \ll m$. Under these conditions, the normalization constant is approximately $|N| = 2\pi^{1/4}\sqrt{m/\sigma}$.

A natural way to see that such an initial state provides a similar description to a free localized Gaussian wave packet with position x_0 and momentum k_0 in non-relativistic quantum mechanics is to compare the expectation value of the energy density $T_{00} = \frac{1}{2}\left[m^2\phi^2 + \dot{\phi}^2 + (\frac{\partial\phi}{\partial x})^2\right]$ for the initial state with the time-dependent probability density of the corresponding wave-function. In the non-relativistic limit, the expectation value of the energy density approximately reduces to a simpler form: $\langle T_{00}\rangle = m^2\langle\phi^2\rangle$, where we have neglected the vacuum energy terms and also $(\frac{\partial\phi}{\partial x})^2$ term since it's proportional to k_0^2, which is small compared with m^2. Note that we also employed the fact that the expectation value of time derivative term reduces to $\frac{1}{2}m^2\langle\phi^2\rangle$ in such limit.

As derived in Appendix C.1, the expectation value of ϕ^2 for $|\psi(0)\rangle$ is given by

$$\langle\psi(0)|\phi\left(t,x\right)^2|\psi(0)\rangle = \frac{1}{m}\left[\frac{\sigma^2}{\pi\left(1+\left(\frac{\sigma^2 t}{m}\right)^2\right)}\right]^{\frac{1}{2}} \exp\left[-\sigma^2\frac{\left(x-x_0-\frac{k_0 t}{m}\right)^2}{1+\left(\frac{\sigma^2 t}{m}\right)^2}\right], \tag{6.5}$$

which coincides with the non-relativistic probability density up to a constant m^{-1} (for quantum mechanical description, see Appendix C.2). From Eq. (6.5), we see the variance of the energy density (probability density) grows with time t, indicating the particle state spreads spatially over time.

Section 6.3

Transition probability of the Unruh-Dewitt detector

The point like Unruh-Dewitt detector can be thought as a two-level system moving along some timelike spacetime trajectory $\mathsf{x}_\mathsf{D}(\tau)$ where τ is the proper time of the detector. The Hilbert space of the detector is spanned by the ground state $|0_D\rangle$ and the excited $|1_D\rangle$ separated by an energy gap Ω. The detector couples to the scalar field locally through the interaction Hamiltonian

$$H_{int}(\tau) = \lambda\chi(\tau)\left(e^{i\Omega\tau}\sigma^{+} + e^{-i\Omega\tau}\sigma^{-}\right)\phi\left[\mathsf{x}_D(\tau)\right], \tag{6.6}$$

where λ is the coupling strength, $\sigma^{+} = |1_D\rangle\langle 0_D|$ and $\sigma^{-} = |0_D\rangle\langle 1_D|$ are ladder operators acting on the detector's Hilbert space, $\chi(t)$ is a compact switching function which controls the switch-on and switch-off moments of the interaction.

In the following, we shall consider an inertial detector at rest at the origin of the coordinate system with its worldline given by the Minkowski coordinate[1]:

$$\mathsf{x}_\mathsf{D}(\tau) = (\tau, 0). \tag{6.7}$$

Such worldline has the simple interpretation that the particle position x_0 is also the separation distance between the particle and the detector.

6.3.1. Transition probability in the vacuum background

Supposing that the detector and the field states are initially prepared in the ground state $|0_D\rangle$ and the vacuum state $|0\rangle$ before the interaction, the transition probability

[1] Without loss of generality, one can always go to the reference frame of the detector, provided that the relative speed between the particle and the detector is non-relativistic.

for the detector to jump to the excited state $|1_D\rangle$ after the interaction has ceased is given to the leading order of the coupling constant by [170]

$$P_v = \lambda^2 \int d\tau d\tau' \chi(\tau)\chi(\tau') e^{-i\Omega(\tau-\tau')} W_v\left(\mathsf{x}_D(\tau), \mathsf{x}_D(\tau')\right), \tag{6.8}$$

where $W_v\left(\mathsf{x}_D(\tau), \mathsf{x}_D(\tau')\right) := \langle 0|\phi(\mathsf{x}_D(\tau))\phi(\mathsf{x}_D(\tau'))|0\rangle$ is the pull back of the vacuum Wightman function to the detector's worldline.

We remark that the vacuum Wightman function in general should be regarded a distribution on the spacetime and one usually needs to consider a smooth switching function $\chi(\tau)$ to cure the possible divergence in Eq. (6.8) in order to obtain unambiguous results for the transition probability. However, as a special case in the two-dimensional Minkowski spacetime for the free massive scalar field, the coincidence singularity of the vacuum Wightman function is only logarithmic [200] and we can consider a sharp switching function:

$$\chi(\tau) = \Theta(\tau - \tau_i)\Theta(\tau_f - \tau), \tag{6.9}$$

where $\Theta(\tau)$ is the Heaviside step function and τ_i (τ_f) indicates the switch-on (off) moment while P_v remains well defined. Note that we have implicitly assumed that $\tau_f \geq \tau_i$, i.e., we always first switch on the interaction and then switch it off with a finite interaction time duration $\Delta\tau := \tau_f - \tau_i$.

The pull back of the vacuum Wightman function for a massive scalar field in the two-dimensional Minkowski spacetime to the detector's worldline is [174, 190]

$$W_v(\tau, \tau') = \frac{1}{2\pi} K_0(m[\epsilon + i(\tau - \tau')]), \tag{6.10}$$

where K_0 is the modified Bessel function of the second kind with limit $\epsilon \to 0^+$ under-

stood.

The transition probability P_v then can be found as [190]

$$P_v = -\frac{\lambda^2}{2m^2}\int_0^{\Delta\tilde{\tau}} du(\Delta\tilde{\tau}-u)[J_0(u)\sin(\mu u)+Y_0(u)\cos(\mu u)], \tag{6.11}$$

where $\Delta\tilde{\tau} = m(\tau_f - \tau_i)$, $\mu = \Omega/m$, J_0 and Y_0 are the Bessel's function of the first kind and the second kind.

6.3.2. Transition probability in the presence of a particle

Now we are ready to discuss the transition probability of the detector in the presence of a non-relativistic particle. Supposing that the field state is prepared as in Eq. (6.4) at $\tau = 0$ with the detector in its ground state $|0_D\rangle$ and adopting the switching function $\chi(\tau)$ in Eq. (6.9) with $\tau_i \geq 0$, the transition probability for the detector to the leading order of the coupling strength is [170]

$$P_p = \lambda^2 \int_{\tau_i}^{\tau_f}\int_{\tau_i}^{\tau_f} d\tau d\tau' e^{-i\Omega(\tau-\tau')}\langle\psi(0)|\phi(\mathsf{x}_D(\tau))\phi(\mathsf{x}_D(\tau'))|\psi(0)\rangle. \tag{6.12}$$

The two-point function in Eq. (6.12) can be expressed as a sum of the vacuum contribution and the matter contribution (see derivation in appendix C.1):

$$\langle\psi(0)|\phi(\mathsf{x}_D(\tau))\phi(\mathsf{x}_D(\tau'))|\psi(0)\rangle = W_v(\tau,\tau') + W_m(\tau,\tau'), \tag{6.13}$$

where

$$W_m(\tau,\tau') = \frac{1}{2\sqrt{\pi}m\sigma}\frac{e^{-im(\tau-\tau')-\frac{k_0^2}{\sigma^2}}}{\sqrt{\left(\frac{1}{\sigma^2}+\frac{i\tau}{m}\right)\left(\frac{1}{\sigma^2}-\frac{i\tau'}{m}\right)}}\exp\left(\frac{\left(\frac{k_0}{\sigma^2}-ix_0\right)^2}{2\left(\frac{1}{\sigma^2}+\frac{i\tau}{m}\right)}+\frac{\left(\frac{k_0}{\sigma^2}+ix_0\right)^2}{2\left(\frac{1}{\sigma^2}-\frac{i\tau'}{m}\right)}\right) + \{\tau \Longleftrightarrow \tau'\}. \tag{6.14}$$

Note that to reach Eq. (6.14), we have taken the non-relativistic limit approximation. Substituting Eq. (6.14) into Eq. (6.12), we then obtain the transition probability as a sum of the vacuum contribution and the matter part contribution:

$$\begin{aligned} P_p &= P_v + P_m \\ &= P_v + \lambda^2 \int_{\tau_i}^{\tau_f} \int_{\tau_i}^{\tau_f} d\tau d\tau' e^{-i\Omega(\tau-\tau')} W_m(\tau,\tau'). \end{aligned} \tag{6.15}$$

The expression of P_m is a complicated integral which does not admit an analytical form in general. In the following two subsections, we shall first discuss a special case of $x_0 = 0$ and $k_0 = 0$, where analytical results can be obtained and then we employ numerical methods to study the dependence of P_m on other parameters.

Analytical results. In case of $x_0 = 0$ and $k_0 = 0$, the point-like detector essentially overlaps with the particle and the matter part contribution to the two-point function simplifies to

$$W_m(\tau,\tau') = \frac{1}{2\sqrt{\pi} m\sigma} \frac{e^{-im(\tau-\tau')}}{\sqrt{\left(\frac{1}{\sigma^2}+\frac{i\tau}{m}\right)\left(\frac{1}{\sigma^2}-\frac{i\tau'}{m}\right)}} + \{\tau \Longleftrightarrow \tau'\}. \tag{6.16}$$

Substituting Eq. (6.16) into Eq. (6.12), we find

$$\begin{aligned} P_m &= \frac{\lambda^2}{2\sqrt{\pi} m\sigma} \int_{\tau_i}^{\tau_f} \int_{\tau_i}^{\tau_f} d\tau d\tau' e^{-i\Omega(\tau-\tau')} \left(\frac{e^{-im(\tau-\tau')}}{\sqrt{\left(\frac{1}{\sigma^2}+\frac{i\tau}{m}\right)\left(\frac{1}{\sigma^2}-\frac{i\tau'}{m}\right)}} + \{\tau \Longleftrightarrow \tau'\} \right) \\ &= \frac{\lambda^2 m}{2\sqrt{\pi}\sigma^3} \left(\left| I(\tau_f,\Omega) - I(\tau_i,\Omega) \right|^2 + \{\Omega \Longleftrightarrow -\Omega\} \right), \end{aligned} \tag{6.17}$$

where we have introduced function $I(\tau,\Omega)$ defined as

$$I(\tau,\Omega) \coloneqq e^{\frac{2m(m+\Omega)}{\sigma^2}} \sqrt{1+\frac{i\tau\sigma^2}{m}} E_{\frac{1}{2}}\left(\frac{m(m+\Omega)}{\sigma^2} + i(m+\Omega)\tau \right), \tag{6.18}$$

with $E_{1/2}$ the exponential integral.

We now discuss properties of P_m in Eq. (6.17). From Eq. (6.17) we see that P_m is invariant under the change of $\Omega \to -\Omega$, indicating that the matter part contribution to the transition probability is the same for both the excitation and the de-excitation of the detector[2]. As a matter of fact, this conclusion also applies to particles with non-zero momentum k_0 and position x_0 since $W_m(\tau, \tau')$ is a symmetrical function of τ and τ' and the transformation of $\Omega \to -\Omega$ in Eq. (6.12) amounts to the exchange of variables τ and τ' in the integral, which then gives the same result. We note that the vacuum Wightman function $W_v(\tau, \tau')$ is, however, non-symmetrical.

A closer study of the function $I(\tau, \Omega)$ reveals more details on how P_m depends on time τ and energy gap Ω. In the long time limit $\tau_f \to +\infty$ (which corresponds to infinite interaction time duration $\Delta\tau \to +\infty$), $I(\tau_f, \Omega)$ approaches zero asymptotically, resulting P_m an initial time τ_i dependent quantity. This asymptotic property of the $I(\tau, \Omega)$ function also means that P_m decreases as τ_i gets larger with a fixed interaction time duration, which is in agreement with the fact that the particle state spreads spatially over time with a decreasing energy/probability density. We note that the exponential integral has an oscillatory dependence on its imaginary component, and therefore P_m also oscillates with interaction time duration $\Delta\tau$. For a positive value of Ω, the first term in Eq. (6.17) is dominated by the second term and the period of P_m is approximately given by $T = 2\pi/(m - \Omega)$. Moreover, as we shall see in the following, there is a strong resonance effect at $\Omega = m$ where P_m obtains its peak value.

We plot P_m as a function of the dimensionless interaction time duration $\Delta\tau\sigma$ and the energy gap Ω/σ with different switch-on moments τ_i in Figs. 6.1 and 6.2. From Fig. 6.1, we see P_m oscillates with a period approximately of $2\pi/(m/\sigma - \Omega/\sigma) = 2\sigma$ and its peak value gradually decreases over time as we remarked previously. Comparing

[2]If Ω is a negative quantity, $|1_D\rangle$ effectively becomes the ground state with $|0_D\rangle$ being the excited state.

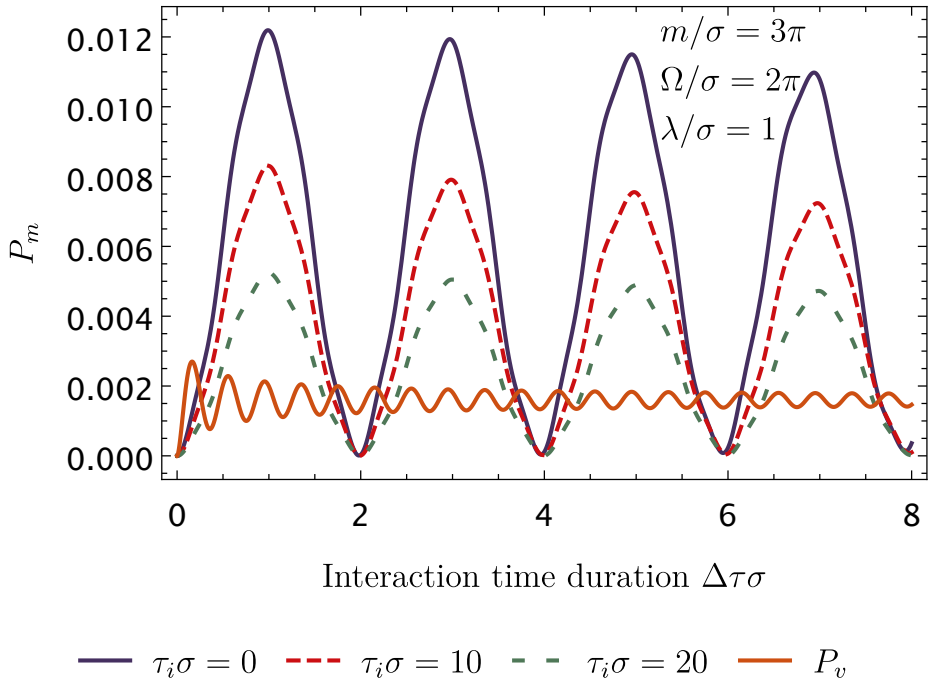

Figure 6.1: The matter part contribution to the transition probability P_m and the vacuum part contribution P_v are plotted as functions of the dimensionless interaction time duration $\Delta\tau\sigma$. We see that both P_m and P_v oscillate with the time duration and its peak value decreases gradually over time.

different switch-on moments $\tau_i\sigma$, we see the transition probability gets smaller for larger values of $\tau_i\sigma$ with a fixed interaction time duration. For a comparison with the vacuum contribution, the dependence on the interaction duration of P_v is also plotted in Fig. 6.1, and it can be seen that the amplitude of P_v is much smaller than P_m here. Fig. 6.2 shows the symmetrical dependence of P_m on the dimensionless energy gap Ω/σ. Moreover, we see from Fig. 6.2 that there is a strong resonance effect for P_m when the energy gap of the detector is tuned to $\Omega = \pm m$. Such resonance should come as no surprise since that the non-relativistic particle would have the same energy as the excited state of the detector in this case. Again, Fig. 6.2 reveals a smaller P_m with larger values of the starting time moment $\tau_i\sigma$ with other parameters fixed.

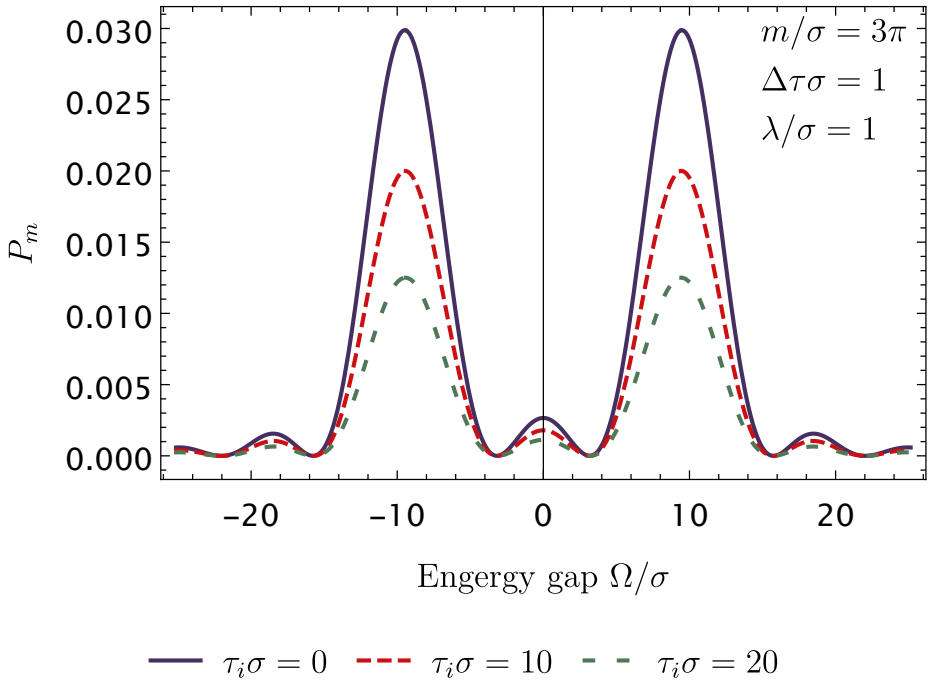

Figure 6.2: The matter part contribution to the transition probability P_m is plotted as a function of the dimensionless detector energy gap Ω/σ. We see a symmetrical dependence of P_m on the energy gap with its peak values obtained in the resonance condition $\Omega = \pm m$.

In Fig. 6.3 we compare the dependence on the dimensionless energy gap Ω/σ for P_m and P_v. It is seen that for positive value of Ω/σ, P_v is dominated by P_m when the energy gap of the detector is close to the resonance condition $\Omega = m$, which is in agreement with Fig 6.1. However, for negative value of Ω/σ, P_v is significantly larger than P_m with its peak around $\Omega = -m$ [190], indicating that the detector has much higher probability to de-excite compared with the excitation rate in the presence of vacuum and it is less sensitive to the matter part contribution for the de-excitation.

We end this subsection with some more discussion on the resonance effect for P_m. Taking $m = \Omega$, the second term in Eq. (6.17) is in fact ill-defined since $E_{1/2}(0)$ is formally infinite. This apparent infinity is due to the improper treatment of the

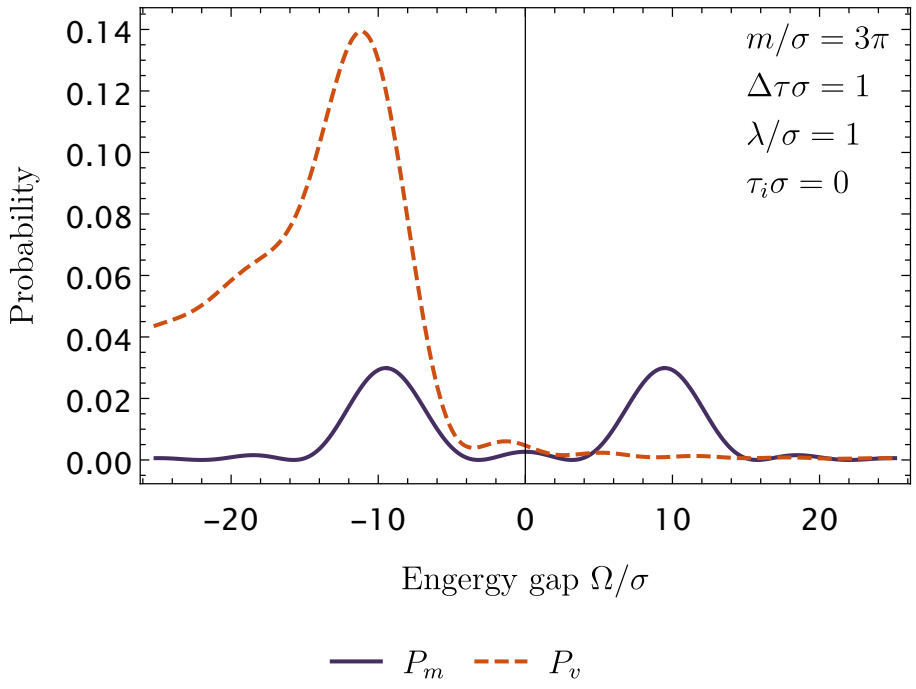

Figure 6.3: The matter part contribution to the transition probability P_m and the vacuum part contribution P_v are plotted as functions of the dimensionless energy gap Ω/σ. We see that P_m dominates P_v for positive value of the energy gap in the resonance region, and for negative value of the energy gap P_v gets significantly larger than P_m with its peak around $\Omega = -m$.

integration in Eq. (6.17). Taking $m = \Omega$ in the integral, we obtain

$$P_m = \frac{\lambda^2 m}{2\sqrt{\pi}\sigma^3}\left[\left|I(\tau_f,\Omega) - I(\tau_i,\Omega)\right|^2 + \left|\sqrt{1-\frac{i\tau_f\sigma^2}{m}} - \sqrt{1-\frac{i\tau_i\sigma^2}{m}}\right|^2\right]. \tag{6.19}$$

The expression of P_m in Eq. (6.19) is, however, also problematical if one consider large difference between τ_f and τ_i as P_m can gets larger than one. Such divergence implies that in the resonance condition, the first order result for the transition probability is invalid for long interaction time duration and one has to take into account the contribution from higher order terms. We note that such first order divergence is due to the stronger infrared divergence in the lower dimensional quantum field theory.

The power of the denominator in Eq. (6.16) increases with the dimension of the spacetime, and therefore Eq. (6.19) would converge in higher dimensional spacetimes.

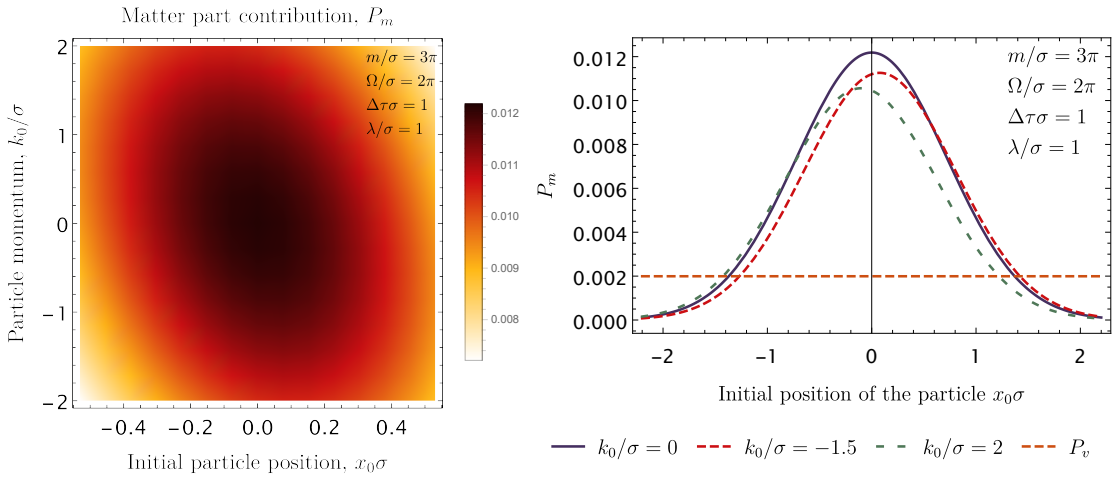

(a) (b)

Figure 6.4: (a) The matter contribution to the transition probability P_m is plotted as a function of the dimensionless initial particle position $x_0\sigma$ and the particle momentum k_0/σ. We see the peak of the probability moves in the opposite directions in the position space as the momentum increases in the positive direction. (b) A more study of P_m is plotted versus initial particle position $x_0\sigma$ with different momentum k_0/σ. The switch-on moments in both (a) and (b) are $\tau_i\sigma = 0$.

Numerical results. The integration for P_m with non-zero initial position x_0 and momentum k_0 can hardly be evaluated analytically. With the dependence on time τ and energy gap Ω discussed in the previous subsection, we shall employ numerical methods in this subsection to focus on exploring the dependence of P_m on x_0 and k_0.

Some comments are in order here before we discuss the numerical plots. Similar to the energy/probability density in Eq. (6.5), it can be seen from Eq. (6.14) that $W_m(\tau, \tau')$ roughly decreases exponentially with the square of the particle position x_0, and therefore P_m would also fall off exponentially with larger value of x_0. Furthermore, since P_v is independent of the particle position x_0, in case of sufficiently large separation between the particle and the detector, the vacuum contribution would

dominate the matter contribution.

Fig. 6.4 displays the numerical plot of P_m. Fig. 6.4 (a) is a density plot of P_m as a function of the dimensionless initial particle position $x_0\sigma$ and the particle momentum k_0/σ, from which one can see that for each fixed value of the momentum k_0/σ, there is a corresponding peak of the probability in the position space. As the particle deviates from such peak position, P_m falls off in both directions quickly. Furthermore, we see that as the momentum k_0/σ increases in the positive direction, the peak of the P_m in the position space moves in the opposite direction to the negative values for $x_0\sigma$. Fig. 6.4 (b) depicts a more detailed numerical study on P_m as a function of the initial particle position $x_0\sigma$ with different momentum k_0/σ as well as the vacuum contribution to the transition probability P_v. We see that as the detector sits sufficiently far from the particle, the vacuum contribution P_v gets greater than the matter contribution P_m and eventually dominates it. Moreover, it can be seen more clearly that for zero momentum, P_m falls off exponentially in both directions in a symmetrical fashion, and in case of the non-zero momentum for the particle, the peak of P_m is shifted in the corresponding direction by a certain value as we have seen in Fig. 6.4 (a). We remark that such behaviour agrees with the energy/probability density dependence in the phase space of the particle. Intuitively one would expect that P_m should be larger if the particle is moving towards the detector during the interaction time interval in contrast to the case when it's moving away from the detector since the average energy/probability density during the interaction time interval at the position of the detector is greater in the former case.

However, the similarity between the non-relativistic probability density and P_m should only be understood in a qualitative sense. To compare the matter part contribution to the transition probability of the detector with the non-relativistic probability density of the particle, we define the averaged probability density at the position

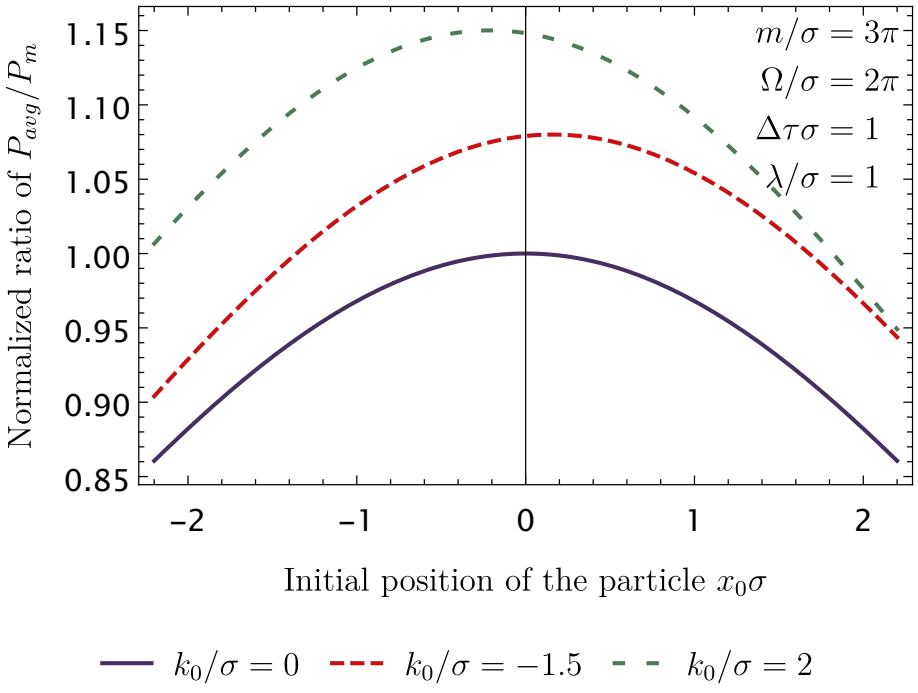

Figure 6.5: The normalized ration of P_{avg}/P_m is plotted as a function of the dimensionless initial particle position $x_0\sigma$ with different momentum k_0/σ. The normalization is taken such that $P_{avg}/P_m = 1$ for $x_0\sigma = 0$ and $k_0/\sigma = 0$.

of the detector as

$$P_{avg} \coloneqq \frac{m}{\tau_f - \tau_i} \int_{\tau_i}^{\tau_f} d\tau \langle \psi(0) | \phi(\tau, 0)\, \phi(\tau, 0) \, | \psi(0) \rangle, \tag{6.20}$$

where we have used the fact that the expectation value of ϕ^2 coincides with the non-relativistic probability density up to a constant m^{-1}. Fig. 6.5 shows the normalized ratio plot of P_{avg}/P_m versus the initial particle position $x_0\sigma$ with different momentum k_0/σ, where an implicit normalization constant has been taken such that P_{avg}/P_m equals to 1 for $x_0 = 0$ and $k_0 = 0$. It can be seen that these two quantities do not have a strict linear relationship and the matter part contribution P_m decays slower over the separation distance between the detector and the particle compared with P_{avg}.

Section 6.4

Conclusion and outlook

In this chapter we studied in detail the transition probability of the UDW detector in the presence of a non-relativistic particle. We introduced an initial state of a massive scalar field that represents a non-relativistic particle and we calculated it's energy density which is shown to be proportional to the corresponding non-relativistic probability density.

Coupling the UDW detector to such an initial field state, we found that the transition probability splits into the vacuum contribution and the matter part contribution. An analytical result for the matter part contribution is obtained in the special case when the particle coincides with the detector during the interaction. It was shown that the matter contribution oscillates with the interaction time duration, and with its peak gradually deceasing over time to its initial time dependent asymptotic value. The frequency of the oscillation is determined by the difference between the mass of the particle and the energy gap of the detector. When the mass equals to the energy gap, we found a strong resonance effect for the transition probability. The comparison between the vacuum contribution and the matter part contribution was performed and we found that for the excitation of the detector, the matter contribution would mostly dominate the vacuum contribution while for the de-excitation of the detector, the situation is reversed. We employed numerical methods to investigate the more general scenarios when the particle does not coincide with the detector and we found that the matter part contribution behaves similar to the averaged energy density of the particle at the position of the detector during the interaction. Such similarity, as

we have checked, should only be understood in a qualitative sense.

Although we have done the analysis in a two-dimensional flat spacetime, we expect that most properties of the matter contribution to the transition probability are still valid in higher dimensional spacetime as the two-point functions for a non-relativistic particle state share similar structures. This chapter has paved the way for operationally investigating field properties in the presence of matter. It would be interesting to extend the analysis to either more general matter distribution scenarios (such as superposition or entangled excitation state) or different interaction types. In particular, it's worth investigating if there exists a type of the interaction between the detector and the field that reproduces exactly non-relativistic probability result. Finally, we notice that it's also interesting to explore how are the entanglement properties of the field influenced by the matter presence as seen by a pair of the UDW detectors, which we postpone to the future work.

Appendix A

Section A.1

Derivation of the model Hamiltonian

Starting from the Lagrangian in Eq. (3.10) and performing a Legendre transformation, the Hamiltonian for the model can be found as

$$H = \int_0^L dx \left[\frac{\pi_z(x,t)^2}{2\rho_m WT} + \frac{F}{2}\left(\frac{\partial u_z}{\partial x}\right)^2 \right] + \frac{Q^2}{2\mathsf{C}[u_z]} + \frac{\Phi^2}{2\mathsf{L}}, \tag{A.1}$$

where Q and π are the corresponding conjugate momenta for the flux and the displacement field:

$$Q = \frac{\delta L}{\delta \dot{\Phi}}, \tag{A.2a}$$

$$\pi_z = \frac{\delta L}{\delta \dot{u}_z}. \tag{A.2b}$$

Since we require that both ends of the strip are fixed with an applied tensile force F, the field u_z then satisfies the boundary condition: $u_z(0) = u_z(L) = 0$, and we can

expand it in the normal mode basis as

$$u_z(x,t) = \sum_{i=1}^{\infty} x_i(t) u_i(x), \tag{A.3}$$

where $u_i(x) = \sin\left(\frac{\pi i x}{L}\right)$, $i = 1, 2, \ldots$. Substituting Eq. (A.3) into Eq. (A.1), the strip Hamiltonian takes the independent harmonic oscillator form:

$$H = \sum_i \left(\frac{1}{2m} p_i^2 + \frac{1}{2} m \omega_i^2 x_i^2 \right) + \frac{Q^2}{2\mathsf{C}} + \frac{\Phi^2}{2\mathsf{L}}, \tag{A.4}$$

where $p_i = m\frac{dx_i}{dt}$, m is the mechanical mode effective strip mass:

$$m = \frac{1}{2}\rho_m W T L, \tag{A.5}$$

and ω_i is the normal mode frequency:

$$\omega_i = \frac{\pi i}{L}\sqrt{\frac{F}{\rho_m W T}}. \tag{A.6}$$

Quantization proceeds by promoting the coordinates Φ, x_i and their conjugate momenta into operators and imposing the usual commutation rules. Introducing the creation/annihilation operators defined by

$$Q = -i\left(\frac{\hbar}{2}\sqrt{\frac{\mathsf{C}}{\mathsf{L}}}\right)^{1/2}(a - a^\dagger), \tag{A.7a}$$

$$\Phi = \left(\frac{\hbar}{2}\sqrt{\frac{\mathsf{L}}{\mathsf{C}}}\right)^{1/2}(a + a^\dagger), \tag{A.7b}$$

$$x_i = \left(\frac{\hbar}{2m\omega_i}\right)^{1/2}(b_i + b_i^\dagger), \tag{A.7c}$$

$$p_i = -i\left(\frac{m\hbar\omega_i}{2}\right)^{1/2}(b_i - b_i^\dagger), \tag{A.7d}$$

the Hamiltonian simplifies to

$$H = \hbar\Omega\left(a^\dagger a + \frac{1}{2}\right) + \sum_n \hbar\omega_i\left(b_i^\dagger b_i + \frac{1}{2}\right), \tag{A.8}$$

where $\Omega = 1/\sqrt{\mathsf{LC}}$; both Ω and the creation/annihilation operators $a^\dagger$, a are functionals of the elastic strip displacement field u_z through their dependence on the strip capacitance $C[u_z]$.

Section A.2

Derivation of the coupling constant λ_i

In order to obtain the optomechanical coupling between the LC circuit and the mechanical mode, we expand Ω to first order in the normal mode displacement coordinates:

$$\begin{aligned}\Omega &\approx \Omega_0 + \sum_i \left.\frac{\partial\Omega}{\partial x_i}\right|_{x_i=0} x_i \\ &= \frac{1}{\sqrt{\mathsf{LC}_0}} - \sum_i \frac{\Omega_0}{2\mathsf{C}_0}\left.\frac{\partial\mathsf{C}}{\partial x_i}\right|_{x_i=0}\left(\frac{\hbar}{2m\omega_i}\right)^{1/2}(b_i + b_i^\dagger) \\ &= \frac{1}{\sqrt{\mathsf{LC}_0}} + \sum_i \Omega_0\lambda_i(b_n + b_n^\dagger),\end{aligned} \tag{A.9}$$

where we define the coupling constant λ_i through the last line of Eq. (A.9). To be consistent with this linear approximation, we must also expand to first order the LC oscillator creation/annihilation operators in the displacement coordinates. This results in additional interaction terms of the form $a^2(b_i + b_i^\dagger)$ and $a^{\dagger 2}(b_i + b_i^\dagger)$, which are usually neglected through the so-called 'rotating wave approximation' [201], hence resulting in the Hamiltonian (4.3).

In order to determine the explicit form of the coupling constant λ_i, we require the mode coordinate derivative of the capacitance. Assuming a positive charge $+Q$

placed on the upper conductor of the capacitor and a negative charge $-Q$ placed on the lower conductor, the electric field between the conductors can be found by solving the Laplace equation for the electric potential ϕ:

$$\frac{\partial^2 \phi}{\partial z^2} = 0, \tag{A.10}$$

where we neglect edge effects and approximate the electric field to be along the z direction within the capacitor. With the lower strip at $z = -d$ and upper strip at $z = u_z(x)$, the boundary conditions for the electric potential are

$$\phi(x, z = -d) = V_l, \tag{A.11a}$$

$$\phi(x, z = u_z(x)) = V_u, \tag{A.11b}$$

where V_l, V_u are the voltages on the lower and upper conductors. Since the displacement field u_z is assumed to be much smaller than d_0, we can write the electric potential as a series expansion $\phi = \phi^{(0)} + \phi^{(1)} + ...$ Substituting this series into the boundary conditions (A.11), we have:

$$\phi^{(0)}(x, -d) = V_l, \tag{A.12a}$$

$$\phi^{(0)}(x, 0) = V_u, \tag{A.12b}$$

and

$$\phi^{(1)}(x, -d) = 0, \tag{A.13a}$$

$$\phi^{(1)}(x, 0) = -\frac{\partial \phi^{(0)}(x, z)}{\partial z}\bigg|_{z=0} u_z(x). \tag{A.13b}$$

Solving the Laplace equation for $\phi^{(0)}$ and $\phi^{(1)}$, and taking the gradient, we obtain

the electric field:

$$\begin{aligned}\mathbf{E} &= -\nabla\left(\phi^{(0)} + \phi^{(1)}\right) \\ &= -\frac{\Delta V}{d}\left(1 - \frac{u_z(x)}{d}\right)\hat{z},\end{aligned} \tag{A.14}$$

where $\Delta V = V_u - V_l$. In order to determine the relationship between the charge Q and the voltage difference ΔV, we apply Gauss's law to a surface that just encloses the upper surface charge and we have:

$$\begin{aligned}Q =& \frac{\epsilon_0 \Delta V W \Delta L}{d} - \frac{\epsilon_0 \Delta V W}{d^2}\int_{\frac{L-\Delta L}{2}}^{\frac{L+\Delta L}{2}} dx u_z(x) \\ =& \mathsf{C}_0 \Delta V - \frac{\mathsf{C}_0}{\Delta L d}\int_{\frac{L-\Delta L}{2}}^{\frac{L+\Delta L}{2}} dx u_z(x).\end{aligned} \tag{A.15}$$

With Eq. (A.15), we have the expression for the capacitance:

$$\mathsf{C} = \frac{Q}{\Delta V} = \mathsf{C}_0 - \frac{1}{\Delta L d}\int_{\frac{L-\Delta L}{2}}^{\frac{L+\Delta L}{2}} dx u_z(x). \tag{A.16}$$

Using the expansion for the displacement field Eq. (A.3) and substituting Eq. (A.16) into Eq. (A.9), we find

$$\lambda_i = -\frac{L}{\pi i d \Delta L}\operatorname{sinc}\left(\frac{\pi i \Delta L}{2L}\right)\sin\left(\frac{\pi i}{2}\right)\left(\frac{\hbar}{2m\omega_i}\right)^{1/2}, \tag{A.17}$$

where $\operatorname{sinc} x \coloneqq \sin x / x$. Expressing the coupling constant λ_i in a frequency dependent form, we finally have the expression for λ_i given by Eq. (3.12):

$$\lambda_i = -\frac{1}{2d}\operatorname{sinc}\left(\frac{\omega_i}{\omega_u}\right)\sin\left(\frac{\pi i}{2}\right)\left(\frac{\hbar}{2m\omega_i}\right)^{1/2}, \tag{A.18}$$

where the upper cut-off frequency is

$$\omega_u = \frac{2}{\Delta L}\sqrt{\frac{F}{\rho_m W T}}. \tag{A.19}$$

Section A.3

Derivation of the strip length condition

From Eq. (A.9), we have:

$$\Omega \approx \Omega_0 + \sum_i \Omega_0 \lambda_i \left(\frac{2m\omega_n}{\hbar}\right)^{1/2} x_n. \tag{A.20}$$

Requiring that the variance of the capacitor frequency to be small compared with the square of its bare frequency Ω_0^2, we have:

$$\left\langle \left(\sum_i \Omega_0 \lambda_i \left(\frac{2m\omega_i}{\hbar}\right)^{1/2} x_i \right)^2 \right\rangle \ll \Omega_0^2. \tag{A.21}$$

For a thermal harmonic oscillator with mass m and frequency ω, the variance for x is:

$$\langle x^2 \rangle = \frac{\hbar}{2m\omega} \coth\left(\frac{\beta\hbar\omega}{2}\right), \tag{A.22}$$

so that Eq. (A.21) becomes

$$\sum_i \lambda_i^2 \coth\left(\frac{\beta\hbar\omega_i}{2}\right) \ll 1, \tag{A.23}$$

where we use the fact that different mechanical modes are statistically independent. Substituting the expression (3.12) for λ_i into Eq. (A.21), we obtain condition (3.17):

$$\sum_i \frac{\hbar}{8m\omega_i d^2} \operatorname{sinc}^2\left(\frac{\omega_i}{\omega_u}\right) \sin^2\left(\frac{\pi i}{2}\right)^2 \coth\left(\frac{\beta\hbar\omega_i}{2}\right) \ll 1. \tag{A.24}$$

Appendix B

Section B.1

Derivation of gravitational wave spacetime Wightman function

Consider a massless scalar field $\phi(\mathsf{x}) = \phi(u, v, x, y)$ in a gravitational wave background satisfying the Klein-Gordon equation $\Box\phi(x) = 0$ in Eq. (5.2). The Klein-Gordon equation is separable in the coordinates (u, v, x, y) and an arbitrary solution can be expanded in the complete set of mode functions

$$u_{\vec{k}}(u, v, x, y) = \frac{\gamma^{-1}(u)}{\sqrt{2k_-}(2\pi)^{3/2}} \exp\left[ik_x x + ik_y y - ik_- v - \frac{i}{4k_-}\int_0^u du\, g^{ab}k_a k_b\right]. \tag{B.1}$$

where $\gamma(u) := (1 - A^2\cos\omega u)^{1/4}$ and the integral evaluates to

$$\begin{aligned}\int_0^u du\, g^{ab}k_a k_b &= \int_0^u du\, \left[k_x^2(1 - A\cos\omega u) + k_y^2(1 + A\cos\omega u)\right] \\ &= \left(k_x^2 + k_y^2\right)u - \left(k_x^2 - k_y^2\right)\frac{A}{\omega}\sin\omega u.\end{aligned} \tag{B.2}$$

These mode functions are normalized and orthogonal to one another with respect to the usual Klein-Gordon inner product [149, 150]. The Wightman function $W(x,x') \coloneqq \langle 0|\phi(x)\phi(x')|0\rangle$ can be expressed in terms of these mode as

$$\begin{aligned} W(\mathsf{x},\mathsf{x}') &= \int d\vec{k}\, u_{\vec{k}}(u,v,x,y), u^*_{\vec{k}'}(u',v',x',y') \\ &= \int d\vec{k} \frac{\gamma^{-1}(u)\gamma^{-1}(u')}{(2\pi)^3 2k_-} e^{ik_x\Delta x + ik_y\Delta y - ik_-\Delta v - \frac{i}{4k_-}(k_x^2+k_y^2)\Delta u + \frac{i}{4k_-}(k_x^2-k_y^2)\frac{A}{\omega}(\sin\omega u - \sin\omega u')} \\ &= \int d\vec{k} \frac{\gamma^{-1}(u)\gamma^{-1}(u')}{(2\pi)^3 2k_-} e^{ik_x\Delta x + ik_y\Delta y - ik_-\Delta v - \frac{ik_x^2}{4k_-}\left[\Delta u - \frac{2A}{\omega}\sin\left(\omega\frac{\Delta u}{2}\right)\cos\left(\omega\frac{u+u'}{2}\right)\right]} \\ &\quad \times e^{-\frac{ik_y^2}{4k_-}\left[\Delta u + \frac{2A}{\omega}\sin\left(\frac{\Delta u}{2}\right)\cos\left(\frac{u+u'}{2}\right)\right]}. \end{aligned} \tag{B.3}$$

Expanding to leading order in A yields

$$\begin{aligned} W(\mathsf{x},\mathsf{x}') = \int \frac{d\mathsf{k}}{(2\pi)^3 2k_-} e^{ik_x\Delta x + ik_y\Delta y - ik_-\Delta v - \frac{i}{4k_-}(k_x^2+k_y^2)\Delta u} \\ \times \left[1 + \frac{iA}{2\omega}\frac{k_x^2-k_y^2}{k_-}\sin\left(\tfrac{\omega}{2}\Delta u\right)\cos\left(\tfrac{\omega}{2}[u+u']\right)\right]. \end{aligned} \tag{B.4}$$

The first term yields the Minkowski space Wightman function

$$W_{\mathcal{M}}(\mathsf{x},\mathsf{x}') = \frac{1}{4\pi i\Delta u}\delta\left(\frac{\sigma_{\mathcal{M}}(\mathsf{x},\mathsf{x}')}{\Delta u}\right) + \mathrm{PV}\,\frac{1}{4\pi^2\sigma_{\mathcal{M}}(\mathsf{x},\mathsf{x}')}, \tag{B.5}$$

and the second term evaluates to

$$\begin{aligned} W_{\mathrm{GW}}(\mathsf{x},\mathsf{x}') &= \frac{iA}{(2\pi)^3 4\omega}\sin\left(\tfrac{\omega}{2}\Delta u\right)\cos\left(\tfrac{\omega}{2}[u+u']\right) \\ &\quad \times \int dk_x dk_y dk_- \, e^{ik_x\Delta x + ik_y\Delta y - ik_-\Delta v - \frac{i}{4k_-}(k_x^2+k_y^2)\Delta u}\frac{k_x^2-k_y^2}{k_-^2} \\ &= \frac{A}{2\omega\pi^2}\frac{\Delta x^2-\Delta y^2}{\Delta u^3}\sin\frac{\omega\Delta u}{2}\cos\frac{\omega(u+u')}{2}\int dk_- k_- e^{ik_-\left(-\Delta v + \frac{\Delta x^2}{\Delta u} + \frac{\Delta y^2}{\Delta u}\right)}. \end{aligned} \tag{B.6}$$

To evaluate the last integral, consider a function $f = f(x)$ and the following integral

$$\int_0^\infty dx\, x e^{ifx} = -i\frac{d}{df}\int_0^\infty dx\, e^{ifx} = -i\frac{d}{df}\left[\pi\delta(f) + \mathrm{PV}\,\frac{i}{f}\right] = -\left[i\delta'(f) + \mathrm{PV}\,\frac{1}{f^2}\right]. \quad \text{(B.7)}$$

Then, the gravitational wave Wightman function becomes

$$W_{\mathrm{GW}}(\mathsf{x},\mathsf{x}') = -\frac{A}{4\pi^2}\frac{\sin\left(\frac{\omega}{2}\Delta u\right)}{\frac{\omega}{2}\Delta u}\cos\left(\tfrac{\omega}{2}[u+u']\right)\frac{\Delta x^2 - \Delta y^2}{\Delta u^2} \times\left[i\pi\delta'\left(\frac{\sigma_{\mathcal{M}}(\mathsf{x},\mathsf{x}')}{\Delta u}\right) + \mathrm{PV}\,\frac{\Delta u^2}{\sigma^2_{\mathcal{M}}(\mathsf{x},\mathsf{x}')}\right]. \quad \text{(B.8)}$$

Section B.2

Computing P, X and C

Derivation of P

Recall from Eq. (5.9) that the probability P for a detector to transition from its ground state to its excited state to leading order in the interaction strength is

$$P = \lambda^2 \int dt dt'\, \chi(t)\chi(t') e^{-i\Omega(t-t')} W(\mathsf{x}_D(t), \mathsf{x}_D(t'))\,, \quad \text{(B.9)}$$

Substituting in the explicit form of the switching functions, it follows that

$$P = \lambda^2 \int dt \int dt' e^{-\frac{(t-t_0)^2+(t'-t_0)^2}{2\sigma^2}} e^{-i\Omega(t-t')} W(\mathsf{x}(t), \mathsf{x}(t')). \quad \text{(B.10)}$$

Consider the trajectory of a single detector in Eq. (5.10); since $\Delta x = \Delta y = 0$, we immediately see that the gravitational wave contribution to the Wightman function in Eq. (5.7) vanishes. Thus, the transition probability of a single detector is unaffected by the presence of a gravitational wave. To evaluate the transition probability, consider

the change of variable $a := \Delta t = t - t'$ and $b := t + t'$, yielding

$$\begin{aligned} P &= \frac{1}{2}\lambda^2 \int da \int db\, e^{-\frac{a^2+(b-2t_0)^2}{4\sigma^2}} e^{-i\Omega a}\left[\frac{1}{4\pi i a}\delta(-a) + \mathrm{PV}\,\frac{1}{4\pi^2(-a^2)}\right] \\ &= \lambda^2\sigma\sqrt{\pi}\int da\, e^{\frac{-a^2}{4\sigma^2}} e^{-i\Omega a}\left[\frac{1}{4\pi i a}\delta(a) + \mathrm{PV}\,\frac{1}{4\pi^2(-a^2)}\right] \\ &= \lambda^2\sigma\sqrt{\pi}\left[\frac{-\Omega}{4\pi} + \frac{1}{4\pi\sqrt{\pi}\sigma}e^{-\sigma^2\Omega^2} + \frac{\Omega\,\mathrm{erf}(\sigma\Omega)}{4\pi}\right] \\ &= \frac{\lambda^2}{4\pi}\left[e^{-\sigma^2\Omega^2} - \sqrt{\pi}\sigma\Omega\,\mathrm{erfc}(\sigma\Omega)\right]. \end{aligned} \tag{B.11}$$

The second last equality follows from the distribution identities: $\frac{\delta(x)}{x} = -\delta'(x)$ and

$$\mathrm{PV}\int_\infty^\infty dx\,\frac{f(x)}{x^2} = \int_0^\infty dx\,\frac{f(x)+f(-x)-2f(0)}{x^2}, \tag{B.12}$$

where it is assumed $f(x)$ reaches 0 as $x \to \pm\infty$.

Derivation of $X_{\mathcal{M}}$

The matrix element is given by

$$\begin{aligned} X_{\mathcal{M}} = -\lambda^2 \int_{-\infty}^{\infty} dt \int_{-\infty}^{t} dt'\, e^{-\frac{(t-t_0)^2+(t'-t_0)^2}{2\sigma^2}} e^{-i\Omega(t+t')} \\ \times \left[W_{\mathcal{M}}(\mathsf{x}_A(t'),\mathsf{x}_B(t)) + W_{\mathcal{M}}(\mathsf{x}_B(t'),\mathsf{x}_A(t))\right]. \end{aligned} \tag{B.13}$$

The Wightman function for Minkowski space for our trajectories becomes

$$W_{\mathcal{M}}(\mathsf{x}_A(t'),\mathsf{x}_B(t)) = -\frac{1}{4\pi i\Delta t}\delta\left(\Delta t - \frac{D^2}{\Delta t}\right) + \mathrm{PV}\,\frac{1}{4\pi^2(-\Delta t^2 + D^2)}. \tag{B.14}$$

By changing variables to $a = \Delta t, b = t + t'$, we find the matrix element X in Minkowski

space

$$
\begin{aligned}
X_{\mathcal{M}} &= -2\lambda^2 \int_{-\infty}^{\infty} dt \int_{-\infty}^{t} dt'\, e^{-\frac{(t-t_0)^2+(t'-t_0)^2}{2\sigma^2}} e^{-i\Omega(t+t')} \\
&\quad \times \left[-\frac{1}{4\pi i \Delta t} \delta\left(\Delta t - \frac{D^2}{\Delta t}\right) + \mathrm{PV}\, \frac{1}{4\pi^2(-\Delta t^2 + D^2)} \right] \\
&= -\lambda^2 \int_{-\infty}^{\infty} db e^{-\frac{(b-2t_0)^2}{4\sigma^2} - i\Omega b} \int_0^{\infty} da\, e^{-\frac{a^2}{4\sigma^2}} \left[\frac{1}{4\pi i a} \delta\left(a - \frac{D^2}{a}\right) + \mathrm{PV}\, \frac{1}{4\pi^2(a^2 - D^2)} \right] \\
&= 2\sigma\sqrt{\pi}\lambda^2 e^{-\Omega^2\sigma^2 - 2i\Omega t_0} \int_0^{\infty} da\, e^{-\frac{a^2}{4\sigma^2}} \left[\frac{1}{4\pi i a} \delta\left(a - \frac{D^2}{a}\right) + \mathrm{PV}\, \frac{1}{4\pi^2(a^2 - D^2)} \right] \\
&= i\frac{\lambda^2\sigma}{4D\sqrt{\pi}} e^{-\sigma^2\Omega^2 - 2i\Omega t_0 - \frac{D^2}{4\sigma^2}} \left[\mathrm{erf}\left(i\frac{D}{2\sigma}\right) - 1 \right]. \qquad \text{(B.15)}
\end{aligned}
$$

where the principal value integration was evaluated using methods similar to those in [141].

Derivation of X_{GW}

The matrix element X is given by [118, 123, 141, 139]

$$
X_{\mathrm{GW}} = -\lambda^2 \int_{-\infty}^{\infty} dt \int_{-\infty}^{t} dt'\, e^{-\frac{t^2+t'^2}{2\sigma^2}} e^{-i\Omega(t+t')} \left[W_{\mathrm{GW}}(\mathsf{x}_A(t'), \mathsf{x}_B(t)) + W_{\mathrm{GW}}(\mathsf{x}_B(t'), \mathsf{x}_A(t)) \right].
$$

From Eq. (5.13), it is seen that $\sigma_{\mathcal{M}}(\mathsf{x}_A(t'), \mathsf{x}_B(t)) = \sigma_{\mathcal{M}}(\mathsf{x}_B(t'), \mathsf{x}_A(t)) = -\Delta t^2 + D^2$. It follows

$$
\begin{aligned}
&W_{\mathrm{GW}}(\mathsf{x}_A(t'), \mathsf{x}_B(t)) = W_{\mathrm{GW}}(\mathsf{x}_B(t'), \mathsf{x}_A(t)) \\
&= -\frac{A}{4\pi^2} \frac{\sin\left(\frac{\omega}{2}\Delta t\right)}{\frac{\omega}{2}\Delta t} \cos\left(\tfrac{\omega}{2}[t+t']\right) \frac{D^2}{\Delta t^2} \left[i\pi\delta'\left(\Delta t - \frac{D^2}{\Delta t}\right) + \mathrm{PV}\left(\frac{\Delta t}{D^2 - \Delta t^2}\right)^2 \right]. \qquad \text{(B.16)}
\end{aligned}
$$

which we note is invariant under $t \leftrightarrow t'$. It follows that X may be expressed as

$$\begin{aligned} X_{\mathrm{GW}} =& A\frac{\lambda^2 D^2}{2\pi^2}\int_{-\infty}^{\infty} dt \int_{-\infty}^{t} dt'\, e^{-i\Omega(t'+t)} e^{-\frac{(t'+t-2t_0)^2}{4\sigma^2}} \cos\left(\tfrac{\omega}{2}[t+t']\right) \\ &\times \frac{e^{-\frac{\Delta t^2}{4\sigma^2}}}{\Delta t^2} \frac{\sin\left(\frac{\omega}{2}\Delta t\right)}{\frac{\omega}{2}\Delta t}\left[i\pi\delta'\left(\Delta t - \frac{D^2}{\Delta t}\right) + \mathrm{PV}\left(\frac{\Delta t}{D^2-\Delta t^2}\right)^2\right]. \end{aligned} \tag{B.17}$$

Changing integration variables to $a \coloneqq \Delta t$ and $b \coloneqq t' + t$, yields

$$\begin{aligned} X_{\mathrm{GW}} =& \frac{A\lambda^2 D^2}{4\pi^2}\int_{-\infty}^{\infty} db\, e^{-i\Omega b} e^{-\frac{(b-2t_0)^2}{4\sigma^2}} \cos\left(\tfrac{\omega}{2}b\right) \int_0^{\infty} da\, \frac{e^{-\frac{a^2}{4\sigma^2}}}{a^2} \frac{\sin\left(\frac{\omega}{2}a\right)}{\frac{\omega}{2}a} \\ &\times \left[i\pi\delta'\left(a - \frac{D^2}{a}\right) + \mathrm{PV}\left(\frac{a}{D^2-a^2}\right)^2\right] \\ =& \frac{A\lambda^2 D^2}{2\pi^2}\sqrt{\pi}\sigma e^{-\left(\frac{\sigma^2\omega^2}{4}+\sigma^2\Omega^2\right)} e^{-2it_0\Omega} \cosh\left(\omega\Omega\sigma^2 - it_0\omega\right) \\ &\times \int_0^{\infty} da\, \frac{e^{-\frac{a^2}{4\sigma^2}}}{a^2} \frac{\sin\left(\frac{\omega}{2}a\right)}{\frac{\omega}{2}a}\left[i\pi\delta'\left(a - \frac{D^2}{a}\right) + \mathrm{PV}\left(\frac{a}{D^2-a^2}\right)^2\right] \\ =& \frac{A\lambda^2}{2D^2\pi^2}\sqrt{\pi}\sigma e^{-\left(\frac{\sigma^2\omega^2}{4}+\sigma^2\Omega^2+2it_0\Omega\right)} \cosh\left(\omega\Omega\sigma^2 - it_0\omega\right)(I_1 + I_2), \end{aligned} \tag{B.18}$$

where the last equality defines the I_1 and I_2 that remain to be evaluated. To evaluate the first integral in Eq. (B.18), note that

$$\frac{d}{da}\delta\left(a - \frac{D^2}{a}\right) = \delta'\left(a - \frac{D^2}{a}\right)\left(\frac{D^2}{a^2}+1\right) \implies \delta'\left(a - \frac{D^2}{a}\right) = \left[\frac{d}{da}\delta\left(a - \frac{D^2}{a}\right)\right]\left(\frac{D^2}{a^2}+1\right)^{-1}. \tag{B.19}$$

Then,

$$\begin{aligned}
I_1 &:= iD^4\pi \int_0^\infty da\, \frac{e^{-\frac{a^2}{4\sigma^2}}}{a^2} \frac{\sin\left(\frac{\omega}{2}a\right)}{\frac{\omega}{2}a} \delta'\left(a - \frac{D^2}{a}\right) \\
&= iD^4\pi \int_0^\infty da \left[\frac{d}{da}\delta\left(a - \frac{D^2}{a}\right)\right]\left(\frac{D^2}{a^2}+1\right)^{-1} \frac{e^{-\frac{a^2}{4\sigma^2}}}{a^2} \frac{\sin\left(\frac{\omega}{2}a\right)}{\frac{\omega}{2}a} \\
&= -iD^4\pi \int_0^\infty da\, \delta\left(\frac{D^2}{a} - a\right) \frac{d}{da}\left[\left(\frac{D^2}{a^2}+1\right)^{-1} \frac{e^{-\frac{a^2}{4\sigma^2}}}{a^2} \frac{\sin\left(\frac{\omega}{2}a\right)}{\frac{\omega}{2}a}\right] \\
&= -iD^4\pi \int_0^\infty da\, \frac{\delta(D-a)}{2} \frac{d}{da}\left[\left(\frac{D^2}{a^2}+1\right)^{-1} \frac{e^{-\frac{a^2}{4\sigma^2}}}{a^2} \frac{\sin\left(\frac{\omega}{2}a\right)}{\frac{\omega}{2}a}\right] \\
&= i\frac{\pi e^{-\frac{D^2}{4\sigma^2}}}{\omega}\left[\left(\frac{D^2}{4\sigma^2}+1\right)\sin\left(\tfrac{\omega}{2}D\right) - \frac{D\omega}{4}\cos\left(\tfrac{\omega}{2}D\right)\right].
\end{aligned} \tag{B.20}$$

Next, evaluating the second integral in Eq. B.18 yields

$$\begin{aligned}
I_2 &:= D^4\,\mathrm{PV}\int_0^\infty da\, e^{-\frac{a^2}{4\sigma^2}} \frac{\sin\left(\frac{\omega}{2}a\right)}{\frac{\omega}{2}a}\left(D^2-a^2\right)^{-2} \\
&= D^4\,\mathrm{PV}\int_{-\infty}^\infty da\, e^{-\frac{a^2}{4\sigma^2}} \frac{\sin\left(\frac{\omega}{2}a\right)}{\omega a}\left(D^2-a^2\right)^{-2} \\
&= \frac{D^4}{\omega}\,\mathrm{PV}\int_{-\infty}^\infty da\, e^{-\frac{a^2}{4\sigma^2}} \sin\left(\tfrac{\omega}{2}a\right)\int_{-\infty}^\infty d\bar{a}\,\delta(\bar{a}-a)\frac{1}{\bar{a}(\bar{a}^2-D^2)^2} \\
&= \frac{D^4}{\omega}\,\mathrm{PV}\int_{-\infty}^\infty da\, e^{-\frac{a^2}{4\sigma^2}} \sin\left(\tfrac{\omega}{2}a\right)\int_{-\infty}^\infty d\bar{a}\left(\frac{1}{2\pi}\int_{-\infty}^\infty ds\, e^{i(\bar{a}-a)s}\right)\frac{1}{\bar{a}(\bar{a}^2-D^2)^2} \\
&= \frac{D^4}{2\pi\omega}\,\mathrm{PV}\int_{-\infty}^\infty ds\left[\int_{-\infty}^\infty da\, e^{-ias}e^{-\frac{a^2}{4\sigma^2}}\sin\left(\tfrac{\omega}{2}a\right)\right]\left[\int_{-\infty}^\infty d\bar{a}\, e^{i\bar{a}s}\frac{1}{\bar{a}(\bar{a}^2-D^2)^2}\right] \\
&= \frac{\sqrt{\pi}\sigma}{2\omega}e^{-\left(\frac{\sigma\omega}{2}\right)^2}\int_{-\infty}^\infty ds\ \mathrm{sgn}(s)\, e^{-\sigma^2s^2}\sinh\left(\sigma^2\omega s\right)\left[2-2\cos(Ds)-Ds\sin(Ds)\right] \\
&= \frac{\pi}{\omega}\left(\mathrm{erf}\left(\frac{\sigma\omega}{2}\right) - e^{-\frac{D^2}{4\sigma^2}}\,\mathrm{Re}\left[e^{i\frac{\omega}{2}D}\left(1+\frac{D^2}{4\sigma^2}-i\frac{D\omega}{4}\right)\mathrm{erf}\left(\frac{\omega}{2}\sigma+\frac{iD}{2\sigma}\right)\right]\right).
\end{aligned} \tag{B.21}$$

Derivation of $C_{\mathcal{M}}$

The expression for $C_{\mathcal{M}}$ is the following

$$C_{\mathcal{M}} = \lambda^2\int_{-\infty}^\infty dt\int_{-\infty}^\infty dt'\, e^{-\frac{(t-t_0)^2+(t'-t_0)^2}{2\sigma^2}} e^{i\Omega(t-t')}W_{\mathcal{M}}(\mathsf{x}_A(t'),\mathsf{x}_B(t)). \tag{B.22}$$

By plugging in the Wightman function in Minkowski space for the trajectories of the detectors and then changing variables to $a = \Delta t, b = t + t'$, we obtain

$$\begin{aligned}
C_{\mathcal{M}} &= \frac{\lambda^2}{2}\int_{-\infty}^{\infty} db e^{-\frac{(b-2t_0)^2}{4\sigma^2}} \int_{-\infty}^{\infty} da e^{-\frac{a^2}{4\sigma^2}+i\Omega a}\left[-\frac{1}{4\pi i a}\delta\left(a-\frac{D^2}{a}\right)+\mathrm{PV}\,\frac{1}{4\pi^2(-a^2+D^2)}\right] \\
&= -\sigma\sqrt{\pi}\lambda^2\int_{-\infty}^{\infty} da e^{-\frac{a^2}{4\sigma^2}+i\Omega a}\left[\frac{1}{4\pi i a}\delta\left(a-\frac{D^2}{a}\right)+\mathrm{PV}\,\frac{1}{4\pi^2(a^2-D^2)}\right] \\
&= \sigma\sqrt{\pi}\lambda^2 e^{-\frac{D^2}{4\sigma^2}}\left[\frac{\sin(\Omega D)}{4D\pi}+\frac{1}{4D\pi}\mathrm{Re}\left(ie^{iD\Omega}\,\mathrm{erf}\left[i\frac{D}{2\sigma}+\sigma\Omega\right]\right)\right] \\
&= \frac{\sigma\lambda^2}{4D\sqrt{\pi}}e^{-\frac{D^2}{4\sigma^2}}\left(\mathrm{Im}\left[e^{iD\Omega}\,\mathrm{erf}\left(i\frac{D}{2\sigma}+\sigma\Omega\right)\right]-\sin\Omega D\right),
\end{aligned} \tag{B.23}$$

where the principal value integration was evaluated using methods similar to those in [141].

Derivation of C_{GW}

The expression for C_{GW} is given by [118, 123, 141, 139]

$$C_{\mathrm{GW}} = \lambda^2\int_{-\infty}^{\infty} dt\int_{-\infty}^{\infty} dt'\, e^{-\frac{(t-t_0)^2+(t'-t_0)^2}{2\sigma^2}} e^{i\Omega(t-t')} W_{\mathrm{GW}}(\mathsf{x}_A(t'),\mathsf{x}_B(t)). \tag{B.24}$$

Using Eq. (B.16) and changing integration variables to $a \coloneqq \Delta t$ and $b \coloneqq t+t'$, Eq. (B.24)

becomes

$$
\begin{aligned}
C_{\mathrm{GW}} &= -\frac{\lambda^2 A D^2}{4\pi^2}\int_{-\infty}^{\infty} dt \int_{-\infty}^{\infty} dt'\, e^{-\frac{\left(t+t'-2t_0\right)^2}{4\sigma^2}} \cos\left(\tfrac{\omega}{2}[t+t']\right) \\
&\quad \times e^{i\Omega\Delta t}\frac{e^{-\frac{\Delta t^2}{4\sigma^2}}}{\Delta t^2}\frac{\sin\left(\frac{\omega}{2}\Delta t\right)}{\frac{\omega}{2}\Delta t}\left[i\pi\delta'\left(\Delta t - \frac{D^2}{\Delta t}\right) + \mathrm{PV}\left(\frac{\Delta t}{D^2-\Delta t^2}\right)^2\right] \\
&= -\frac{\lambda^2 A D^2}{8\pi^2}\int_{-\infty}^{\infty} db\, e^{-\frac{(b-2t_0)^2}{4\sigma^2}} \cos\left(\tfrac{\omega}{2}b\right)\int_{-\infty}^{\infty} da\, e^{i\Omega a}\frac{e^{-\frac{a^2}{4\sigma^2}}}{a^2}\frac{\sin\left(\frac{\omega}{2}a\right)}{\frac{\omega}{2}a} \\
&\quad \times\left[i\pi\delta'\left(a - \frac{D^2}{a}\right) + \mathrm{PV}\left(\frac{a}{D^2-a^2}\right)^2\right] \\
&= -\frac{\lambda^2 A D^2}{8\pi^2}\left[2\sqrt{\pi}\sigma e^{-\left(\frac{\omega}{2}\sigma\right)^2}\cos\left(\omega t_0\right)\right]\int_{-\infty}^{\infty} da\, e^{i\Omega a}\frac{e^{-\frac{a^2}{4\sigma^2}}}{a^2}\frac{\sin\left(\frac{\omega}{2}a\right)}{\frac{\omega}{2}a} \\
&\quad \times\left[i\pi\delta'\left(a - \frac{D^2}{a}\right) + \mathrm{PV}\left(\frac{a}{D^2-a^2}\right)^2\right] \\
&= -\frac{\lambda^2 A\sigma}{4D^2\pi^{3/2}} e^{-\left(\frac{\omega}{2}\sigma\right)^2}\cos\left(\omega t_0\right)\left(I_3 + I_4\right), \qquad \text{(B.25)}
\end{aligned}
$$

where

$$
\begin{aligned}
I_3 &:= iD^4\pi\int_{-\infty}^{\infty} da\, e^{i\Omega a}\frac{e^{-\frac{a^2}{4\sigma^2}}}{a^2}\frac{\sin\left(\frac{\omega}{2}a\right)}{\frac{\omega}{2}a}\delta'\left(a - \frac{D^2}{a}\right) \\
&= iD^4\pi\int_{-\infty}^{\infty} da\, e^{i\Omega a}\frac{e^{-\frac{a^2}{4\sigma^2}}}{a^2}\frac{\sin\left(\frac{\omega}{2}a\right)}{\frac{\omega}{2}a}\left[\frac{d}{da}\delta\left(a - \frac{D^2}{a}\right)\right]\left(\frac{D^2}{a^2}+1\right)^{-1} \\
&= -iD^4\pi\int_{-\infty}^{\infty} da\,\delta\left(a - \frac{D^2}{a}\right)\frac{d}{da}\left[e^{i\Omega a}\frac{e^{-\frac{a^2}{4\sigma^2}}}{a^2}\frac{\sin\left(\frac{\omega}{2}a\right)}{\frac{\omega}{2}a}\left(\frac{D^2}{a^2}+1\right)^{-1}\right] \\
&= -iD^4\pi\int_{-\infty}^{\infty} da\,\frac{\delta\left(D+a\right)+\delta\left(D-a\right)}{2}\frac{d}{da}\left[e^{i\Omega a}\frac{e^{-\frac{a^2}{4\sigma^2}}}{a^2}\frac{\sin\left(\frac{\omega}{2}a\right)}{\frac{\omega}{2}a}\left(\frac{D^2}{a^2}+1\right)^{-1}\right] \\
&= \frac{\pi e^{-\frac{D^2}{4\sigma^2}}}{4\omega}\Bigg[\left(D\omega + 2D\Omega\right)\sin\left(D\left[\frac{\omega}{2}+\Omega\right]\right) + \left(D\omega - 2D\Omega\right)\sin\left(D\left[\frac{\omega}{2}-\Omega\right]\right) \\
&\quad + \left(\frac{D^2}{\sigma^2}+4\right)\left(\cos\left(D\left[\frac{\omega}{2}+\Omega\right]\right) - \cos\left(D\left[\frac{\omega}{2}-\Omega\right]\right)\right)\Bigg] \qquad \text{(B.26)}
\end{aligned}
$$

and

$$
\begin{aligned}
I_4 &\coloneqq D^4\,\mathrm{PV}\int_{-\infty}^{\infty} da\, e^{i\Omega a}\frac{\sin\left(\frac{\omega}{2}a\right)}{\frac{\omega}{2}a}\frac{e^{-\frac{a^2}{4\sigma^2}}}{\left(a^2-D^2\right)^2}\\
&= \frac{2D^4}{\omega}\,\mathrm{PV}\int_{-\infty}^{\infty} da\, e^{i\Omega a}\sin\left(\tfrac{\omega}{2}a\right)e^{-\frac{a^2}{4\sigma^2}}\int_{-\infty}^{\infty} d\bar{a}\,\delta(\bar{a}-a)\frac{1}{\bar{a}\left(\bar{a}^2-D^2\right)^2}\\
&= \frac{2D^4}{\omega}\,\mathrm{PV}\int_{-\infty}^{\infty} da\, e^{i\Omega a}\sin\left(\tfrac{\omega}{2}a\right)e^{-\frac{a^2}{4\sigma^2}}\int_{-\infty}^{\infty} d\bar{a}\left(\frac{1}{2\pi}\int_{-\infty}^{\infty} ds\, e^{i(\bar{a}-a)s}\right)\frac{1}{\bar{a}\left(\bar{a}^2-D^2\right)^2}\\
&= \frac{D^4}{\pi\omega}\,\mathrm{PV}\int_{-\infty}^{\infty} ds\int_{-\infty}^{\infty} da\, e^{i(\Omega-s)a}\sin\left(\tfrac{\omega}{2}a\right)e^{-\frac{a^2}{4\sigma^2}}\int_{-\infty}^{\infty} d\bar{a}\,\frac{e^{i\bar{a}s}}{\bar{a}\left(\bar{a}^2-D^2\right)^2}\\
&= \frac{\pi}{\omega}\left(\mathrm{erf}\left[\sigma\left(\frac{\omega}{2}-\Omega\right)\right]+\mathrm{erf}\left[\sigma\left(\frac{\omega}{2}+\Omega\right)\right]-e^{-\frac{D^2}{4\sigma^2}}\,\mathrm{Re}\left[Q_+R_+ + Q_-R_-\right]\right),
\end{aligned}
\tag{B.27}
$$

where we have defined $Q_\pm \coloneqq -ie^{iD\left(\frac{\omega}{2}\pm\Omega\right)}\,\mathrm{erf}\left[i\frac{D}{2\sigma}+\sigma\left(\frac{\omega}{2}\pm\Omega\right)\right]$ and $R_\pm \coloneqq \frac{D}{2}\left(\frac{\omega}{2}\pm\Omega\right)+i\left(1+\frac{D^2}{4\sigma^2}\right)$.

Section B.3

The effect of gravitational waves on vacuum correlations

In Sec. 5.3.3, the dependence of the concurrence on the properties of gravitational waves and detectors was investigated, which quantifies the harvested entanglement in the final state of the detectors and is interpreted as a proxy for field entanglement. However, these detectors also harvest classical correlations from the vacuum. Thus, to quantify the total correlations harvested by a pair of detectors, interpreted analogously as a proxy for correlations between the region in which detectors interact, the correlations between local energy measurements (i.e., measurements of σ_z) can be computed. Such correlations are quantified by the correlation function [139, 141]

$$
\mathrm{corr}\,\rho_{AB} \coloneqq \frac{|X|^2+|C|^2}{P}+\mathcal{O}\left(\lambda^4\right) = \Psi_{\mathcal{M}}+\Psi_{\mathrm{GW}}+\mathcal{O}(\lambda^4),
\tag{B.28}
$$

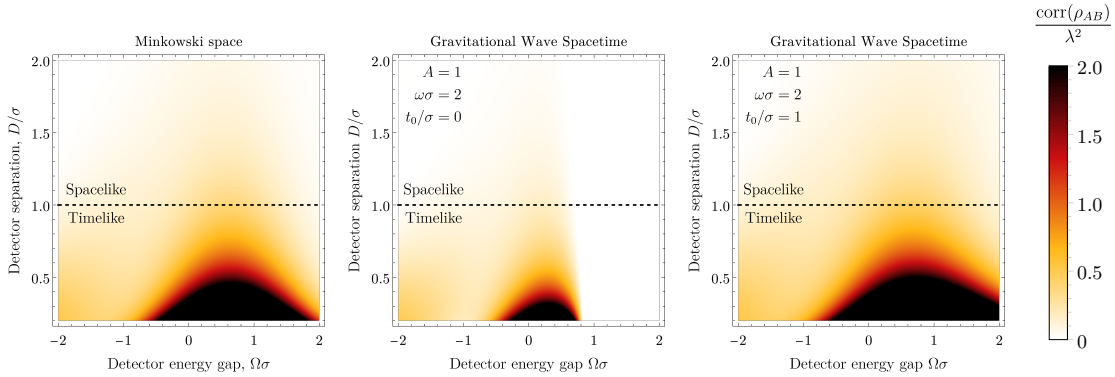

(a) (b) (c)

Figure B.1: The correlation function $\mathrm{corr}(\rho_{AB})/\lambda^2$ is plotted as a function of the detectors' energy $\Omega\sigma$ and the detectors' average proper separation D/σ for detectors in (a) Minkowski space and detectors in a gravitational wave spacetime for (b) $t = 0$ and (c) $t \neq 0$. Analogous to the concurrence, we see that correlations between two detectors can be degraded or amplified depending on the value of t_0

where in the second equality the correlation function has been expressed as a sum of the Minkowski space and gravitational wave contributions to the correlation function, defined respectively as

$$\Psi_{\mathcal{M}} \coloneqq \frac{|X_{\mathcal{M}}|^2 + |C_{\mathcal{M}}|^2}{P}, \tag{B.29}$$

$$\Psi_{\mathrm{GW}} \coloneqq 2\frac{\mathrm{Re}[X_{\mathrm{GW}}X^*_{\mathcal{M}}] + \mathrm{Re}[C_{\mathrm{GW}}C^*_{\mathcal{M}}]}{P}. \tag{B.30}$$

To examine the effect a gravitational wave has on the correlations harvested by the detectors, Fig. B.1 compares correlations between detectors in Minkowski space with detectors in a gravitational wave spacetime, revealing similar behaviour as the concurrence depicted in Fig. 5.1. The gravitational wave contribution to the correlation function Ψ_{GW} is plotted in Figs. B.2 and B.3 for $t_0 = 0$ and $t_0 \neq 0$, respectively. Similar to the concurrence, the correlation function exhibits a resonance around $\omega \approx 2\Omega$ and oscillatory behaviour for nonzero t_0.

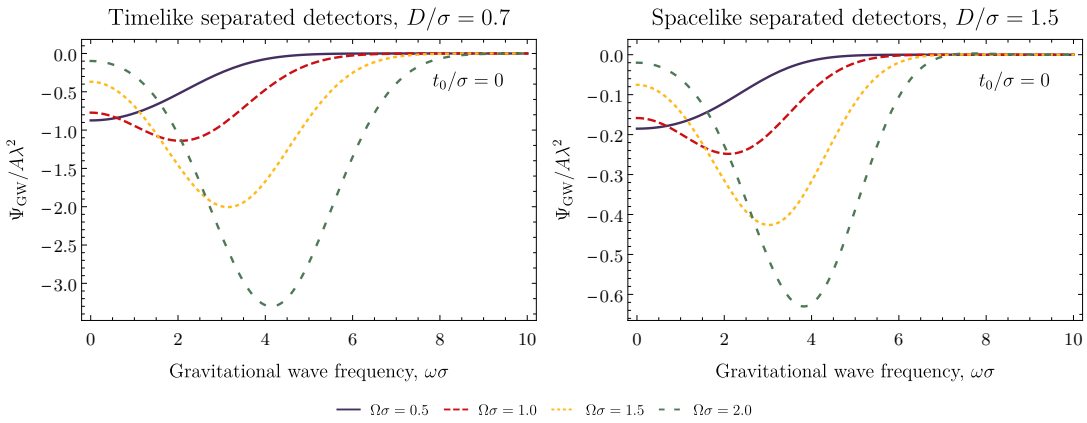

Figure B.2: The gravitational wave contribution $\Psi_{GW}/A\lambda^2$ to the correlation function is plotted as a function of the gravitational wave frequency $\omega\sigma$ for both timelike (*left*) and spacelike (*right*) separated detectors for $t_0/\sigma = 0$ for different values of the detectors energy $\Omega\sigma$. Similar to Θ_{GW}, Ψ_{GW} is always negative, which implies that detector correlations are always degraded for $t_0 = 0$.

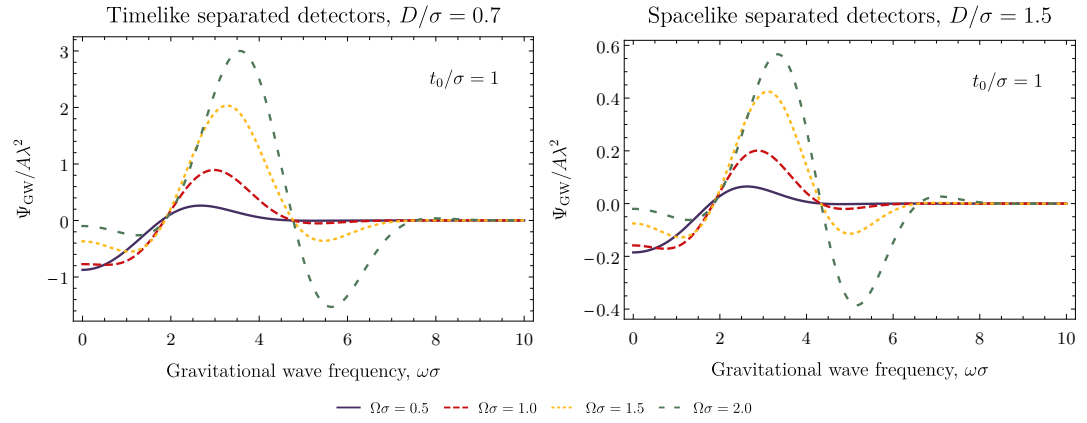

Figure B.3: The gravitational wave contribution $\Psi_{GW}/A\lambda^2$ to the correlation function is plotted as a function of the gravitational wave frequency $\omega\sigma$ for both timelike (*left*) and spacelike (*right*) separated detectors for $t_0/\sigma = 1$ for different values of the detectors energy $\Omega\sigma$. Similar to Θ_{GW}, Ψ_{GW} can be both positive and negative implying that a gravitational wave can amplify and degrade detector correlations.

Appendix C

Section C.1

Derivation of the two point function

The purpose of this section is twofold. We shall first derive the expectation value of ϕ^2 as in Eq. (6.5) and then calculate the two point function as in Eq. (6.14).

Using the expression of the initial field state in Eq. (6.4) and sandwiching two field operators in between, we have:

$$\begin{aligned}\langle\psi(0)|\phi(x,t)\,\phi(x',t')\,|\psi(0)\rangle = |N|^2 \int \frac{dk_1}{(2\pi)^{1/2}(2\omega_{k_1})^{1/2}} e^{-\frac{1}{2\sigma^2}(k_1-k_0)^2 - ik_1 r_0} \\ \int \frac{dk_2}{(2\pi)^{1/2}(2\omega_{k_2})^{1/2}} e^{-\frac{1}{2\sigma^2}(k_2-k_0)^2 + ik_2 r_0} \int \frac{dk}{(2\pi)^{1/2}(2\omega_k)^{1/2}} \int \frac{dk'}{(2\pi)^{1/2}(2\omega_{k'})^{1/2}} \\ \langle 0|a(k_2)\left(a(k)a^\dagger(k')e^{ix^\mu k_\mu - ix'^\mu k'_\mu} + a^\dagger(k)a(k')e^{ix'^\mu k'_\mu - ik_\mu x^\mu}\right)a^\dagger(k_1)|0\rangle. \end{aligned} \tag{C.1}$$

where we have dropped odd multiples of creation/anihilation operators since they give vanishing result. Using the commutation relation $[a(k), a^\dagger(k')] = \delta(k-k')$, the

expectation values of the operator products in Eq. (C.1) can be simplified to

$$\langle 0|a(k_2)a(k)a^\dagger(k')a^\dagger(k_1)|0\rangle = \delta(k-k')\delta(k_1-k_2) + \delta(k-k_1)\delta(k'-k_2), \tag{C.2}$$

and

$$\langle 0|a(k_2)a^\dagger(k)a(\mathbf{k}')a^\dagger(k_1)|0\rangle = \delta(k_1-k')\delta(k_2-k). \tag{C.3}$$

Substituting Eq. (C2) and Eq. (C3) into Eq. (C.1) we then have:

$$\begin{aligned}\langle\psi(0)|\phi(x,t)\,\phi(x',t')\,|\psi(0)\rangle &= |N|^2\int\frac{dk_1}{4\pi\omega_{k_1}}e^{-\frac{1}{\sigma^2}(k_1-k_0)^2}\int\frac{dk}{4\pi\omega_k}e^{ik_\mu(x-x')^\mu}\\ &+|N|^2\int\frac{dk_1}{4\pi\omega_{k_1}}e^{-\frac{1}{2\sigma^2}(k_1-k_0)^2-ik_1x_0+ik_{1\mu}x^\mu}\int\frac{dk_2}{4\pi\omega_{k_2}}e^{-\frac{1}{2\sigma^2}(k_2-k_0)^2+ik_2x_0-ik_{2\mu}x'^\mu}\\ &+|N|^2\int\frac{dk_1}{4\pi\omega_{k_1}}e^{-\frac{1}{2\sigma^2}(k_1-k_0)^2-ik_1x_0+ik_{1\mu}x'^\mu}\int\frac{dk_2}{4\pi\omega_{k_2}}e^{-\frac{1}{2\sigma^2}(k_2-k_0)^2+ik_2x_0-ik_{2\mu}x^\mu}.\end{aligned} \tag{C.4}$$

As can be easily checked, the first line of Eq. (C4) is just the vacuum Wightman function of the scalar field.

We now first derive the energy density term in Eq. (6.5). Setting $x = x'$ and $t = t'$, Eq. (C4) reduces to

$$\begin{aligned}\langle\psi(0)|\phi(x,t)\,\phi(x,t)\,|\psi(0)\rangle =&|N|^2\int\frac{dk_1}{4\pi\omega_{k_1}}e^{-\frac{1}{\sigma^2}(k_1-k_0)^2}\int\frac{dk}{4\pi\omega_k}\\ &+2|N|^2\left|\int\frac{dk_1}{4\pi\omega_{k_1}}e^{-\frac{1}{2\sigma^2}(k_1-k_0)^2-ik_1x_0+ik_{1\mu}x^\mu}\right|^2\end{aligned} \tag{C.5}$$

The first integral corresponds to the infinite vacuum energy term which we shall ignore. To evaluate the second integral, we employ the non-relativistic approximation by expanding the $\omega_k t$ phase terms to second order in k and making the approximation $\omega_k = m$ for the terms appearing in the denominators, the resulting approximate

Gaussian integral is

$$\langle\psi(0)|\phi(t,x)\,\phi(t,x)\,|\psi(0)\rangle = \frac{1}{m}\left[\frac{\sigma^2}{\pi\left(1+\left(\frac{\sigma^2 t}{m}\right)^2\right)}\right]^{\frac{1}{2}} \exp\left[-\sigma^2\frac{\left(x-x_0-\frac{k_0 t}{m}\right)^2}{1+\left(\frac{\sigma^2 t}{m}\right)^2}\right], \quad \text{(C.6)}$$

which is Eq. (6.5).

Next we calculate the pull back of the two-point function to the detector worldline which is given in Eq. (6.7). Replacing the operator $\phi(x,t)\,\phi(x',t')$ by $\phi(0,\tau)\,\phi(0,\tau')$ in Eq. (C4) and adopting the similar approximation methods, we have

$$\langle\psi(0)|\phi(0,\tau)\,\phi(0,\tau')\,|\psi(0)\rangle = W_v(\tau,\tau') + W_m(\tau,\tau'), \quad \text{(C.7)}$$

where $W_v(\tau,\tau')$ is given in Eq. (6.10) and $W_m(\tau,\tau')$ can be found as

$$\begin{aligned} W_m(\tau,\tau') =& \frac{1}{2\sqrt{\pi}m\sigma}\frac{e^{-im(\tau-\tau')-\frac{k_0^2}{\sigma^2}}}{\sqrt{\left(\frac{1}{\sigma^2}+\frac{i\tau}{m}\right)\left(\frac{1}{\sigma^2}-\frac{i\tau'}{m}\right)}}\exp\left(\frac{\left(\frac{k_0}{\sigma^2}-ix_0\right)^2}{2\left(\frac{1}{\sigma^2}+\frac{i\tau}{m}\right)}+\frac{\left(\frac{k_0}{\sigma^2}+ix_0\right)^2}{2\left(\frac{1}{\sigma^2}-\frac{i\tau'}{m}\right)}\right) \\ &+\{\tau\Longleftrightarrow\tau'\}. \end{aligned} \quad \text{(C.8)}$$

Section C.2

A free quantum particle description

Consider a Gaussian wave packet state that describes a particle with position x_0 and momentum k_0:

$$\Psi(x,t=0) = N\int dk e^{-\frac{1}{2\sigma^2}(k-k_0)^2+ik(x-x_0)} = N(2\pi\sigma^2)^{3/2}e^{-\frac{\sigma^2}{2}(x-x_0)^2}e^{ik_0(x-x_0)} \quad \text{(C.9)}$$

where $N = (2\sigma\pi^{3/2})^{-3/2}$ is the normalization constant. The time evolution of the particle state can be obtained by solving the Schrödinger equation for the free Hamiltonian

$H = p^2/(2m)$, and we have

$$\Psi(\mathbf{r},t) = \left[\frac{\sigma}{\sqrt{\pi}\,(1+it\sigma^2/m)}\right]^{1/2} \exp\left[-\frac{\sigma^2}{2}\frac{(x-x_0-k_0t/m)^2}{1+i\sigma^2t/m} + ik_0\,(x-x_0) - ik_0^2t/(2m)\right], \tag{C.10}$$

from which one then finds probability density as

$$|\Psi(\mathbf{r},t)|^2 = \left[\frac{\sigma^2}{\pi\left(1+\left(\frac{\sigma^2t}{m}\right)^2\right)}\right]^{1/2} \exp\left[-\sigma^2\frac{(x-x_0-k_0t/m)^2}{1+\left(\frac{\sigma^2t}{m}\right)^2}\right]. \tag{C.11}$$

We see this result coincides with the expectation value of ϕ^2 in Eq. (6.5) up to a constant of m.

Bibliography

[1] H. Walther, B. T. Varcoe, B.-G. Englert, and T. Becker, "Cavity quantum electrodynamics," *Reports on Progress in Physics*, vol. 69, no. 5, p. 1325, 2006.

[2] A. Blais, A. L. Grimsmo, S. Girvin, and A. Wallraff, "Circuit quantum electrodynamics," *Reviews of Modern Physics*, vol. 93, no. 2, p. 025005, 2021.

[3] M. Aspelmeyer, T. J. Kippenberg, and F. Marquardt, "Cavity optomechanics," *Reviews of Modern Physics*, vol. 86, no. 4, p. 1391, 2014.

[4] W. G. Unruh, "Notes on black-hole evaporation," *Physical Review D*, vol. 14, no. 4, p. 870, 1976.

[5] S. Hawking and W. Israel, "General relativity: an einstein centenary survey," *General Relativity: an Einstein Centenary Survey*, 2010.

[6] S. B. Giddings and S. Weinberg, "Gauge-invariant observables in gravity and electromagnetism: black hole backgrounds and null dressings," *Physical Review D*, vol. 102, no. 2, p. 026010, 2020.

[7] T. Oniga and C. H.-T. Wang, "Quantum coherence, radiance, and resistance of gravitational systems," *Physical Review D*, vol. 96, no. 8, p. 084014, 2017.

[8] E. Witten, "Aps medal for exceptional achievement in research: Invited article on entanglement properties of quantum field theory," *Reviews of Modern Physics*, vol. 90, no. 4, p. 045003, 2018.

[9] A. O. Caldeira and A. J. Leggett, "Quantum tunnelling in a dissipative system," *Annals of Physics*, vol. 149, no. 2, pp. 374–456, 1983.

[10] E. Joos and H. D. Zeh, "The emergence of classical properties through interaction with the environment," *Zeitschrift für Physik B Condensed Matter*, vol. 59, no. 2, pp. 223–243, 1985.

[11] W. H. Zurek, "Decoherence and the transition from quantum to classical–revisited," *arXiv preprint quant-ph/0306072*, 2003.

[12] M. P. Blencowe, "Effective field theory approach to gravitationally induced decoherence," *Physical Review Letters*, vol. 111, no. 2, p. 021302, 2013.

[13] C. Anastopoulos and B. L. Hu, "A master equation for gravitational decoherence: probing the textures of spacetime," *Classical and Quantum Gravity*, vol. 30, no. 16, p. 165007, 2013.

[14] T. Oniga and C. H.-T. Wang, "Quantum gravitational decoherence of light and matter," *Physical Review D*, vol. 93, no. 4, p. 044027, 2016.

[15] A. Bassi, A. Großardt, and H. Ulbricht, "Gravitational decoherence," *Classical and Quantum Gravity*, vol. 34, no. 19, p. 193002, 2017.

[16] C. DeLisle, J. Wilson-Gerow, and P. Stamp, "Gravitational decoherence, asymptotic quantization, and entanglement measures," *arXiv preprint arXiv:1905.05333*, 2019.

[17] L. Asprea, G. Gasbarri, and A. Bassi, "Gravitational decoherence: A general nonrelativistic model," *Physical Review D*, vol. 103, no. 10, p. 104041, 2021.

[18] C. Anastopoulos, M. Blencowe, and B.-L. Hu, "Gravitational decoherence in deep space experiments," *arXiv preprint arXiv:2111.05441*, 2021.

[19] R. Kaltenbaek, M. Aspelmeyer, P. F. Barker, A. Bassi, J. Bateman, K. Bongs, S. Bose, C. Braxmaier, Č. Brukner, B. Christophe, *et al.*, "Macroscopic quantum resonators (maqro): 2015 update," *EPJ Quantum Technology*, vol. 3, no. 1, p. 5, 2016.

[20] J. F. Donoghue, "General relativity as an effective field theory: The leading quantum corrections," *Physical Review D*, vol. 50, no. 6, p. 3874, 1994.

[21] D. Arteaga, R. Parentani, and E. Verdaguer, "Propagation in a thermal graviton background," *Physical Review D*, vol. 70, no. 4, p. 044019, 2004.

[22] E. A. Calzetta and B.-L. Hu, *Nonequilibrium Quantum Field Theory*. Cambridge, England: Cambridge University Press, 2008.

[23] H. J. Carmichael, *Statistical Methods in Quantum Optics 1: Master Equations and Fokker-Planck Equations*. Springer, Berlin, 1999.

[24] F. Petruccione and H.-P. Breuer, *The Theory of Open Quantum Systems*. Oxford University Press, Oxford, 2002.

[25] C. Gardiner and P. Zoller, *Quantum Noise: a Handbook of Markovian and Non-Markovian Quantum Stochastic Methods with Applications to Quantum Optics*, vol. 56. Springer, Berlin, 2004.

[26] T. Oniga and C. H.-T. Wang, "Quantum coherence, radiance, and resistance of gravitational systems," *Physical Review D*, vol. 96, no. 8, p. 084014, 2017.

[27] T. Kovachy, P. Asenbaum, C. Overstreet, C. A. Donnelly, S. M. Dickerson, A. Sugarbaker, J. M. Hogan, and M. A. Kasevich, "Quantum superposition at the half-metre scale," *Nature*, vol. 528, no. 7583, p. 530, 2015.

[28] V. Xu, M. Jaffe, C. D. Panda, S. L. Kristensen, L. W. Clark, and H. Müller, "Probing gravity by holding atoms for 20 seconds," *Science*, vol. 366, p. 745, 2019.

[29] Y. Y. Fein, P. Geyer, P. Zwick, F. Kiałka, S. Pedalino, M. Mayor, S. Gerlich, and M. Arndt, "Quantum superposition of molecules beyond 25 kda," *Nature Physics*, vol. 15, no. 12, pp. 1242–1245, 2019.

[30] T. Li, S. Kheifets, and M. G. Raizen, "Millikelvin cooling of an optically trapped microsphere in vacuum," *Nature Physics*, vol. 7, no. 7, p. 527, 2011.

[31] O. Romero-Isart, A. C. Pflanzer, M. L. Juan, R. Quidant, N. Kiesel, M. Aspelmeyer, and J. I. Cirac, "Optically levitating dielectrics in the quantum regime: Theory and protocols," *Physical Review A*, vol. 83, no. 1, p. 013803, 2011.

[32] S. Bose, A. Mazumdar, G. W. Morley, H. Ulbricht, M. Toroš, M. Paternostro, A. A. Geraci, P. F. Barker, M. Kim, and G. Milburn, "Spin entanglement witness for quantum gravity," *Physical Review Letters*, vol. 119, no. 24, p. 240401, 2017.

[33] U. Delić, D. Grass, M. Reisenbauer, T. Damm, M. Weitz, N. Kiesel, and M. Aspelmeyer, "Levitated cavity optomechanics in high vacuum," *Quantum Science and Technology*, vol. 5, no. 2, p. 025006, 2020.

[34] D. Boyanovsky, H. J. de Vega, R. Holman, S. P. Kumar, and R. D. Pisarski, "Real-time relaxation and kinetics in hot scalar qed: Landau damping," *Physical Review D*, vol. 58, no. 12, p. 125009, 1998.

[35] M. Aspelmeyer, T. J. Kippenberg, and F. Marquardt, "Cavity optomechanics," *Reviews of Modern Physics*, vol. 86, no. 4, p. 1391, 2014.

[36] J. D. Thompson, B. M. Zwickl, A. M. Jayich, F. Marquardt, S. Girvin, and J. Harris, "Strong dispersive coupling of a high-finesse cavity to a micromechanical membrane," *Nature*, vol. 452, no. 7183, p. 72, 2008.

[37] Q. Xu and M. P. Blencowe, "Cavity mode dephasing via the optomechanical interaction with an acoustic environment," *Physical Review A*, vol. 104, no. 6, p. 063509, 2021.

[38] L. Gilles and P. L. Knight, "Two-photon absorption and nonclassical states of light," *Physical Review A*, vol. 48, no. 2, p. 1582, 1993.

[39] S. Bose, K. Jacobs, and P. L. Knight, "Preparation of nonclassical states in cavities with a moving mirror," *Physical Review A*, vol. 56, no. 5, p. 4175, 1997.

[40] S. Bose, K. Jacobs, and P. L. Knight, "Scheme to probe the decoherence of a macroscopic object," *Physical Review A*, vol. 59, no. 5, p. 3204, 1999.

[41] J. Anglin, J. P. Paz, and W. H. Zurek, "Deconstructing decoherence," *Physical Review A*, vol. 55, no. 6, p. 4041, 1997.

[42] W. B. Case, "Wigner functions and weyl transforms for pedestrians," *American Journal of Physics*, vol. 76, no. 10, pp. 937–946, 2008.

[43] E. Cortés, B. J. West, and K. Lindenberg, "On the generalized langevin equation: Classical and quantum mechanicala," *The Journal of Chemical Physics*, vol. 82, no. 6, pp. 2708–2717, 1985.

[44] Z. Leghtas, S. Touzard, I. M. Pop, A. Kou, B. Vlastakis, A. Petrenko, K. M. Sliwa, A. Narla, S. Shankar, M. J. Hatridge, *et al.*, "Confining the state of light to a quantum manifold by engineered two-photon loss," *Science*, vol. 347, no. 6224, pp. 853–857, 2015.

[45] C. Gardiner, *Handbook of Stochastic Methods, Third Edition*. Springer, Berlin, 2004.

[46] J. R. Johansson, P. D. Nation, and F. Nori, "Qutip 2: A python framework for the dynamics of open quantum systems," *Computer Physics Communications*, vol. 184, no. 4, pp. 1234–1240, 2013.

[47] W. P. Bowen and G. J. Milburn, *Quantum Optomechanics*. CRC press, 2015.

[48] D. E. Bruschi, "Time evolution of coupled multimode and multiresonator optomechanical systems," *Journal of Mathematical Physics*, vol. 60, p. 062105, June 2019.

[49] W. H. Renninger, P. Kharel, R. O. Behunin, and P. T. Rakich, "Bulk crystalline optomechanics," *Nature Physics*, vol. 14, pp. 601–607, June 2018.

[50] Y. Minoguchi, P. Kirton, and P. Rabl, "Environment-induced rabi oscillations in the optomechanical boson-boson model," *arXiv: 1904.02164*, 2019.

[51] Q. Xu and M. P. Blencowe, "Toy models for gravitational and scalar qed decoherence," *arXiv: 2005.02554*, 2020.

[52] K. H. Michel, S. Costamagna, and F. M. Peeters, "Theory of thermal expansion in 2D crystals: Theory of thermal expansion in 2D crystals," *physica status solidi (b)*, vol. 252, pp. 2433–2437, Nov. 2015.

[53] D. P. Clougherty, "Quantum sticking of atoms on membranes," *Physical Review B*, vol. 90, p. 245412, Dec. 2014.

[54] S. Sengupta, V. N. Kotov, and D. P. Clougherty, "Infrared dynamics of cold atoms on hot graphene membranes," *Physical Review B*, vol. 93, p. 235437, June 2016.

[55] D. P. Clougherty and S. Sengupta, "Infrared problem in quantum acoustodynamics," *Physical Review A*, vol. 95, p. 052110, May 2017.

[56] D. P. Clougherty, "Infrared problem in quantum acoustodynamics at finite temperature," *Physical Review B*, vol. 96, p. 235404, Dec. 2017.

[57] S. Sengupta and D. P. Clougherty, "Radiative corrections to quantum sticking on graphene," *Physical Review B*, vol. 96, p. 035419, July 2017.

[58] S. Sengupta, "Theory of phonon-assisted adsorption in graphene: Many-body infrared dynamics," *Physical Review B*, vol. 100, p. 075429, Aug. 2019.

[59] A. J. Leggett, S. Chakravarty, A. T. Dorsey, M. P. A. Fisher, A. Garg, and W. Zwerger, "Dynamics of the dissipative two-state system," *Reviews of Modern Physics*, vol. 59, pp. 1–85, Jan. 1987.

[60] R. Schilling, H. Schütz, A. H. Ghadimi, V. Sudhir, D. J. Wilson, and T. J. Kippenberg, "Near-field integration of a sin nanobeam and a sio_2 microcavity for heisenberg-limited displacement sensing," *Phys. Rev. Applied*, vol. 5, p. 054019, May 2016.

[61] M. Reagor, W. Pfaff, C. Axline, R. W. Heeres, N. Ofek, K. Sliwa, E. Holland, C. Wang, J. Blumoff, K. Chou, M. J. Hatridge, L. Frunzio, M. H. Devoret, L. Jiang, and R. J. Schoelkopf, "Quantum memory with millisecond coherence in circuit QED," *Physical Review B*, vol. 94, p. 014506, July 2016.

[62] K. X. Wei, I. Lauer, S. Srinivasan, N. Sundaresan, D. T. McClure, D. Toyli, D. C. McKay, J. M. Gambetta, and S. Sheldon, "Verifying multipartite entangled Greenberger-Horne-Zeilinger states via multiple quantum coherences," *Physical Review A*, vol. 101, p. 032343, Mar. 2020.

[63] H. Zhang, S. Chakram, T. Roy, N. Earnest, Y. Lu, Z. Huang, D. Weiss, J. Koch, and D. I. Schuster, "Universal Fast-Flux Control of a Coherent, Low-Frequency Qubit," *Physical Review X*, vol. 11, p. 011010, Jan. 2021.

[64] M. J. Underwood, *Cryogenic optomechanics with a silicon nitride membrane*. Ph.D. thesis, Yale University., 2016.

[65] G. Brooker, *Modern classical optics*. No. 8 in Oxford master series in physics, Oxford; New York: Oxford University Press, 2003.

[66] J. Guo and Y. Liu, "A modified Euler–Maclaurin formula in 1D and 2D with applications in statistical physics," *Communications in Theoretical Physics*, vol. 73, p. 075002, July 2021.

[67] M. Underwood, D. Mason, D. Lee, H. Xu, L. Jiang, A. B. Shkarin, K. Børkje, S. M. Girvin, and J. G. E. Harris, "Measurement of the motional sidebands of a nanogram-scale oscillator in the quantum regime," *Physical Review A*, vol. 92, p. 061801, Dec. 2015.

[68] W. H. Zurek, "Environment-induced superselection rules," *Physical Review D*, vol. 26, no. 8, p. 1862, 1982.

[69] E. Joos and H. D. Zeh, "The emergence of classical properties through interaction with the environment," *Zeitschrift für Physik B Condensed Matter*, vol. 59, no. 2, pp. 223–243, 1985.

[70] W. H. Zurek, "From quantum to classical," *Physics Today*, vol. 44, p. 36, 1991.

[71] D. Braun, "Creation of entanglement by interaction with a common heat bath," *Physical Review Letters*, vol. 89, no. 27, p. 277901, 2002.

[72] F. Benatti, R. Floreanini, and M. Piani, "Environment induced entanglement in markovian dissipative dynamics," *Physical Review Letters*, vol. 91, no. 7, p. 070402, 2003.

[73] R. Romano and D. D'Alessandro, "Environment-mediated control of a quantum system," *Physical Review Letters*, vol. 97, no. 8, p. 080402, 2006.

[74] A. Ferreira, A. Guerreiro, and V. Vedral, "Macroscopic thermal entanglement due to radiation pressure," *Physical Review Letters*, vol. 96, no. 6, p. 060407, 2006.

[75] L. Contreras-Pulido and R. Aguado, "Entanglement between charge qubits induced by a common dissipative environment," *Physical Review B*, vol. 77, no. 15, p. 155420, 2008.

[76] J. P. Paz and A. J. Roncaglia, "Dynamics of the entanglement between two oscillators in the same environment," *Physical Review Letters*, vol. 100, no. 22, p. 220401, 2008.

[77] D. P. McCutcheon, A. Nazir, S. Bose, and A. J. Fisher, "Long-lived spin entanglement induced by a spatially correlated thermal bath," *Physical Review A*, vol. 80, no. 2, p. 022337, 2009.

[78] T. Zell, F. Queisser, and R. Klesse, "Distance dependence of entanglement generation via a bosonic heat bath," *Physical Review Letters*, vol. 102, no. 16, p. 160501, 2009.

[79] F. Galve, L. A. Pachón, and D. Zueco, "Bringing entanglement to the high temperature limit," *Physical Review Letters*, vol. 105, no. 18, p. 180501, 2010.

[80] P. Eastham, P. Kirton, H. Cammack, B. Lovett, and J. Keeling, "Bath-induced coherence and the secular approximation," *Physical Review A*, vol. 94, no. 1, p. 012110, 2016.

[81] L.-Z. Hu, Z.-X. Man, and Y.-J. Xia, "Steady-state entanglement and thermalization of coupled qubits in two common heat baths," *Quantum Information Processing*, vol. 17, no. 3, pp. 1–14, 2018.

[82] A. Retzker, J. I. Cirac, and B. Reznik, "Detecting vacuum entanglement in a linear ion trap," *Physical Review Letters*, vol. 94, no. 5, p. 050504, 2005.

[83] C. Sabín, J. J. García-Ripoll, E. Solano, and J. León, "Dynamics of entanglement via propagating microwave photons," *Physical Review B*, vol. 81, no. 18, p. 184501, 2010.

[84] C. Sabín, B. Peropadre, M. del Rey, and E. Martín-Martínez, "Extracting past-future vacuum correlations using circuit qed," *Physical Review Letters*, vol. 109, no. 3, p. 033602, 2012.

[85] M. Cattaneo, G. L. Giorgi, S. Maniscalco, G. S. Paraoanu, and R. Zambrini, "Bath-induced collective phenomena on superconducting qubits: Synchronization, subradiance, and entanglement generation," *Annalen der Physik*, vol. 533, no. 5, p. 2100038, 2021.

[86] L. Aolita, F. De Melo, and L. Davidovich, "Open-system dynamics of entanglement: a key issues review," *Reports on Progress in Physics*, vol. 78, no. 4, p. 042001, 2015.

[87] B. S. DeWitt, *Quantum Gravity: the new synthesis*, pp. 680–745. Cambridge University Press, 1 1979.

[88] S.-Y. Lin and B.-L. Hu, "Backreaction and the unruh effect: New insights from exact solutions of uniformly accelerated detectors," *Physical Review D*, vol. 76, no. 6, p. 064008, 2007.

[89] B. Reznik, "Entanglement from the vacuum," *Foundations of Physics*, vol. 33, no. 1, pp. 167–176, 2003.

[90] B. Reznik, A. Retzker, and J. Silman, "Violating bell's inequalities in vacuum," *Physical Review A*, vol. 71, no. 4, p. 042104, 2005.

[91] E. Martín-Martínez, E. G. Brown, W. Donnelly, and A. Kempf, "Sustainable entanglement production from a quantum field," *Physical Review A*, vol. 88, no. 5, p. 052310, 2013.

[92] G. Salton, R. B. Mann, and N. C. Menicucci, "Acceleration-assisted entanglement harvesting and rangefinding," *New Journal of Physics*, vol. 17, no. 3, p. 035001, 2015.

[93] S.-Y. Lin and B. L. Hu, "Entanglement creation between two causally disconnected objects," *Physical Review D*, vol. 81, no. 4, p. 045019, 2010.

[94] P. Simidzija, R. H. Jonsson, and E. Martín-Martínez, "General no-go theorem for entanglement extraction," *Physical Review D*, vol. 97, p. 125002, June 2018.

[95] M. P. Blencowe, "Effective field theory approach to gravitationally induced decoherence," *Physical Review Letters*, vol. 111, no. 2, p. 021302, 2013.

[96] Q. Xu and M. P. Blencowe, "Toy models for gravitational and scalar qed decoherence," *arXiv preprint arXiv:2005.02554*, 2020.

[97] Q. Xu and M. P. Blencowe, "Cavity mode dephasing via the optomechanical interaction with an acoustic environment," *Physical Review A*, vol. 104, no. 6, p. 063509, 2021.

[98] S. Bose, A. Mazumdar, G. W. Morley, H. Ulbricht, M. Toroš, M. Paternostro, A. A. Geraci, P. F. Barker, M. Kim, and G. Milburn, "Spin entanglement witness for quantum gravity," *Physical Review Letters*, vol. 119, no. 24, p. 240401, 2017.

[99] C. Marletto and V. Vedral, "Gravitationally induced entanglement between two massive particles is sufficient evidence of quantum effects in gravity," *Physical Review Letters*, vol. 119, no. 24, p. 240402, 2017.

[100] D. Carney, "Newton, entanglement, and the graviton," *arXiv preprint arXiv:2108.06320*, 2021.

[101] R. H. Jonsson, E. Martin-Martinez, and A. Kempf, "Quantum signaling in cavity qed," *Physical Review A*, vol. 89, no. 2, p. 022330, 2014.

[102] D. M. T. Benincasa, L. Borsten, M. Buck, and F. Dowker, "Quantum information processing and relativistic quantum fields," *Classical and Quantum Gravity*, vol. 31, no. 7, p. 075007, 2014.

[103] G. Vidal and R. F. Werner, "Computable measure of entanglement," *Physical Review A*, vol. 65, no. 3, p. 032314, 2002.

[104] R. Schilling, H. Schütz, A. Ghadimi, V. Sudhir, D. J. Wilson, and T. J. Kippenberg, "Near-field integration of a sin nanobeam and a sio 2 microcavity for heisenberg-limited displacement sensing," *Physical Review Applied*, vol. 5, no. 5, p. 054019, 2016.

[105] M. Hofheinz *et al.*, "Synthesizing arbitrary quantum states in a superconducting resonator," *Nature*, vol. 459, no. 7246, pp. 546–549, 2009.

[106] A. Nersisyan *et al.*, "Manufacturing low dissipation superconducting quantum processors," in *2019 IEEE International Electron Devices Meeting (IEDM)*, (San Francisco, CA, USA), pp. 31.1.1–31.1.4, IEEE, Dec. 2019.

[107] R. J. Marshman, A. Mazumdar, and S. Bose, "Locality and entanglement in table-top testing of the quantum nature of linearized gravity," *Physical Review A*, vol. 101, no. 5, p. 052110, 2020.

[108] A. Matsumura, "Field-induced entanglement in spatially superposed objects," *Physical Review D*, vol. 104, p. 046001, 2021.

[109] A. Mari, G. De Palma, and V. Giovannetti, "Experiments testing macroscopic quantum superpositions must be slow," *Scientific reports*, vol. 6, no. 1, pp. 1–9, 2016.

[110] A. Belenchia, R. M. Wald, F. Giacomini, E. Castro-Ruiz, Č. Brukner, and M. Aspelmeyer, "Quantum superposition of massive objects and the quantization of gravity," *Physical Review D*, vol. 98, no. 12, p. 126009, 2018.

[111] D. L. Danielson, G. Satishchandran, and R. M. Wald, "Gravitationally mediated entanglement: Newtonian field vs. gravitons," *arXiv preprint arXiv:2112.10798*, 2021.

[112] D. E. Bruschi, "Time evolution of coupled multimode and multiresonator optomechanical systems," *Journal of Mathematical Physics*, vol. 60, no. 6, p. 062105, 2019.

[113] S. J. Summers and R. Werner, "Bell's Inequalities and Quantum Field Theory. II. Bell's Inequalities are Maximally Violated in the Vacuum," *J. Math. Phys.*, vol. 28, p. 2448, 1987.

[114] S. J. Summers and R. Werner, "Bell's Inequalities and Quantum Field Theory. I. General Setting," *J. Math. Phys.*, vol. 28, p. 2440, 1987.

[115] S. J. Summers and R. Werner, "The vacuum violates Bell's inequalities," *Phys. Lett. Letters A*, vol. 110, pp. 257–259, July 1985.

[116] A. Valentini, "Non-local correlations in quantum electrodynamics," *Phys. Lett. A*, vol. 153, p. 321, 1991.

[117] B. Reznik, "Entanglement from the vacuum," *Foundations of Physics*, vol. 33, p. 167, 2003.

[118] B. Reznik, A. Retzker, and J. Silman, "Violating Bell's inequalities in vacuum," *Phys. Rev. A*, vol. 71, p. 042104, 2005.

[119] E. Martín-Martínez, E. G. Brown, W. Donnelly, and A. Kempf, "Sustainable entanglement production from a quantum field," *Phys. Rev. A*, vol. 88, no. 5, p. 052310, 2013.

[120] G. Salton, R. B. Mann, and N. C. Menicucci, "Acceleration-assisted entanglement harvesting and rangefinding," *New J. Phys.*, vol. 17, p. 035001, Mar. 2015.

[121] T. C. Ralph and N. Walk, "Quantum key distribution without sending a quantum signal," *New J. Phys.*, vol. 17, p. 063008, June 2015.

[122] A. Pozas-Kerstjens and E. Martín-Martínez, "Harvesting correlations from the quantum vacuum," *Phys. Rev. D*, vol. 92, p. 064042, Sep 2015.

[123] A. Pozas-Kerstjens and E. Martín-Martínez, "Entanglement harvesting from the electromagnetic vacuum with hydrogenlike atoms," *Phys. Rev. D*, vol. 94, p. 064074, 2016.

[124] E. Martín-Martínez and B. C. Sanders, "Precise space–time positioning for entanglement harvesting," *New J. Phys.*, vol. 18, p. 043031, Apr. 2016.

[125] A. Sachs, R. B. Mann, and E. Martín-Martínez, "Entanglement harvesting and divergences in quadratic Unruh-DeWitt detector pairs," *Phys. Rev. D*, vol. 96, p. 085012, Oct. 2017.

[126] J. S. Ardenghi, "Entanglement harvesting in double-layer graphene by vacuum fluctuations in a microcavity," *Phys. Rev. D*, vol. 98, p. 045006, Aug. 2018.

[127] J. Trevison, K. Yamaguchi, and M. Hotta, "Pure state entanglement harvesting in quantum field theory," *Prog. Theor. Exp. Phys.*, vol. 2018, Oct. 2018.

[128] E. Martin-Martinez and P. Rodriguez-Lopez, "Relativistic Quantum Optics: On the relativistic invariance of the light-matter interaction models," *Phys. Rev. D*, vol. 97, p. 105026, May 2018.

[129] P. Simidzija and E. Martín-Martínez, "Harvesting correlations from thermal and squeezed coherent states," *Phys. Rev. D*, vol. 98, p. 085007, Oct. 2018.

[130] W. Cong, E. Tjoa, and R. B. Mann, "Entanglement harvesting with moving mirrors," *J. High Energ. Phys.*, vol. 2019, p. 21, June 2019.

[131] L. J. Henderson and N. C. Menicucci, "Bandlimited Entanglement Harvesting," May 2020.

[132] L. J. Henderson, A. Belenchia, E. Castro-Ruiz, C. Budroni, M. Zych, v. C. Brukner, and R. B. Mann, "Quantum Temporal Superposition: the case of QFT," 2020.

[133] R. Faure, T. R. Perche, and B. d. S. L. Torres, "Particle detectors as witnesses for quantum gravity," Apr. 2020.

[134] M. B. Plenio and S. Virmani, "An Introduction to entanglement measures," *Quant. Inf. Comput.*, vol. 7, pp. 1–51, 2007.

[135] G. Ver Steeg and N. C. Menicucci, "Entangling power of an expanding universe," *Phys. Rev. D*, vol. 79, p. 044027, 2009.

[136] E. Martin-Martinez and N. C. Menicucci, "Cosmological quantum entanglement," *Class. Quant. Grav.*, vol. 29, p. 224003, 2012.

[137] E. Martín-Martínez and N. C. Menicucci, "Entanglement in curved spacetimes and cosmology," *Classical and Quantum Gravity*, vol. 31, no. 214001, p. 41, 2014.

[138] Z. Huang and Z. Tian, "Dynamics of quantum entanglement in de Sitter spacetime and thermal Minkowski spacetime," *Nuclear Physics B*, vol. 923, pp. 458–474, Oct. 2017.

[139] E. Martín-Martínez, A. R. H. Smith, and D. R. Terno, "Spacetime structure and vacuum entanglement," *Phys. Rev. D*, vol. 93, p. 044001, Feb. 2016.

[140] S.-Y. Lin, C.-H. Chou, and B.-L. Hu, "Entanglement dynamics of detectors in an einstein cylinder," *Journal of High Energy Physics*, vol. 2016, no. 3, p. 47, 2016.

[141] A. R. H. Smith, *Detectors, Reference Frames, and Time*. Springer Theses, Cham: Springer International Publishing, 2019.

[142] M. Cliche and A. Kempf, "Vacuum entanglement enhancement by a weak gravitational field," *Phys. Rev. D*, vol. 83, p. 045019, Feb. 2011.

[143] K. K. Ng, R. B. Mann, and E. Martín-Martínez, "Unruh-DeWitt detectors and entanglement: The anti–de Sitter space," *Phys. Rev. D*, vol. 98, p. 125005, Dec. 2018.

[144] K. K. Ng, R. B. Mann, and E. Martín-Martínez, "New techniques for entanglement harvesting in flat and curved spacetimes," *Phys. Rev. D*, vol. 97, p. 125011, June 2018.

[145] L. J. Henderson, R. A. Hennigar, R. B. Mann, A. R. H. Smith, and J. Zhang, "Entangling detectors in anti-de Sitter space," *J. High Energ. Phys.*, vol. 2019, no. 5, p. 178, 2019.

[146] L. J. Henderson, R. A. Hennigar, R. B. Mann, A. R. H. Smith, and J. Zhang, "Harvesting entanglement from the black hole vacuum," *Class. Quantum Grav.*, vol. 35, p. 21LT02, Oct. 2018.

[147] W. Cong, C. Qian, M. R. R. Good, and R. B. Mann, "Effects of Horizons on Entanglement Harvesting," June 2020.

[148] G. W. Gibbons, "Quantized fields propagating in plane-wave spacetimes," *Comm. Math. Phys.*, vol. 45, no. 2, pp. 191–202, 1975.

[149] J. Garriga and E. Verdaguer, "Scattering of quantum particles by gravitational plane waves," *Phys. Rev. D*, vol. 43, pp. 391–401, Jan. 1991.

[150] N. Birrell and P. Davies, *Quantum Fields in Curved Space*. Cambridge Monographs on Mathematical Physics, Cambridge, UK: Cambridge Univ. Press, 2 1984.

[151] R. M. Wald, *Quantum Field Theory in Curved Space-Time and Black Hole Thermodynamics*. Chicago Lectures in Physics, Chicago: University of Chicago Press, 10 1995.

[152] P. D. Mannheim, "Light-front quantization is the same as instant-time quantization," 2020.

[153] W. G. Unruh, "Notes on black-hole evaporation," *Phys. Rev. D*, vol. 14, pp. 870–892, Aug. 1976.

[154] E. Martín-Martínez, M. Montero, and M. del Rey, "Wavepacket detection with the Unruh-DeWitt model," *Phys. Rev. D*, vol. 87, no. 6, p. 064038, 2013.

[155] Á. M. Alhambra, A. Kempf, and E. Martín-Martínez, "Casimir forces on atoms in optical cavities," *Phys. Rev. A*, vol. 89, no. 3, p. 033835, 2014.

[156] J. Louko and A. Satz, "Transition rate of the Unruh-DeWitt detector in curved spacetime," *Class. Quant. Grav.*, vol. 25, p. 055012, 2008.

[157] J. Louko and A. Satz, "How often does the Unruh-DeWitt detector click? Regularisation by a spatial profile," *Class. Quant. Grav.*, vol. 23, pp. 6321–6344, 2006.

[158] D. Su, C. T. M. Ho, R. B. Mann, and T. C. Ralph, "Black hole squeezers," *Phys. Rev. D*, vol. 96, p. 065017, Sep 2017.

[159] W. K. Wootters, "Entanglement of Formation and Concurrence," *Quantum Inf. Comput.*, vol. 1, no. 1, pp. 27–44, 2001.

[160] B. P. Abbott, R. Abbott, T. Abbott, M. Abernathy, F. Acernese, K. Ackley, C. Adams, T. Adams, P. Addesso, R. Adhikari, *et al. Phys. Rev. Lett.*, vol. 116, p. 061102, Feb 2016.

[161] D. Christodoulou, "Nonlinear nature of gravitation and gravitational wave experiments," *Phys. Rev. Lett.*, vol. 67, pp. 1486–1489, 1991.

[162] A. G. Wiseman and C. M. Will, "Christodoulou's nonlinear gravitational wave memory: Evaluation in the quadrupole approximation," *Phys. Rev. D*, vol. 44, no. 10, pp. 2945–2949, 1991.

[163] P. Candelas and D. W. Sciama, "Irreversible thermodynamics of black holes," *Physical Review Letters*, vol. 38, no. 23, p. 1372, 1977.

[164] P. C. Davies, "Thermodynamics of black holes," *Reports on Progress in Physics*, vol. 41, no. 8, p. 1313, 1978.

[165] S. Gutti, S. Kulkarni, and L. Sriramkumar, "Modified dispersion relations and the response of the rotating unruh-dewitt detector," *Physical Review D*, vol. 83, no. 6, p. 064011, 2011.

[166] V. Husain and J. Louko, "Low energy lorentz violation from modified dispersion at high energies," *Physical review letters*, vol. 116, no. 6, p. 061301, 2016.

[167] N. Alkofer, G. D'Odorico, F. Saueressig, and F. Versteegen, "Quantum gravity signatures in the unruh effect," *Physical Review D*, vol. 94, no. 10, p. 104055, 2016.

[168] S. Schlicht, "Considerations on the unruh effect: Causality and regularization," *Classical and Quantum Gravity*, vol. 21, no. 19, p. 4647, 2004.

[169] P. Langlois, "Causal particle detectors and topology," *Annals of Physics*, vol. 321, no. 9, pp. 2027–2070, 2006.

[170] J. Louko and A. Satz, "How often does the unruh–dewitt detector click? regularization by a spatial profile," *Classical and Quantum Gravity*, vol. 23, no. 22, p. 6321, 2006.

[171] A. Satz, "Then again, how often does the unruh–dewitt detector click if we switch it carefully?," *Classical and Quantum Gravity*, vol. 24, no. 7, p. 1719, 2007.

[172] E. Martín-Martínez, M. Montero, and M. del Rey, "Wavepacket detection with the unruh-dewitt model," *Physical Review D*, vol. 87, no. 6, p. 064038, 2013.

[173] B. Iyer and A. Kumar, "Detection of dirac quanta in rindler and black hole space-times and the ξ quantisation scheme," *Journal of Physics A: Mathematical and General*, vol. 13, no. 2, p. 469, 1980.

[174] S. Takagi, "Vacuum noise and stress induced by uniform accelerationhawking-unruh effect in rindler manifold of arbitrary dimension," *Progress of Theoretical Physics Supplement*, vol. 88, pp. 1–142, 1986.

[175] D. Hümmer, E. Martín-Martínez, and A. Kempf, "Renormalized unruh-dewitt particle detector models for boson and fermion fields," *Physical Review D*, vol. 93, no. 2, p. 024019, 2016.

[176] J. Louko and V. Toussaint, "Unruh-dewitt detector's response to fermions in flat spacetimes," *Physical Review D*, vol. 94, no. 6, p. 064027, 2016.

[177] L. C. Crispino, A. Higuchi, and G. E. Matsas, "The unruh effect and its applications," *Reviews of Modern Physics*, vol. 80, no. 3, p. 787, 2008.

[178] B. Hu, S.-Y. Lin, and J. Louko, "Relativistic quantum information in detectors–field interactions," *Classical and quantum gravity*, vol. 29, no. 22, p. 224005, 2012.

[179] E. Martin-Martinez and N. C. Menicucci, "Entanglement in curved spacetimes and cosmology," *Classical and Quantum Gravity*, vol. 31, no. 21, p. 214001, 2014.

[180] E. Martín-Martínez, A. R. Smith, and D. R. Terno, "Spacetime structure and vacuum entanglement," *Physical Review D*, vol. 93, no. 4, p. 044001, 2016.

[181] A. Sachs, R. B. Mann, and E. Martín-Martínez, "Entanglement harvesting and divergences in quadratic unruh-dewitt detector pairs," *Physical Review D*, vol. 96, no. 8, p. 085012, 2017.

[182] J. S. Ardenghi, "Entanglement harvesting in double-layer graphene by vacuum fluctuations in a microcavity," *Physical Review D*, vol. 98, no. 4, p. 045006, 2018.

[183] J. Trevison, K. Yamaguchi, and M. Hotta, "Pure state entanglement harvesting in quantum field theory," *Progress of Theoretical and Experimental Physics*, vol. 2018, no. 10, p. 103A03, 2018.

[184] L. J. Henderson, A. Belenchia, E. Castro-Ruiz, C. Budroni, M. Zych, Č. Brukner, and R. B. Mann, "Quantum temporal superposition: The case of quantum field theory," *Physical review letters*, vol. 125, no. 13, p. 131602, 2020.

[185] R. Faure, T. R. Perche, and B. de SL Torres, "Particle detectors as witnesses for quantum gravity," *Physical Review D*, vol. 101, no. 12, p. 125018, 2020.

[186] G. Ver Steeg and N. C. Menicucci, "Entangling power of an expanding universe," *Physical Review D*, vol. 79, no. 4, p. 044027, 2009.

[187] Z. Huang and Z. Tian, "Dynamics of quantum entanglement in de sitter spacetime and thermal minkowski spacetime," *Nuclear Physics B*, vol. 923, pp. 458–474, 2017.

[188] Q. Xu, S. A. Ahmad, and A. R. Smith, "Gravitational waves affect vacuum entanglement," *Physical Review D*, vol. 102, no. 6, p. 065019, 2020.

[189] Z. Liu, J. Zhang, and H. Yu, "Harvesting entanglement by uniformly accelerated detectors in the presence of a reflecting boundary," *arXiv preprint arXiv:2101.00114*, 2021.

[190] V. Toussaint and J. Louko, "Detecting the massive bosonic zero-mode in expanding cosmological spacetimes," *arXiv preprint arXiv:2102.04284*, 2021.

[191] A. R. Lee and I. Fuentes, "Spatially extended unruh-dewitt detectors for relativistic quantum information," *Physical Review D*, vol. 89, no. 8, p. 085041, 2014.

[192] S. Das and S. Shankaranarayanan, "How robust is the entanglement entropy-area relation?," *Physical Review D*, vol. 73, no. 12, p. 121701, 2006.

[193] M. Caprio, P. Cejnar, and F. Iachello, "Excited state quantum phase transitions in many-body systems," *Annals of Physics*, vol. 323, no. 5, pp. 1106–1135, 2008.

[194] R. D. Sorkin, "Impossible measurements on quantum fields," in *Directions in general relativity: Proceedings of the 1993 International Symposium, Maryland*, vol. 2, pp. 293–305, 1993.

[195] S.-Y. Lin, "Notes on nonlocal projective measurements in relativistic systems," *Annals of Physics*, vol. 351, pp. 773–786, 2014.

[196] L. Borsten, I. Jubb, and G. Kells, "Impossible measurements revisited," *Physical Review D*, vol. 104, no. 2, p. 025012, 2021.

[197] H. Bostelmann, C. J. Fewster, and M. H. Ruep, "Impossible measurements require impossible apparatus," *Physical Review D*, vol. 103, no. 2, p. 025017, 2021.

[198] J. Polo-Goméz, L. J. Garay, and E. Martín-Martínez, "A detector-based measurement theory for quantum field theory," 2021.

[199] Q. Xu and M. Blencowe, "work in progress," *work in progress*.

[200] Y. Décanini and A. Folacci, "Hadamard renormalization of the stress-energy tensor for a quantized scalar field in a general spacetime of arbitrary dimension," *Physical Review D*, vol. 78, no. 4, p. 044025, 2008.

[201] C. K. Law, "Interaction between a moving mirror and radiation pressure: A Hamiltonian formulation," *Physical Review A*, vol. 51, pp. 2537–2541, Mar. 1995.